Electronic Theses and Dissertations

Theses, Dissertations, and Major Papers

2012

FLOW OVER A TRAPEZOIDAL CAVITY UNDER VARYING REYNOLDS NUMBER AND TURBULENCE CHARACTERISTICS

Saeed Zeinalidanaloo
University of Windsor

Follow this and additional works at: https://scholar.uwindsor.ca/etd

-FLOW OVER A TRAPEZOIDAL CAVITY UNDER VARYING REYNOLDS

NUMBER AND TURBULENCE CHARACTERISTICS

by

SAEED ZEINALIDANALOO

A Thesis

Submitted to the Faculty of Graduate Studies
through Mechanical, Automotive, and Materials Engineering
in Partial Fulfillment of the Requirements for
the Degree of Master of Applied Science at the
University of Windsor
Windsor, Ontario, Canada
2012

FLOW OVER A TRAPEZOIDAL CAVITY UNDER VARYING REYNOLDS

NUMBER AND TURBULENCE CHARACTERISTICS

by

SAEED ZEINALIDANALOO

APPROVED BY:

_____

Dr. Tirupati Bolisetti (Outside Program Reader)

Department of Civil and Environmental Engineering

_____

Dr. Gary Rankin (Program Reader)

Department of Mechanical, Automotive and Materials Engineering

_____

Dr. David Ting (Co-Adviser)

Department of Mechanical, Automotive and Materials Engineering

_____

Dr. Xiaohong Xu (Co-Adviser)

Department of Civil and Environmental Engineering

_____

Dr. Andrzej Sobiesiak (Chair of Defense)

Department of Mechanical, Automotive and Materials Engineering

20 Nov 2012

DECLARATION OF ORIGINALITY

I hereby certify that I am the sole author of this thesis and that no part of this thesis has been published or submitted for publication.

I certify that, to the best of my knowledge, my thesis does not infringe upon anyone's copyright nor violate any proprietary rights and that any ideas, techniques, quotations, or any other material from the work of other people included in my thesis, published or otherwise, are fully acknowledged in accordance with the standard referencing practices. Furthermore, to the extent that I have included copyrighted material that surpasses the bounds of fair dealing within the meaning of the Canada Copyright Act, I certify that I have obtained a written permission from the copyright owner(s) to include such material(s) in my thesis and have included copies of such copyright clearances to my appendix.

I declare that this is a true copy of my thesis, including any final revisions, as approved by my thesis committee and the Graduate Studies office, and that this thesis has not been submitted for a higher degree to any other University or Institution.

ABSTRACT

The effect of Reynolds number (Re), turbulence intensity (Tu) and aspect ratio (W/D) on flow above and inside a trapezoidal cavity is studied in terms of the vortex characteristics inside the cavity and the normalized volumetric air exchanged rate from the cavity ($Q_{normalized}$). A CFD model has been set and validated based on limited wind tunnel data.

With increasing Re (60000, 123000, and 181000), the center of vortex moved toward the trailing edge of the cavity, $Q_{normalized}$ increased, and the vortex inside the cavity had more strength (Vorticity magnitude increased). With increasing Tu (0.67%, 5%, and 15%), the center of vortex moved toward the leading edge in W/D of 2, and $Q_{normalized}$ did not change significantly. With increasing W/D (2, 4, and 6), the center of vortex moved toward the leading edge, and $Q_{normalized}$ increased significantly. W/D was found to be the most significant factor affecting vortex characteristics and $Q_{normalized}$. The cavity was "open" in W/D of 2 and 4, whereas, the cavity was found to be "closed and transitional" in W/D of 6.

This thesis is dedicated to my parents.

for their endless support and love

ACKNOWLEDGEMENTS

TABLE OF CONTENTS

LIST OF FIGURES

LIST OF TABLES

LIST OF SYMBOLS

CFD   Computational Fluid Dynamics

D   Cavity's depth [m]

FEM   Finite Element Method

FVM   Finite Volume Method

L   Cavity's mouth length [m]

LDV   Laser Doppler Velocimetry

LES   Large Eddy Simulation

PIV   Particle Image Velocimetry

Q   Volumetric flow rate [$\frac{m^3}{s}$]

Re   Reynolds number $= \frac{\rho U D}{\mu}$

Tu   Turbulence intensity (%)

u   X-component of the velocity [$\frac{m}{s}$]

u' Instantaneous fluctuating velocity

$u'v'$ Turbulence shear stress [$\frac{m^2}{s^2}$]

u_{rms} Root mean square of u' [$\frac{m}{s}$]

$U_{upstream}$ Inlet velocity [$\frac{m}{s}$]

$\bar{U}$ Time averaged velocity [$\frac{m}{s}$]

v   Y-component of the velocity [$\frac{m}{s}$]

W	Cavity's width [m]
y^+	Non- dimensional distance from wall, $\dfrac{u_\tau y}{\nu}$

GREEK SYMBOLS

β	Side angle of the cavity
Γ	Cavity's length [m]
δ	Boundary layer thickness [mm]
υ	Air kinematic viscosity $[\dfrac{m^2}{s}]$
ξ	Vorticity $[\dfrac{1}{s}]$
ρ	Air density $[\dfrac{kg}{m^3}]$
φ	Fluid's property

CHAPTER I

INTRODUCTION

1.1. Engineering applications of cavities

"Cavity" refers to a hollow space within a solid object. A cavity can be characterized with respect to its geometry, i.e. rectangular, trapezoidal, triangular or circular. A cavity's Width (W) to Depth (D) ratio (W/D) has been commonly used to identify how deep or shallow a cavity is. Cavities can be found in many engineering applications such as roadway configurations or street canyons (Lawson and Barakos, 2011). Moreover, due to the simplicity of the geometry and complexity of flow patterns and possible vortices inside it, there has been an effort to better understand flow inside the cavities numerically (Erturk, 2009).

A cavity could be representing the geometry of a roadway or street configuration as well. For example, for a roadway with length of 4 m and air velocity of 5 m/s (Re $\approx$ 6.4×10^5) can be considered as a cavity. In this specific application, flow patterns, i.e. vortex characteristics, and pollutant dispersion inside the cavity are the main concerns (Ahmad et al., 2005). There has been an intense research on this specific application because despite improvements in fuels and engines, most of air pollution in urban areas is traffic induced emissions (Fenger, 1999).

Furthermore, cavity flows can be found in coating and polishing industry (Shankar and Deshpande, 2000), as Aidun et al. (1991) first emphasized the application of cavity flows in coaters and melt-spinning process. Therefore, understanding flow over a cavity is of great importance.

1

1.2. Objectives

Although there has been much study on rectangular cavities, flow over trapezoidal cavities has not been yet fully identified. The primary objective of this study is to investigate the flow field above a shallow trapezoidal cavity. This was to be accomplished by developing a numerical model to be validated using limited experimental data conducted in a wind tunnel. The cavity is studied under varying Reynolds number (60000, 123000 and 181000), turbulence intensity (0.67%, 5% and 15%) and W/D (2, 4 and 6).

The specific objectives are to:

I.   Develop an experimental setup capable of generating a perpendicular boundary layer entering a shallow trapezoidal cavity.

II. Conduct velocity measurements above and behind the experimental model.

III. Develop a numerical model for the study and validate it using data collected from wind tunnel experiments.

IV. Characterize flow over a shallow trapezoidal cavity using the results of CFD model simulation.

V.   Analyze the CFD results to find the effect of each factor on vortex characteristics inside, shear layer grow above and the air exchange rate from the trapezoidal cavity.

CHAPTER II

THEORETICAL BACKGROUND AND LITERATURE REVIEW

2.1. Classification of cavities

Cavities can be classified with respect to different factors. Shape wise, they are classified into rectangular, trapezoidal and triangular cavities, as shown in Fig. 2.1. Rectangular cavities are divided into shallow and deep cavities with respect to their Width (W) to Depth (D) ratio. Shallow cavities have W/D greater than one, and deep cavities have W/D smaller than one (Lawson and Barakos, 2011).

Both trapezoidal and triangular cavities' geometry can also be described using their width to depth ratio and the side angle (β). By the analogy we may borrow from rectangular cavities, let the trapezoidal cavities with W/D greater than one be shallow and W/D smaller than one deep.
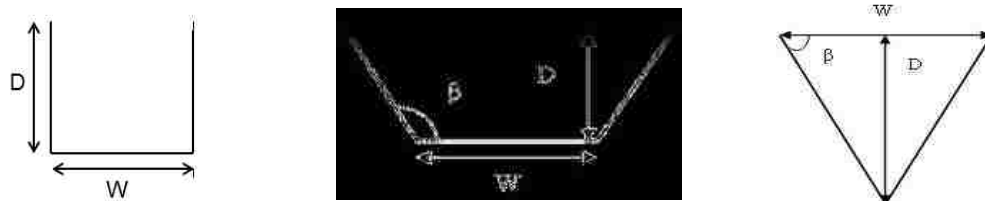
Fig. 2.1. Rectangular cavity, Trapezoidal cavity and Triangular cavity

Moreover, cavities can be classified with respect to the flow pattern inside them. In "closed and transitional" cavities the flow does not have enough energy to bridge the cavity. Therefore, there is a separation point at the beginning of the mouth of the cavity and somewhere on the bottom (see Fig. 2.2.a).

In "open" cavities flow has enough energy to bridge the cavity. Therefore, a complete vortex can be seen inside the cavity and there is no separation point inside the cavity (see Fig. 2.2.b). Sometimes, in "open" cavities, secondary vortices can be seen inside the cavity as well. The presence of these vortices and shape of them depend on Re and geometry of the cavity (Lawson and Barakos, 2011).

a) Closed cavity   b) Open cavity
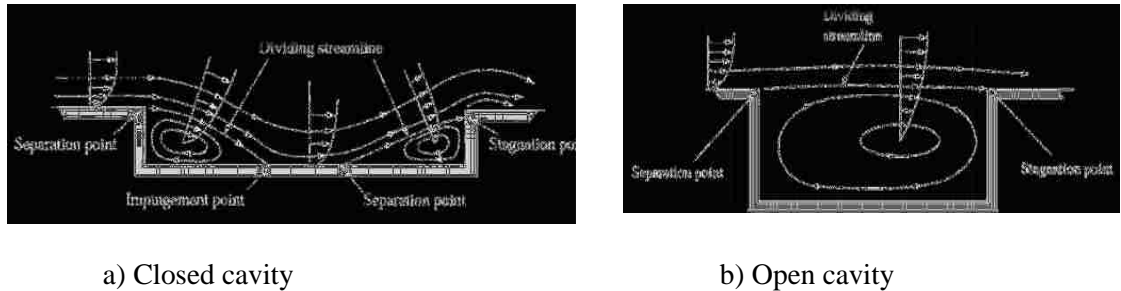
Fig. 2.2. Classification of cavities with respect to the vortex structure inside them (Lawson and Barakos, 2011).

The 2D schematic of a trapezoidal cavity can be described with W, D and β (side angle of the cavity). The third dimension of the cavity is called the length of the cavity (Γ). The ratio of the Length of the cavity to its Depth is used to characterize the cavities. Γ/D ratio affects the flow behavior inside the cavity. The higher the Γ/D ratio is, the more the flow shows 2D behavior in the middle section. The 2D or 3D behavior of the flow is also dependent on W/D of the cavity and Re (Reynolds number) and Tu (turbulence intensity) of the upstream flow. For their studied range of Re (1150 to10670), Faure et al. (2007) reported that flow inside and above the cavity with Γ /D ratio of 6 is mostly 2D rather than 3D.

4

2.2. Turbulent boundary layer

Flow regimes can be classified into laminar, transitional and turbulent. This classification is mostly based on the value of Re. In low Re, the viscous forces are dominant. Therefore, any disturbance in the flow is damped by the viscous forces (Pope, 2000). In laminar regime, the boundary layer consists of parallel stream lines with no mixing between them. However, by increasing Re, the inertia forces become dominant. Eventually, the disturbances in flow are not damped with viscous forces. This causes a chaotic manner in the flow. It is worth noting that flow transfers from laminar to turbulent through a transitional regime. In turbulent boundary layer, mixing occurs between the layers and the boundary layer thickness is less in comparison with the laminar case (Pope, 2000). Figure 2.3 shows the laminar, transitional and turbulent regimes on a flat plate.
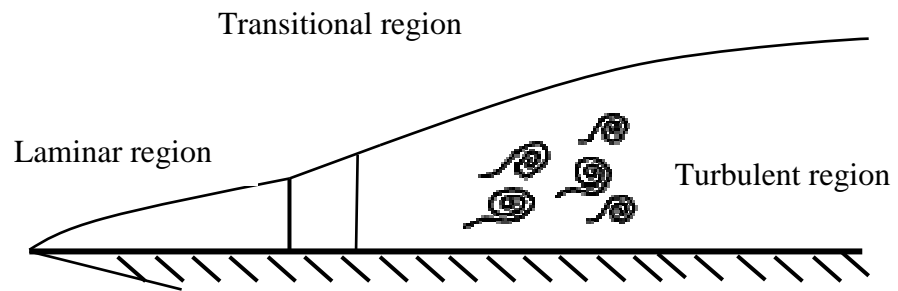
Fig. 2.3. Different flow regimes on a flat plate

Turbulence intensity (Tu) signifies the level of fluctuation in the flow and is defined as (Pope, 2000):

$$Tu = \frac{u'_{RMS}}{\bar{u}} \times 100 \qquad (2.1)$$

where, u' is the fluctuating portion of the velocity and can be written as:

$$u' = u(t) - \bar{u} \qquad (2.2)$$

and u(t) is the instantaneous velocity at time (t) and $\bar{u}$ is the mean value of velocity.

Moreover, the term τ_{ij} (Reynolds stress) is defined as:

$$\tau_{ij} = \rho \overline{u_\iota u_J} \qquad (2.3)$$

The turbulent boundary consists of four main regions (Akinlade 2005). These regions are defined based on the distance from the wall. The dimensionless distance from the wall is:

$$y^+ = \frac{u_\tau y}{v} \qquad (2.4)$$

where u_τ is the friction velocity, y is the distance from the wall [m] and v $[\frac{m^2}{s}]$ is the local kinematic viscosity.

$$u_\tau \equiv \sqrt{\frac{\tau_w}{\rho}} \qquad (2.5)$$

where τ_w is the wall shear stress and ρ $[\frac{kg}{m^3}]$ is the fluid density at the wall. The viscous sublayer is defined as the area very close to the wall, i.e. $z<z_f$, where z_f is the distance at Re $_{BL}$ =1. This Re_{BL} is calculated having z as the characteristic length. In this area, friction is very important (y^+ <30). The initial sublayer is defined as the area far away

from the boundary between $z=z_f$ and $z=\delta$ and δ is the boundary layer thickness. The region is similar to the inertial range in the homogenous turbulence.

Inner and outer regions are defined with respect to y^+. Fig. 2.4 shows these two regions. It can be seen that there is an overlap region ($30 < y^+ < 300$).
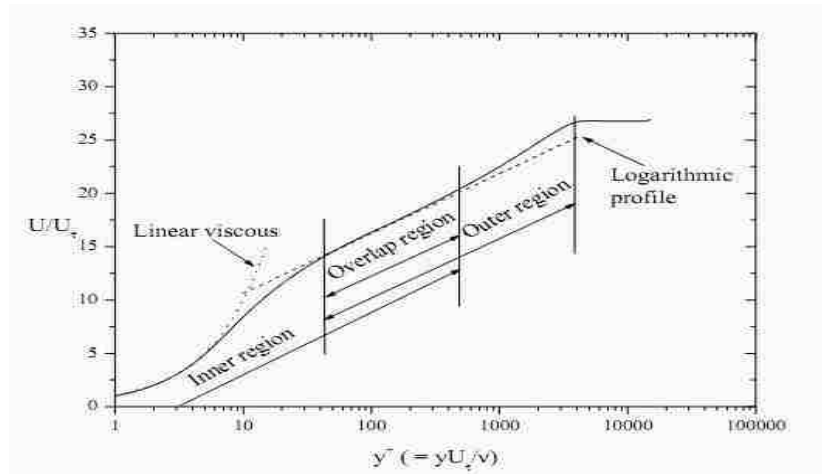
Fig. 2.4. Schematic of the inner, outer and overlap region (Akinlade, 2005)

According to Prandtl the flow in the inner layer is highly affected by the viscosity and shear stress (Akinlade, 2005). In the outer layer, at very high Re, i.e. beyond the critical Re, the flow motion is not a function of viscosity. The critical Re varies for different cases and geometries. For example, for the flow in pipes, the critical Re is ≈ 2300 and is calculated based on the diameter of the pipe. The law of wall is presented in the inner region which relates the u^+ to y^+ u^+ and y^+ are the dimensionless values of the velocity and distance from wall. This number is used to identify the regime of flow, i.e. for Re< Re_{cr} flow is laminar.

The law of wall states that in the overlap region, the dimensionless velocity is proportional to the logarithm of the dimensionless distance from that point to the "wall" (Akinlade, 2005).

$$u^+ = \frac{1}{k}\ln(y^+) + C^+ \qquad (2.6)$$

where u^+ is $\frac{u}{u_\tau}$ and C^+ is a constant. In ($y^+<5$),

$$u^+ \approx y^+ \qquad (2.7)$$

However, for the region of $5<y^+<30$, neither of the above estimations are applicable. Therefore, in the CFD model (see Appendix A.1), y^+ should be either kept below 5 or between 30 and 300, depending on the turbulence modeling and wall treatment used.

2.3. Vorticity

Motion of flow in circular pattern makes a vortex. Vortex is known by vortex lines. Vortex lines are the lines on which the line's tangent on any point gives the local vorticity direction. According to the definition Vorticity is defined as the curl function of velocity (Kundo, 1990):

$$\xi = \nabla u \qquad (2.8)$$

For the case of flow movement in Cartesian plane, the Vorticity line would be in Z-direction and it can be calculated by (Kundo, 1990):

$$\xi = \frac{\partial v}{\partial x} - \frac{\partial u}{\partial y} \qquad (2.9)$$

In the following sections a list of related researches and a summary of the area of interest in this field has been discussed. The studies have been divided into experimental and numerical studies.

Different experimental techniques have been used for cavity research by researchers. Particle Image Velocimetry (PIV) (Melling, 1997), Laser Doppler Velocimetry (LDV) (Tropea, 1995) and hot-wire anemometry (Comte-Bellot, 1976) have been commonly used in the papers reviewed. The experimental studies have been classified with respect to the method they used.

2.4. Experimental studies

In one of the earliest studies on cavities Roshko (1955) conducted experiments to measure velocity and pressure on the walls of a rectangular cavity. The upstream velocity was 22.86 and 64 m/s (75 and 210 ft /sec). The main conclusion of the work was that in order to balance any unstable pressures there should be a momentum transfer at the mouth of the cavity. Moreover, drag coefficient was reported to be only a function of pressures on the walls of the cavity. Later on, many other researchers continued this research with newer techniques and ideas.

<u>**Rectangular cavities**</u>

➢ **PIV studies**

Faure et al., (2007) conducted wind tunnel experiments using PIV to study a rectangular cavity. W/D of the cavity was 0.5, 1, 1.5 and 2, with free stream velocities of 0.69, 1.21 and 1.6 m/s. The Γ/D ratio of the experimental model was 6. In addition, the

upstream boundary layer was laminar. Flow visualizations were conducted mainly to emphasize the 3-D flow generation inside the cavity. In all the cases considered, the cavity was found to be "open". Moreover, it was found that the injection of flow into the cavity was more a 2-D phenomenon in that range of Re from 1150 to 10670. Figure 2.5 presents the flow visualization in two vertical planes for three different upstream velocities. These plots are for the cavity with W/D of 1.

The flow patterns in the two planes are very similar. Also it can be seen that the flow behavior is becoming more 3D with increasing upstream velocity. There are other plots in the paper concluding that for shallower cavities the flow shows more of 3D behavior especially at higher upstream velocities. The main conclusion, however, is that the flow is primarily 2D inside the cavity in this range of Re.
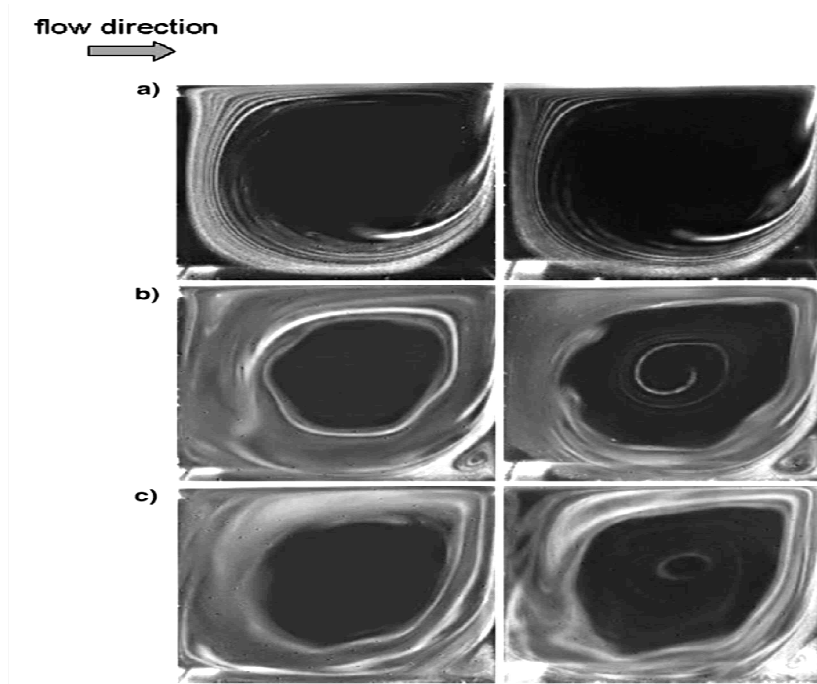
Fig. 2.5. Flow visualization for two vertical planse in the length of the cavity for upstream velocity of a) 0.61 m/s, b) 1.21 m/s and c) 1.6 m/s (Faure et al., 2007)

Ozsoy et al. (2005) performed experiments on a rectangular 2-D cavity with W/D =4 for Re of 4000, 9000 and 13000 using PIV. The incoming boundary layer was set laminar. In all cases the cavity was found to be open and with increasing Re the downstream vortex became larger and the center of the vortex moved toward the leading edge.

Salizzoni et al. (2011) studied a rectangular deep cavity (W/D=1) with the application for a street canyon. Turbulent urban boundary layer was generated in the wind tunnel. Velocity measurements were conducted using PIV and hot-wire anemometry. The upstream velocity was set at 6.75 m/s. They found that the momentum transfer and vortex shape inside the cavity was dependent on the type of the urban boundary layer generated and one dominant vortex inside the cavity was detectable.

➤ **LDV studies**

Grace and Dewar (2004) conducted measurements using LDV and HW for a shallow rectangular cavity with W/D=4. The upstream boundary layer was set both laminar and turbulent and upstream velocity was changed for two levels (7.5 and 15 m/s). They found the cavity to be "open" in all the cases. Vortex inside the cavity was stronger for the case of laminar upstream boundary layer in comparison with turbulent case. Figure 2.6 shows the dimensionless plots of $u'v'$ in two vertical lines among the cavity's width. Shear stress is close to zero inside the cavity and there is a peak in shear stress at the mouth of the cavity (y/L = 0) for the turbulent incoming boundary layer. However, $\frac{u'v'}{U^2}$ value is negligible in comparison with $\frac{u'u'}{U^2}$. Figure 2.7 shows the dimensionless

11

plots of $u'u'$ in different vertical lines among the cavity's mouth. It can be seen that Reynolds shear stress is higher in the turbulent case.
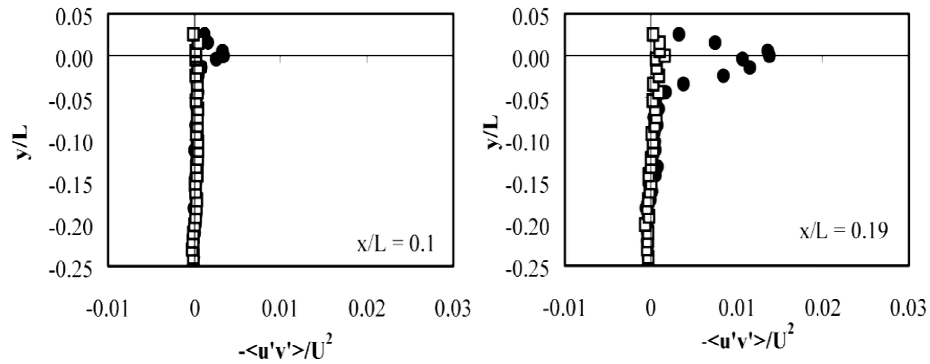
Fig. 2.6. Dimensionless shear stress in two vertical lines among the cavity for laminar (square) and turbulent (circle) upstream boundary layer (Grace and Dewar, 2004)
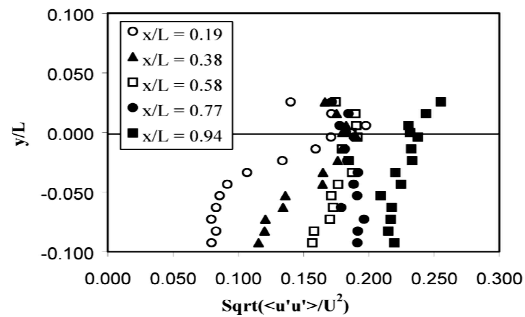
Fig. 2.7. Dimensionless shear stress in two vertical lines among the cavity for laminar (square) and turbulent (circle) upstream boundary layer (Grace and Dewar, 2004)

Esteve et al. (2000) did experiments on a shallow cavity with W/D of 10 using two components LDV. The incoming boundary layer was turbulent (Tu = 1%) and upstream velocities were 10 and 20 m/s. They found that the cavity is in transitional region. They found no reattachment of flow inside the cavity and a stagnation point has been detected inside the cavity.

Yang et al. (2002) conducted experiments and developed a CFD model to study a rectangular cavity. Experiments were done using LDV in a water tunnel and a FVM

(Finite Volume Method) (Patankar, 1980) code was used for the numerical model. The cavity was a shallow one with different aspect ratios (2, 4, 8 and 16) with upstream velocities (0.28, 0.53, 1.12 and 2.23 cm/s) with laminar boundary layer that for each aspect ratio resulting Re = 50, 100, 200 and 400. They found the critical Re of ≈ 295 and that for Re > Re$_{cr}$ flow becomes unstable. They also predicted the critical Re to be larger in the case of turbulent incoming boundary layer.

  ➢ **Hot-wire Studies**

Hardin and Block (1979) studied flow over rectangular cavities using hot wire anemometry. The main objective of their work was to conduct experimental data for their discrete vortex model. The discrete vortex model was presented in their previous work (Hardin and Block, 1977) to evaluate cavity noise production. The experiments were conducted in Re = $5{\times}10^{5}$, and the characteristic length was half of the cavity's length. W/D was also changed in three levels (0.78, 2.35 and 5.01). They found that the vortex model had a good performance in terms of predicting the mean velocity profiles. However, the model tended to overestimate the value of the turbulence intensity.

Triangular/Trapezoidal and Semi Circular Cavities

Of the very few papers on other geometries, Ozalp et al. (2010) studied triangular, rectangular and semi-circular cavities with W/D=2 using PIV. The experiments were conducted in three different upstream velocities resulting Re of 1230, 1470 and 1700. The effect of cavity's shape has been studied on the vortex structure inside the cavity. They found that cavity's shape was the most effective parameter influencing the vortex

shape inside the cavity. However, with varying Re slightly different vortex characteristics and turbulence intensities were observed.

2.5. Numerical Studies

<u>Rectangular Cavities</u>

Ritchie et al. (2010) presents results from a URANS CFD model validated by their PIV experiments on two shallow cavities (W/D of 5 and 14). They varied the upstream velocities to characterize open and close cavities in transonic speeds. Moreover, they used realizable kε turbulence modeling which has been known to give better results in high shear flows in comparison with standard kε (Launder and Spalding, 1972).

Larchevequ et al. (2003) used Large Eddy Simulation (LES) (Sagaut and Meneveaue 1998) in Re= 6×105 on a deep cavity with W/D=0.41. They found the shear layer to be highly dependent on the incoming flow turbulence.

Assimakopoulos et al. (2003) studied two rectangular cavities with W/D ratios of 0.5, 1, 2 and 3 with an environmental application. The cavities were representing street canyons. They used MIMO model (Kunz and Moussiopoulos, 1995) with k-ε as the turbulence modeling. They found the cavity to be "open" in all the cases and further discussion was made on pollutant dispersion inside the cavity. Figure 2.8 shows the streamlines around the cavity for one of the configurations studied. A dominant vortex inside the cavity is detectable and the cavity is "open".
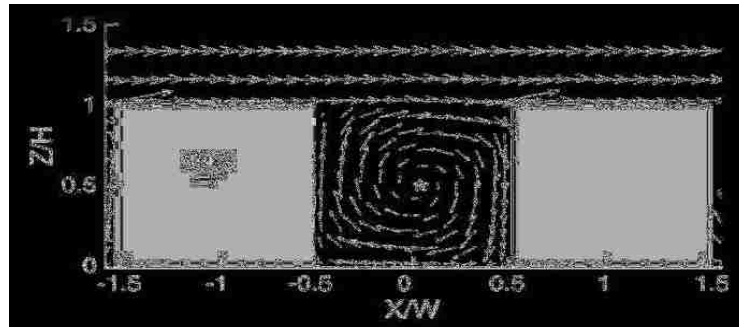
Fig. 2.8. Streamlines and vortex generated inside the cavity (Assimakopoulos et al , 2002)

<u>Triangular/Trapezoidal Cavities</u>

Gaskell et al. (1999) developed an FEM (Finite Element Method) (Patankar, 1980) code to solve Navier-Stokes equations for laminar condition. They studied Re in the range of $2\sqrt{3}$ to $1000\sqrt{3}$. They varied W/D ratio and β (the bottom angle of the triangle) and plotted streamlines. They found one up to four vortices formed inside the cavity. Four vortices were formed in the deepest cavity. They found the geometry to be an important factor on vortex characteristics in comparison with Re.

Although rectangular cavities have been deeply studied, there are not many papers on flow over trapezoidal cavities. William et al. (1992) developed a FDM code to study a simple geometry of a trapezoidal cavity with one moving wall. Moving wall is referring to the boundary condition of $U = U_{wall}$ in the mouth of the cavity. In other words a cavity with moving wall can be described as a closed system and flow movement inside the cavity is due to the movement of the mouth of the cavity. With their code, they could just validate their results for Re<500. They found the vortex inside the cavity become more circular with increasing Re.

15

Zhang et al. (2010) developed a numerical method for simple trapezoidal cavities with one moving wall for very low Re using Latice Boltzman (Chen and Doolen, 1998) for different Re, between 100 and 15000. They found the vortex dynamics to become more complex with increasing Re. The W/D was set 1.8 and β was 60. Figure 2.9 shows the streamlines inside the cavity for Re =1000. A dominant vortex with a small vortex in the downstream part of the cavity are detectable.
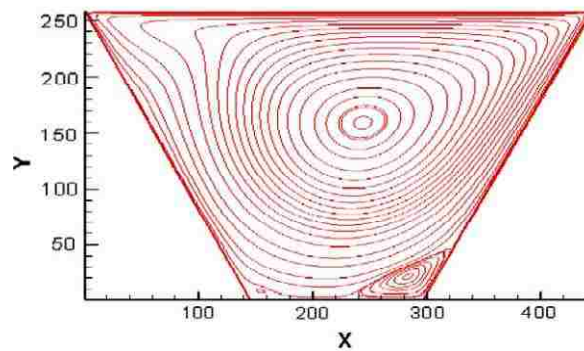
Fig. 2.9. Stream line function for Re = 1000 (Zhang et al., 2010)

2.6. Summary of literature review

In this chapter some theoretical background and summary of literature in the area of flow over cavities was reviewed. Different experimental and numerical methods have been used to investigate cavity flows. Rectangular cavity has been studied for a wide range of Re, turbulence intensities and W/D ratios. However, there are relatively less papers found on trapezoidal cavities and flow over trapezoidal cavities has not been yet well described.

16

CHAPTER III

METHODOLOGY

In this work, a combination of wind tunnel experiments and numerical simulation has been applied. A CFD model has been developed and validated using limited experimental data. Three factors have been selected for the study. Re (60000 [$U_{upstream}$= 5m/s], 123000 [$U_{upstream}$= 9.5 m/s] and 181000 [$U_{upstream}$= 15 m/s]), Tu (0.67%, 5% and 15%) and W/D (2, 4 and 6). The combination of factors and levels give 27 possible cases. The results from the CFD model and experiment are compared for one case (W/D=2, Re=123000 and Tu=0.67%) to check the performance of the model. After making sure that the results of the model are in agreement with the experimental results, the model was ran for 27cases and the results are analyzed.

The experimental setup and apparatus details and the CFD model developed as well as the design of the study will be presented in this chapter.

3.1. Wind tunnel experiments

3.1.1. Closed loop wind tunnel

The experiments were conducted in a closed loop wind tunnel located in B05 Essex Hall, University of Windsor, with a test section of 4.0 m as shown in Fig. 3.1. The cross section of the wind tunnel in the test section is 30 inches (762 mm) high and 30 inches (762 mm) wide. The maximum free stream velocity in the wind tunnel is 20 m/s when the test section is empty. In the presence of the perforated plates and/or setup, the maximum free-stream velocity is approximately 11 m/s.

17

The setup was placed close to the end of test section as shown in Figs. 3.2. and 3.3. The inlet flow in the empty wind tunnel is laminar and the velocity profile inside the wind tunnel is assumed to be uniform.

The upstream velocity in this work is defined as the velocity before the setup and Re was calculated based on this velocity, using the width of the cavity as the specific length. The free-stream velocity was measured with the pitot-static tube and a digital manometer. The Pitot - static tube was placed at the center of the wind tunnel before the test section. In order to reach to the steady state condition, a period of 15 minutes is required and experiments were done after 15 minutes of warm up. The turbulence intensity of the flow in the empty wind tunnel (without perforated plates) was measured as to be 0.67%.

Fig. 3.1. Overall view of the closed loop wind tunnel
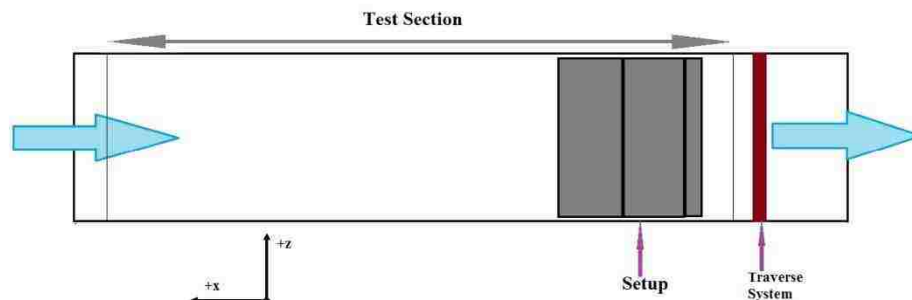
Fig. 3.2. Top view schematic of the closed wind tunnel

18

The setup was placed in the middle of the wind tunnel to avoid wind tunnel's boundary layer effect. Moreover, the model had to be suspended in wind tunnel; otherwise, the bottom of the wind tunnel had to be cut.

3.1.2. Traverse system

The probe was moved with a 2D traverse system with a resolution of 0.1 inches (2.54 mm). The traverse system was fixed with wood pieces to reduce the vibration induced by wind and was controlled with a computer program. Figure 3.3 shows the 2D traverse system installed in the wind tunnel.

Fig. 3.3. The 2D traverse system

3.1.3. Experimental model

The experimental setup was built out of wood. The schematic views of the designed model can be seen in Fig. 3.4. Solid wood was chosen to have a smooth surface with reasonable weight. The weight of the model was very important because the cavity had to be suspended in the wind tunnel.
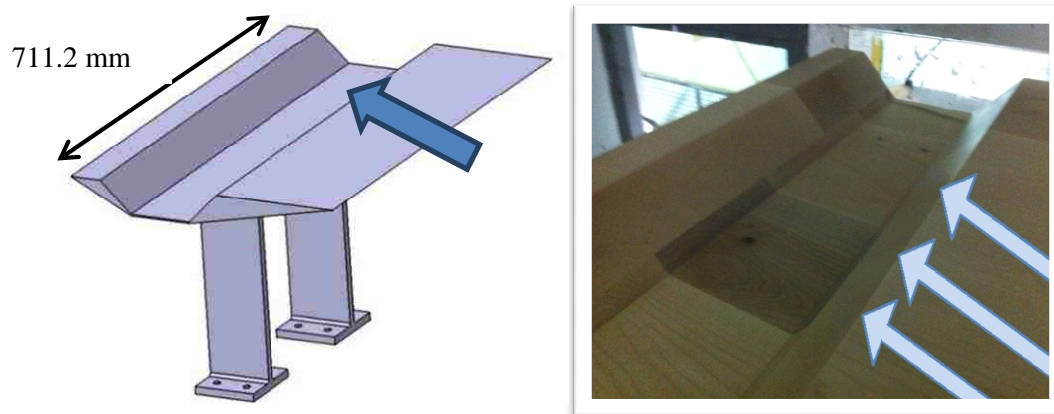
Fig. 3.4. Schematic view of the model and the model in the wind tunnel

The dimensions of the trapezoidal cavity are shown in Fig. 3.5. The blockage factor for this work is 7% which is acceptable (Barlow, 1999). The blockage factor is defined as the ratio of the setup's depth to the wind tunnel's height.
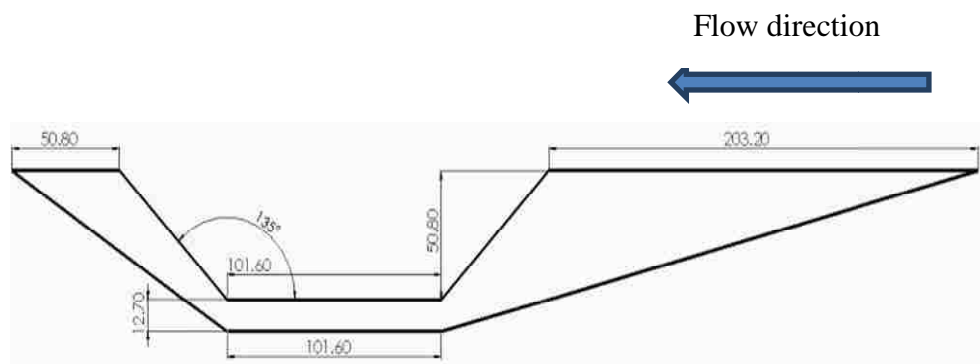
Fig. 3.5. Dimensions of the trapezoidal cavity in (mm) (cross section)

The columns of the setup keep the cavity 355.6 mm from the wind tunnel's floor (see Fig. 3.4.). The flow separates at the beginning of the leading edge (sharp edge). The

length of the leading edge of the cavity which is 203.2 mm (8 in) is to give space to flow to reattach and form the boundary layer on it.

The length of the cavity (Γ) is 711.2 mm (28 in). This length was chosen to be large enough to have a 2D cavity. In a 2D cavity the flow characteristics can be presented in two dimensions (x and z in this case). In the case of this study as Γ/D is 14 flow characteristics can be considered 2D according to Faure et al., (2007). Furthermore, the length of the cavity should be less than the wind tunnel width for installing and removing of the setup. As the width of the wind tunnel is 762 mm (30 in), there is a 25.4 mm (1 in) gap on each side.

3.1.4. Hot-wire anemometer

Velocity measurements are conducted using a 1D boundary layer hot-wire probe type 55P15 which is installed on a Dantec streamline 55C90 constant-temperature anemometer (CTA). The original data from hot-wire anemometer is in terms of voltages and further is converted into velocity using a MATLAB code. The experiments were conducted at a sampling frequency of 80 kHz. In the present work, the analog signal from the hotwire was low pass filtered at 30 kHz. The sampling frequency of 80 kHz is chosen to be more than twice the Nyquist frequency to avoid aliasing problems (Proakis and Manolakis, 1992).Furthermore, at each point, a sample of 2×10^6 is taken (see Appendix A.2.).

The streamline probe calibration system is used to find the relation between the voltage reads and the velocity. The calibration unit (Dantec 90H10) consists of a calibration module, and a nozzle for the flow. To calibrate the probe, the probe's wire

should be mounted at the opening of the nozzle and at the center of it. There are some

preset values for velocities and the device calibrates the velocity with those values within

some iterations. After the iterations, the system gives five coefficients, C_0, C_1, C_2, C_3, and

C_4 to relate voltages to velocity values.

$$U= C_0 + C_1E^1 + C_2E^2 + C_3E^3 + C_4E^4 \tag{3.1}$$

Fig. 3.6. The calibration box

3.2. CFD model simulation

A CFD model has been developed to study the flow over and inside a trapezoidal

cavity. As the experimental data collected from wind tunnel was used for the validation

of the CFD model, the dimensions of the CFD model are set the same as the experimental

setup.

ANSYS FLUENT 14 has been used for this research which works based on Finite

Volume Difference (FVM method). ANSYS FLUENT has been known to give accurate

results for different fluid engineering applications. The grid was generated with GAMBIT software. After building up the mesh, it was imported into the FLUENT software. The next step was to set the software's options appropriately. These options identify the solver, boundary conditions, equations to be solved and time step for the simulation (ANSYS FLEUENT manual).

3.2.1. Grid Generation

A 2D fully structured multi block quad mesh with 732700 elements has been generated using GAMBIT software. As the length to depth ratio of the cavity is very high (14), the nature of flow inside the cavity has been assumed as to be 2D. The hypothesis of 2D flow in this case is reasonable. In some references it has been stated that for the cases with Γ /D ratio greater than 7 the 2D flow scenario is realistic (Faure et al., 2007).

In mesh generation, there has been an effort to have finer elements in the areas expecting sharp gradients in flow properties. In the grid domain, if the length of the setup is M, a distance of 6M has been left from the inlet to the cavity. This distance has been chosen to let the flow coming from the inlet to become fully developed. The 16.8M distance behind the cavity has been left to completely capture the interaction between the flow going above and underneath of the cavity (See Fig. 3.7. a). The flow going underneath of the cavity will affect the flow above the cavity.

23

.a.)The schematic of the simulation domain
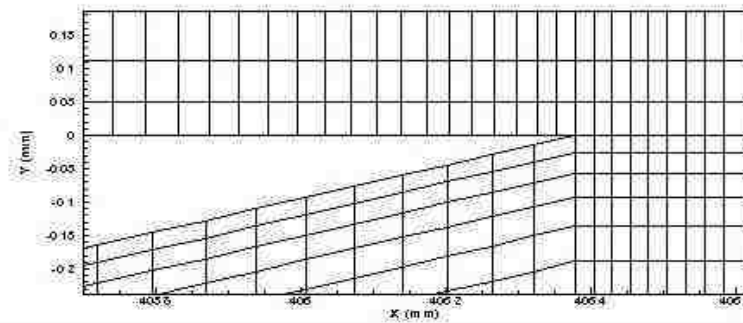
.b) The boundary layer mesh on the edge of cavity

Fig.3.7. Simulation domain and boundary layer mesh

Figure 3.7.b shows the boundary layer mesh on the edges of the cavity. The boundary layer mesh on the edges gives more control on the value of y^+ on the edges. The value of y^+ can be checked in FLUENT and it was less than one on the edges of the cavity as part of requirements of the turbulence modeling approach used in this work. According to y^+ definition, to have lower value of y^+ (as the value of y^+ is calculated by the first row's element size.), finer mesh is required on the edges and hence, more number of elements in the domain.

A zoomed in view of the mesh generated close to the cavity can be found in Fig. 3.8. It can be seen that there has been an effort to have finer mesh at the corners and edges.
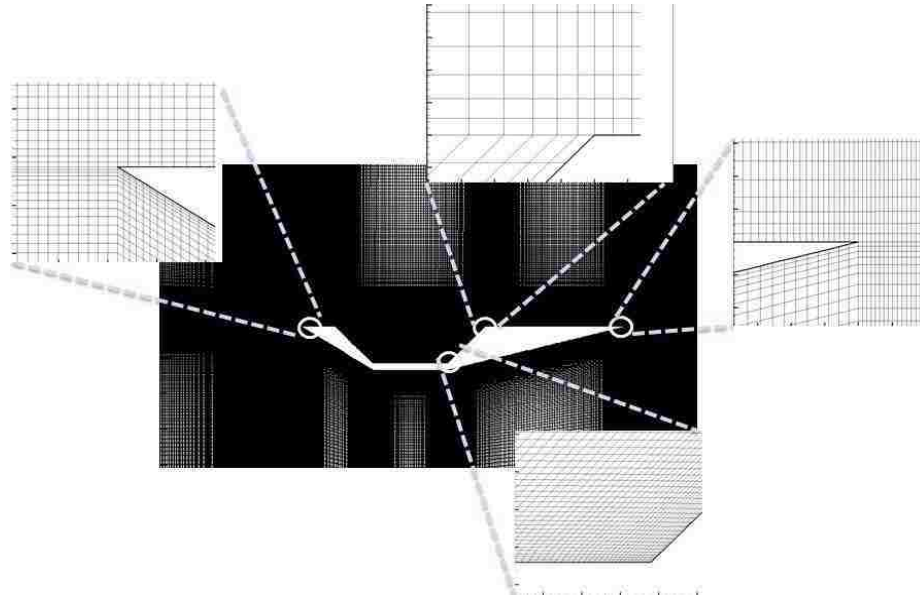
Fig. 3.8. Overall view of the mesh around the cavity

3.2.2. Boundary Conditions

The boundary conditions chosen for this simulation were velocity inlet in the inlet, outflow in the outlet and wall on the cavity surfaces and wind tunnel walls. Two parameters should be set to describe the turbulence characteristics of the flow in the inlet. These two parameters are turbulent intensity and turbulent length scale. For example, in the specific case that has been used for model validation, the turbulent intensity is 0.67% which is the level of turbulence measured in the empty wind tunnel and the depth of the cavity has been chosen as the length scale for the turbulent flow.

No slip stationary wall is the boundary condition set for all the edges. The roughness height of the experimental model has been measured and imported into the CFD model to make the conditions of the CFD model as close as possible to the experimental setup (see Appendix A.3).

3.2.3. Governing equations

Continuity equation coupled with momentum equations are solved simultaneously in the domain. For the turbulence modeling different turbulence modeling methods have been tested. Standard k-ε (Launder and Sharma, 1974), k-ω standard (Wilcox, 1998), k-ω SST (Menter et al., 2003), k-kl-ω (Walters and Cokljat, 2008) and Reynolds Shear Method (RSM) (Sarkar and Balakrishnan, 1990) were tested. In all the turbulence modeling approaches enhanced wall treatment was applied.

Instead of wall treatments, wall functions can be applied which are empirical functions for the velocity boundary layer in the area close to the wall. They are less precise in comparison with wall treatment. It does not require very fine mesh on the walls which reduces the computational cost. Using wall function is useful in industrial applications which do not require too much precision (Help FLUENT).

Turbulence modeling approaches add some additional equations to continuity and momentum equations. Modeling approaches of k-ε and two k-ω add two equations. The k-kl-ω modeling approach adds three equations and Reynolds Shear Stress (RSM) adds five. The k-kl-ω model can be used effectively where there is transition between laminar and turbulent regime. In addition, k-ε does not give accurate results in the presence of adverse pressure gradient (Help FLUENT). In this work k-kl-ω has been chosen. The governing equations and turbulence modeling formulation are brought in (Appendix A.4) in more detail.

3.2.4. Solver

A 2D transient pressure-based solver with time step of 0.05 sec was used. The general options for the solver can be found Fig. 3.9. The figure shows the solution methods and the special discretization method used for each differential governing equation. The transient simulation gives the same results with the steady state simulation case.

As it can be seen, the Semi-Implicit Method for Pressure-Linked Equations (SIMPLE) (S.V. Patankar and Spalding, 1972) scheme has been used for this work.
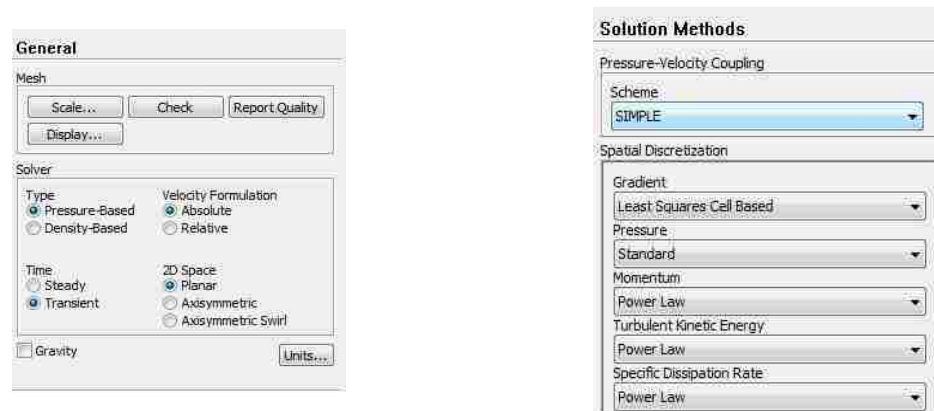
Fig. 3.9. General setup and Solution methods and discretization

3.3. Study design

A CFD model has been built up for this study as explained. A set of wind tunnel experiments have been used to validate the model. The results from experiments and the CFD model have been compared for the case with the upstream velocity of 9.5m/s, turbulence intensity of 0.67% and for the cavity with aspect ratio of 2. The turbulence intensity of 0.67% is the value of turbulence intensity measured in the empty wind tunnel at 9.5 m/s. Moreover, the dimensions of the experimental setup and CFD model are the

same. In addition, the roughness of the experimental setup has been imported into the model.

In this study, upstream velocity ($U_{upstream}$) and turbulence intensity (Tu) of the upstream flow are referring to the velocity and Tu of the flow at inlet. The velocity right before the cavity is the same as the velocity in the inlet as the wind tunnel's cross section is constant. However, the Tu of the flow when reaches the cavity is lower in comparison to the Tu of the flow in inlet as the turbulence of the flow is damped. For the case with Tu of 0.67% the difference between the turbulence level in the inlet and before the cavity is negligible. Hence, the case with Tu of 0.67% has been chosen for validation purpose (Details can be found in Appendix A.7). For the case with 5% of turbulence, around 1.4% reaches to the cavity and for the case with 15%, the level of turbulence of the flow is only around 4.5% when flow reaches to the cavity.

The effect of Re ($U_{upstream}$) and Tu of the flow on vortex characteristics, shear layer growth of the cavity and flow field inside the cavity and the air exchange volumetric flow rate from the cavity have been investigated.

To understand the effect of W/D, the CFD model has been modified to have cavities of aspect ratio of 4 and 6 as well. It should be mentioned that, the grid generation for all the models have follow certain instruction, i.e. element sizes, stretch factors, etc. are the same for all three cases. As the width of the cavity remains constant for all the cases (see Fig. 3.10), in this work Re is calculated based on cavity's width to have the same Re for all aspect ratios at each upstream velocity. Re based on cavity width is calculated as to be

$\approx$ 60000 for $U_{upstream}$ = 5 m/s, 123000 for $U_{upstream}$ = 9.5 m/s and 181000 for $U_{upstream}$ = 15 m/s. Table- 3.1 shows a summary of effective parameters and their levels:

Table- 3.1- Summary of the parametric study

Factor / Level	W/D	$U_{upstream}$ (m/s)	Tu (%)
1	2	5	0.67
2	4	9.5	5
3	6	15	15
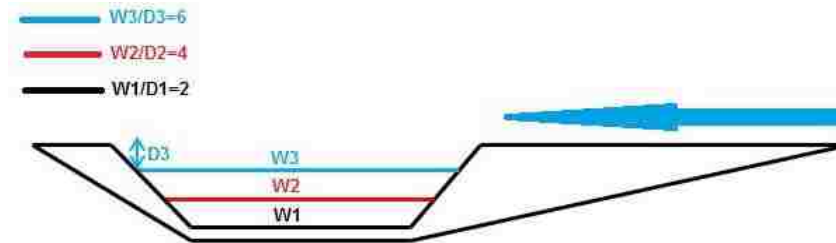
Fig. 3.10. Different aspect ratios of the cavity

As there are three factors for this study (W/D, $U_{upstream}$ and Tu) and each factor has three levels, there are possible 27 cases in hand (3×3 = 27). The model has been run for all the 27 cases. The effect of W/D, $U_{upstream}$ (Re) and Tu has been studied statistically using Minitab software. The effect of these parameters is studied on the normalized air exchange volumetric flow rate from the cavity ($Q_{normalized}$), the normalized horizontal position of the center of vortex (x/L), the normalized vertical position of the center of vortex (y/D), the cavity type ("open" or "closed and transitional") and number of vortices inside the cavity.

The center of vortex is identified by zooming in into the streamlines inside the cavity. The air exchange volumetric flow rate is calculated by integration on the vertical velocity profile at the mouth of the cavity. The cavity type is identified based on the definition of "open" and "closed and transitional" cavities (see page 4).

The air exchange volumetric flow rate from the cavity is normalized by the volume of the cavity. The horizontal position of the center of the vortex is normalized by the length of the mouth of the cavity. The vertical position of the center of the vortex is normalized by the depth of the cavity.

The effect of W/D, $U_{upstream}$ and Tu on vortex characteristic and shear layer growth above the cavity and vorticity inside the cavity has been studied in more detail as well. Results from the few cases of the CFD runs are presented and discussed in more details. More results are presented in Appendix. A.8.

3.4. Experiment details

Six velocity profiles are measured above and behind the cavity. The lines of velocity measurements and their positions are shown in Fig. 3.11.

Lines 1, 2 and 3 : 3 inches = 76.2 mm
Lines 4, 5 and 6 : 6 inches = 152.4 mm
Distance between lines lines behind the cavity : 5 inches = 127 mm
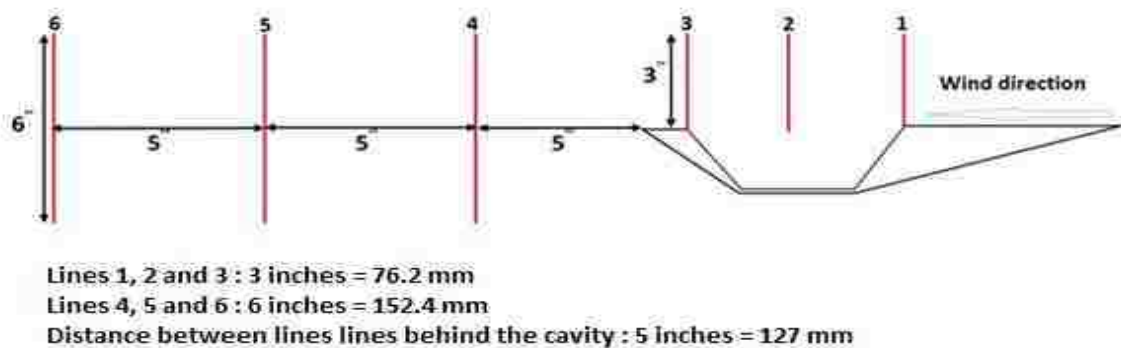
Fig. 3.11. Position of lines of velocity measurements

Velocity profile on Line 1 is the profile of the flow that enters the cavity and Line 2 is right in the middle of cavity's width and Line 3 is the velocity profile of the flow leaving the cavity. Hence, a distance of 4 inches (101.6 mm) is in between each two of the lines. Moreover, velocity profiles on three vertical lines behind the cavity have been measured to check the performance of the model to predict the wake behind the cavity. Line 4 is 5 inches (76.2 mm) behind the cavity to check the wake behind the cavity from CFD and experiment. Lines 5 and 6 are at the distance of 5 inches (76.2 mm) farther downstream.

All the experimental results are conducted with an inlet velocity of 9.5 m/s and Tu of 0.67%. In addition, the setup was fixed close to the end of the test section of the wind tunnel and the distance of the leading edge of the cavity from the beginning of the test section was 3.5 m.

For velocity measurements on Lines 1 and 3, the probe was placed at 0.1 inches (2.54 mm) above the cavity's mouth level. The probe was moved up 2.9 inches (73.66 mm) 0.1 inches at each step by traverse system. Therefore, after 30 points of measurement the probe was placed 3 inches (76.2 mm) above the cavity.

Five replications have been done to measure the velocity profiles above the cavity. The reason of these replications was to reduce the effect of human error and check the experiment's repeatability. For each replication the setup was installed inside the wind tunnel and the position of the setup was marked in the wind tunnel and the velocity was set to be 9.5 m/s with pitot-static tube. Re is calculated based on the cavity's mouth

length for the upstream velocity of 9.5 m/s. The uncertainty analysis for Re have been

calculated in (Appendix A.5).

$$Re = \frac{UL}{\vartheta} = (9.5 \times 0.2033)/(15.68 \times 10^{-6})) = 123112 \pm 471 \qquad (3.2)$$

Cavities with aspect ratio of 2 and 4 have been studied for rectangular cavities (Grace

and Dewar; Lin and Rockwell, 2001). The aspect ratio of 2 can be representing a

roadway with two lanes with a trapezoidal section. The aspect ratio of 4 can be

representing a wider road and the aspect ratio of 6 can be assumed as a highway.

Although the results of this work cannot be interpreted into the real case geometry

without scaling study, it is better to study the geometries that can have applications in the

real world. Moreover, the upstream velocities of this work have been studied for

rectangular cavities previously (Grace and Dewar, 2004). Tu in the study is referring to

the Tu of the flow in inlet. The Tu = 0.67 is the level of turbulence measured in the empty

wind tunnel representing the laminar flow that approaches the setup. The other two levels

of turbulence intensity are to see how increasing the turbulence intensity will affect flow

characteristics above and inside the cavity as usually in engineering applications the

working flow is turbulent. It should be mentioned that as the cavity has been placed

suspended inside the wind tunnel, the boundary layer on the leading edge of cavity is

turbulent due to the presence of cavity and the turbulence generated by the setup.

In this chapter, the experimental apparatus, the CFD model options, and details for

the experiments were presented. Furthermore, the design of the study, the effective

parameters and their levels were presented. In the next chapter, the experimental result

and CFD results will be presented and discussed.

CHAPTER IV

RESULTS AND DISCUSSION

4.1. Experimental results

Figure 4.1.shows the velocity profiles for Lines 1 to 3. In the plots the velocity at each point has been non-dimensionalized with the upstream velocity and the probe position has been non–dimensionalized with the cavity's depth which is 2 inches (50.8 mm).

Five replications are in hand for these lines. Experiments A, B, C, D and E were done at the same W/D (W/D = 2) and velocity in the inlet ($U_{upstream}$= 9.5 m/s) and Tu= 0.67%. The relative bias uncertainty in the value of $\overline{U}$ has been found to be ≈ 3% at this Re. However, taking the replications into account, for a point on Line 3 that has the closest distance to the cavity's edge, the total uncertainty has been found ≈ 14%. As hotwire has been known to have better results far away from the walls, total uncertainty has been calculated on a point very close to the cavity's edge as an example. Calculations for the uncertainty analysis of hot-wire measurement can be found in Appendix A.6.
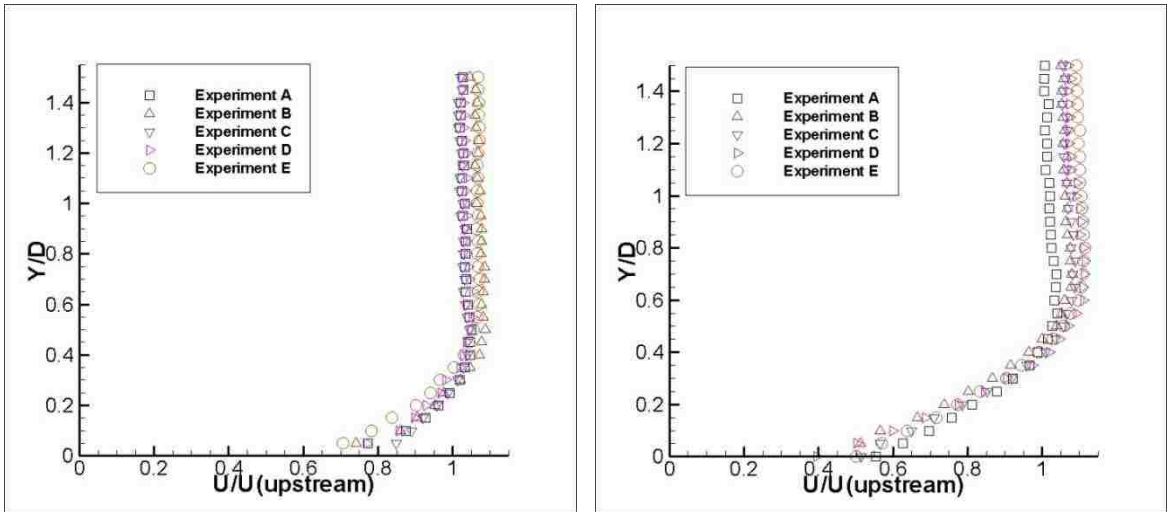
a) Velocity Profiles on Line. 1

b) Velocity Profiles on Line. 2
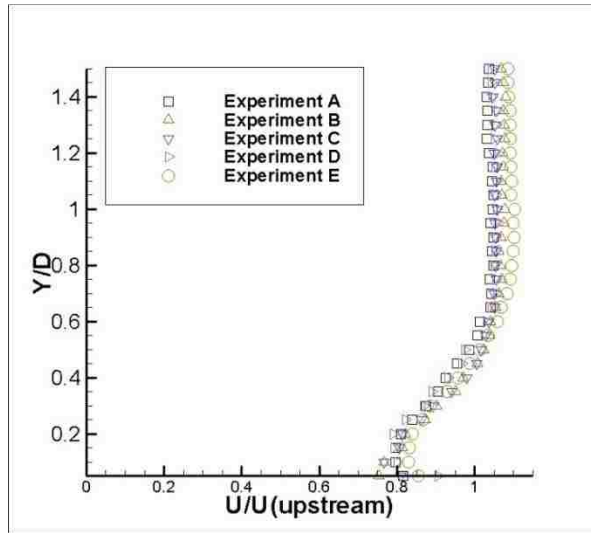
c) Velocity Profiles on Line. 3

Fig. 4.1. Velocity Profiles above the cavity

Figure 4.2 shows the velocity profiles behind the cavity for Lines 4, 5 and 6 respectively. It can be seen that Line 4 has the most drastic velocity drop because it is the closest one to the cavity. Hence, this area is in the strong wake area behind the cavity.

Moving farther downstream, it is visible that the velocity drop has been reduced and the velocity profile is closer to a uniform profile.
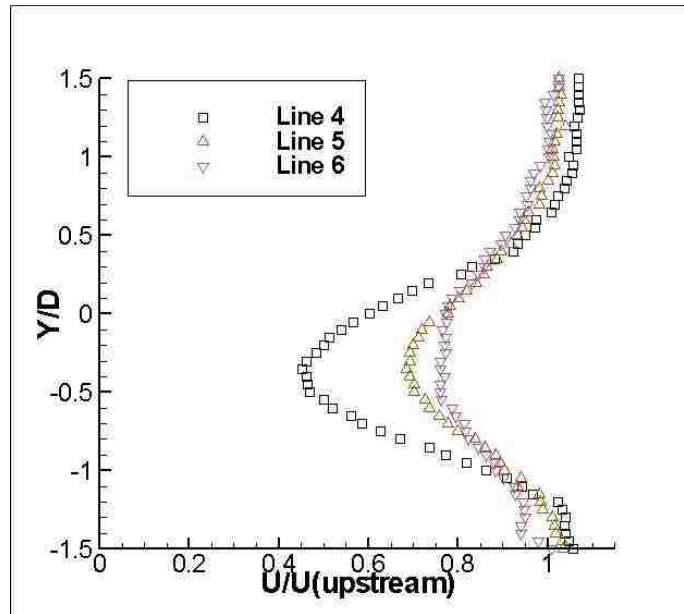
Fig. 4.2. Velocity profiles for Lines 4, 5 and 6

4.2. CFD model validation

To check the validation of the model, first it is required to check that the results of the model are not dependant on the grid generated. The effect of number of elements in the grid on velocity pofile on Line.2 has been checked for an example that the the results of the CFD simulation are grid indipendent, i.e. the grid is fine enough.

Figure 4.3 shows the non–dimensionalized velocity profiles on Line 2 for different grids. The 89000 element grid is the coarsest grid and the 879000 element grid was the finest grid checked. It can be seen that the profile does not change significantly when the number of elements increase from 590000 elements on. The grid with 732700 elements was chosen to keep the y^+ below 1 as part of the requirements for the turbulence

35

modeling which is chosen for the CFD model. The velocity profile obtained from the chosen grid is not different with the ones from 590000 and 879000 element grids. Hence, the results from the CFD model are grid indipendent.
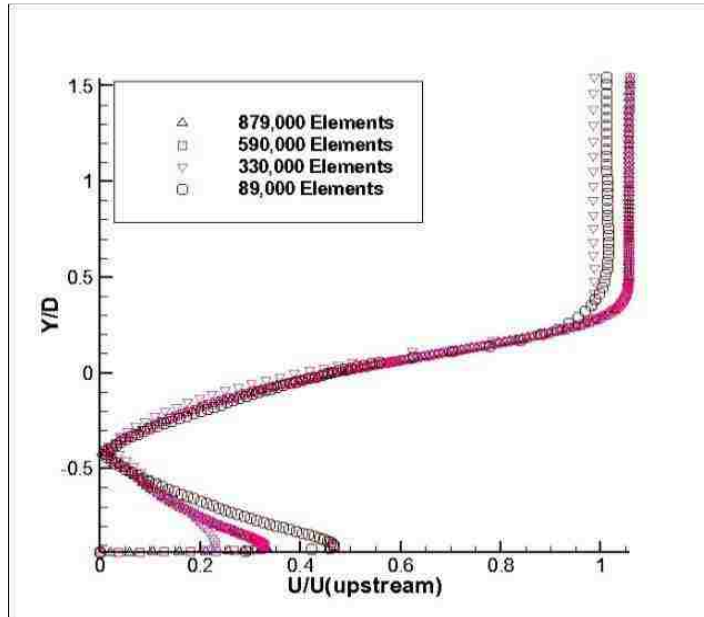
Fig. 4.3. Velocity profile on line 2 (Different grids with different number of elements)

After checking the grid independency of the model the results of the model are compared with experimental results obtained from conducted wind tunnel experiments. Velocity profiles on 3 vertical lines above the cavity and 3 vertical lines behind the cavity from the CFD model are compared with the experimental results to see the performance of the model. The velocity in inlet was set as to be 9.5 m/s and the Tu was set 0.67% to duplicate the conditions of the experimental results. The model was run with different turbulence modeling approaches to see which turbulence model gives better results.

Figures 4.4 and 4.5 show the velocity profiles on the lines 1 to 6. For Lines 1 to 3 five replications were in hand and the average value of the measurements at each point was taken.
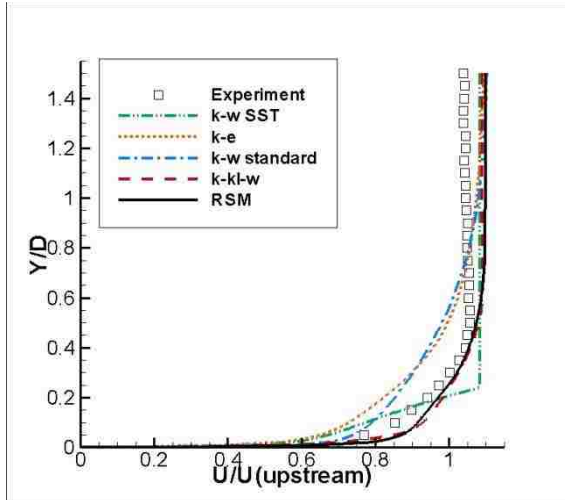
36

a) Velocity profiles on Line. 1
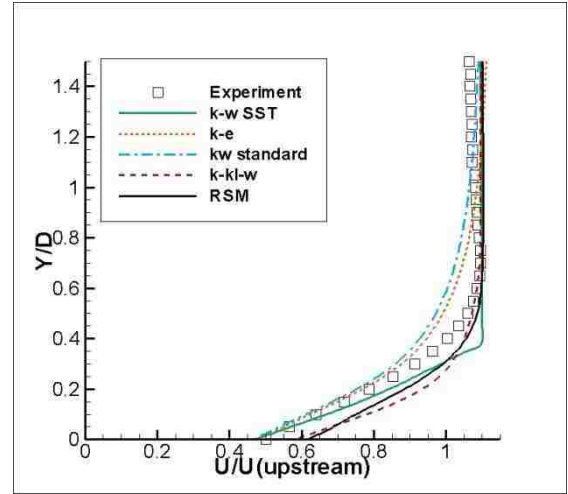
b) Velocity profiles on Line. 2
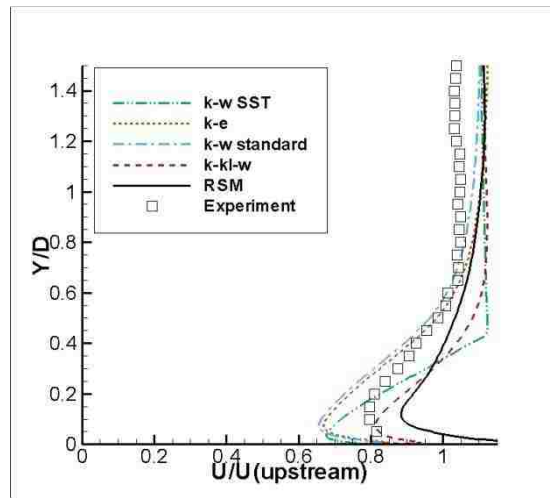
c) Velocity profiles on Line. 3

Fig. 4.4. Velocity profiles on lines 1, 2 and 3 (Comparison between results from experiment and the CFD model with different turbulence modeling)
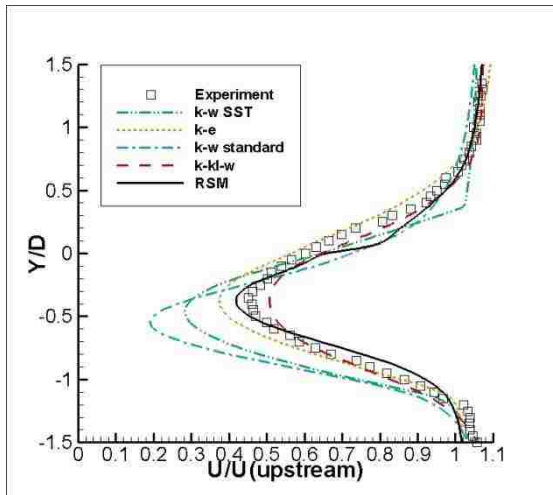
a) Velocity profiles on line. 4   b) Velocity profiles on line. 5
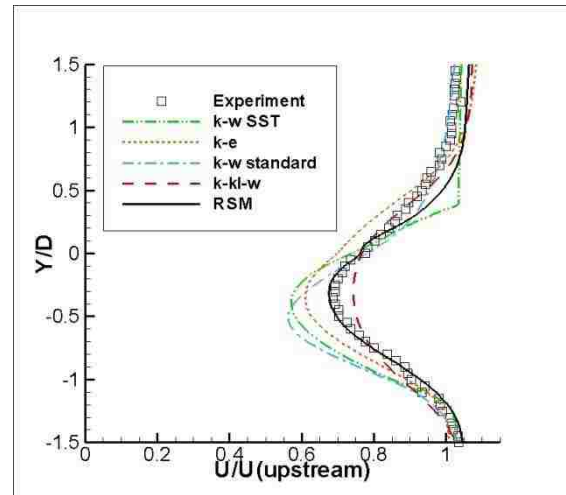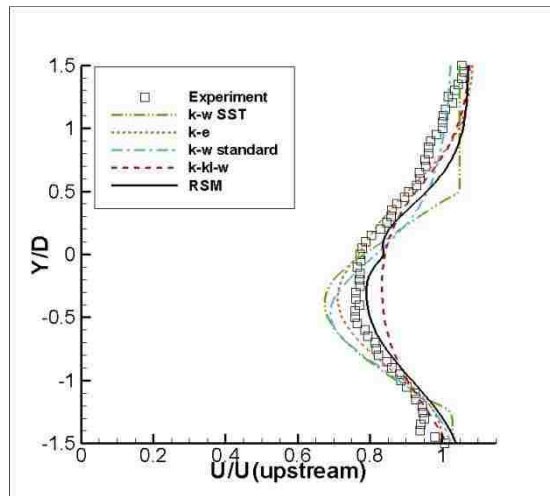
Velocity profiles on line. 6

Fig. 4.5. Velocity profiles on lines 4, 5 and 6 (Comparison between results from experiment and the CFD model with different turbulence modeling)

It can be seen from the figures that k-kl-ω and RSM are giving closest results to the experimental data. K-ω-SST predicts a sharp gradient in the boundary layer above the cavity which is unrealistic. The biggest difference between the experimental and numerical results happens on Line.3 and close to the wall. The difference is because of the separation of the flow at the trailing edge of the cavity. It is worth noting that this

38

profile can only be seen right on the trailing edge of the cavity according to the CFD model. It has been seen that this unique profile is not detectable if the location of the line is moved 0.1 inches (2.54 mm) either upstream or downstream. Therefore, experimental results on this line are very sensitive to the probe positioning. However, there is a reasonable agreement between the experimental and numerical results.

To check the performance of the model quantitatively, the local difference between the results from experiment and CFD has been calculated. The local difference (Δ) is presented as:

$$\Delta= |\frac{(U_i(exp) - U_i(num))}{\frac{(U_i(exp) + U_i(num))}{2}}| \times 100 \qquad (4.2)$$

Figure 4.6 shows the local difference versus vertical position for lines 1 and 3. The local difference has been calculated for k-kl-ω and RSM. It can be seen that the maximum difference occurs close to the wall for both lines and the two models show quit the same performance in terms of predicting the velocity profiles on these lines. One explanation on the big local difference close to the wall is that velocity is lower close to the wall and $(U_i(exp) - U_i(num))$ is divided to a smaller value. Hence, the local difference increases significantly getting close to the wall.

Therefore, the CFD model with k-kl-ω and RSM turbulence modeling methods is valid to an acceptable level. From Fig. 4.6. , it can be observed that k-kl-ω is having lower value of local difference in some regions. RSM found to have convergence issues and required very small time steps in the simulation, i.e. the time step for k-kl-ω was set 0.1 seconds whereas for RSM a minimum time step of 10^{-5} was required for the

39

simulation. It is worth mentioning that as RSM adds 5 equations to the model and due to the very small time step required, hence, the computational cost drastically. Hence, k-kl-ω model was chosen for this study.
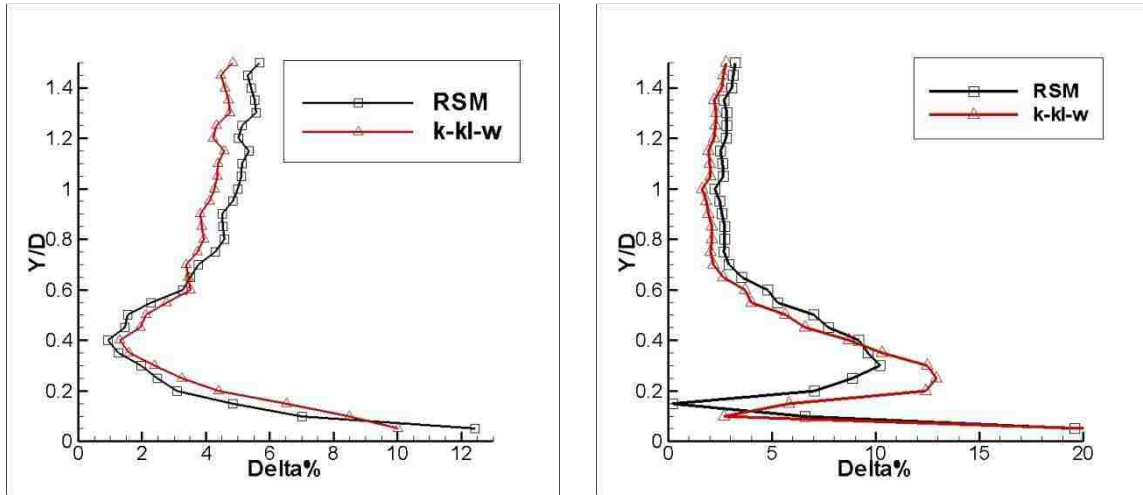
a) Local difference vs. vertical
position on Line.1

b) Local difference vs. vertical
position on Line 3

Fig. 4.6. The local difference vs. non-dimensional vertical position (Lines 1 and 3)

After checking the performance of the model with experimental results the CFD results for the tested model can be discussed. Flow characteristics, i.e. streamlines, pressure domain, Vorticity magnitude contour inside the cavity and velocity contour around the cavity are discussed for the case that has been compared with experimental data.

Figure 4.7 shows the position of the coordinate system that the CFD results have been presented with respect to, as well as the position of three lines (b1, b2 and b3). These lines will be used to plot some properties on them. These lines start from the bottom of the cavity and end 3 inches (76.2 mm) above the cavity.
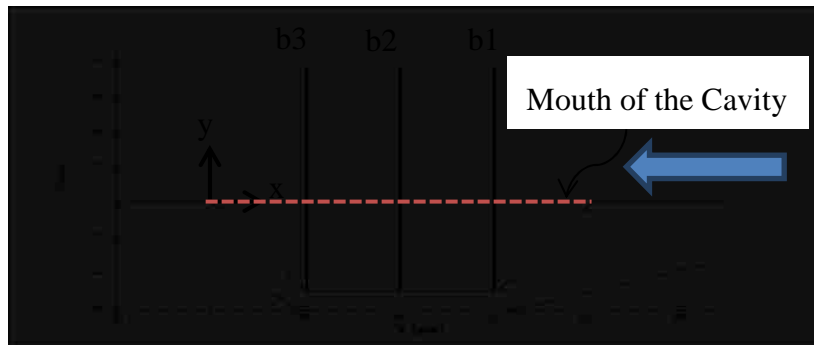
Fig. 4.7. The coordinate system set for the CFD results

Figure 4.8 shows the flow streamlines around the cavity. It can be seen that the flow separates when hitting the leading edge of the setup and reattaches the surface. The vortex size on the separation point is around 25 mm along the leading edge of the cavity which is fairly small in comparison with the length of the leading edge which is 203.2 mm.

Moreover, one dominant vortex can be seen inside the cavity which rotates counterclockwise and a very small vortex is detectable in the leading corner which is rotating clockwise. Hence, the cavity is open. In addition, two vortexes are illustrated in the wake region behind the cavity.
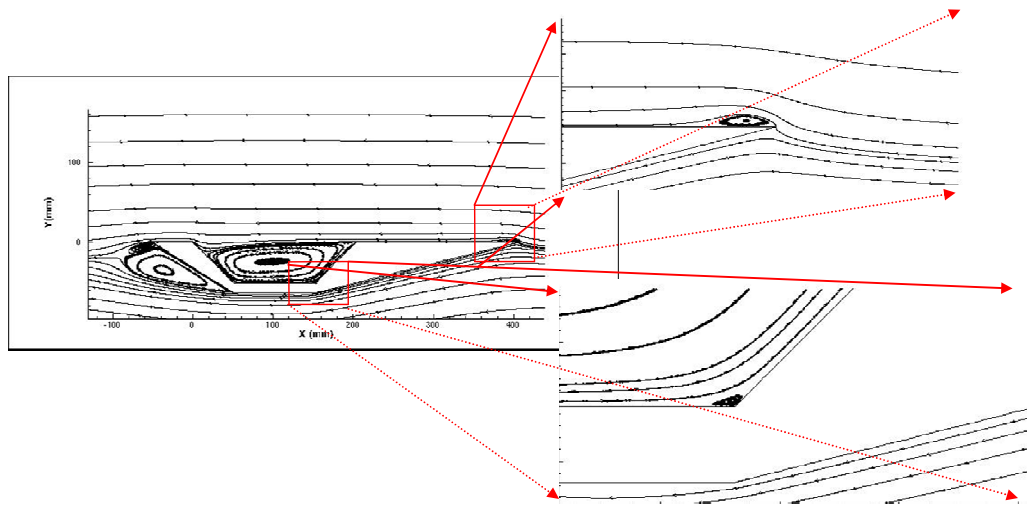
Fig. 4.8. Flow streamlines in the baseline simulation

The static pressure contour around the cavity has been illustrated in Fig. 4.9. A closer view of the beginning of the leading edge has been shown with streamlines on it to better see the vortex due to the flow separation. It can be seen that the static pressure remains constant on the leading edge and an area of high static pressure can be seen underneath of the cavity and gradients in static pressure are detectable.
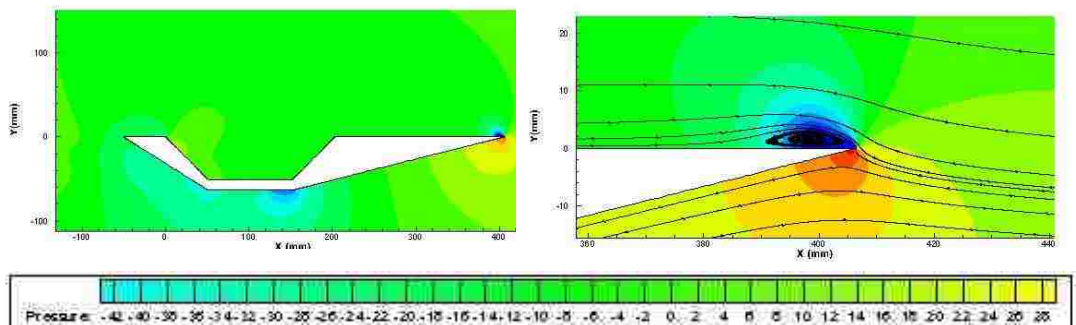
Fig. 4.9. Static pressure contour around the cavity (Pa)

The contours of velocity and Z-vorticity magnitude can be seen in Figs. 4.10. and 4.11. It is obvious that the Z-vorticity in this case is in + direction according to the velocity direction and the coordinate system chosen as the vortex inside the cavity is counterclockwise.
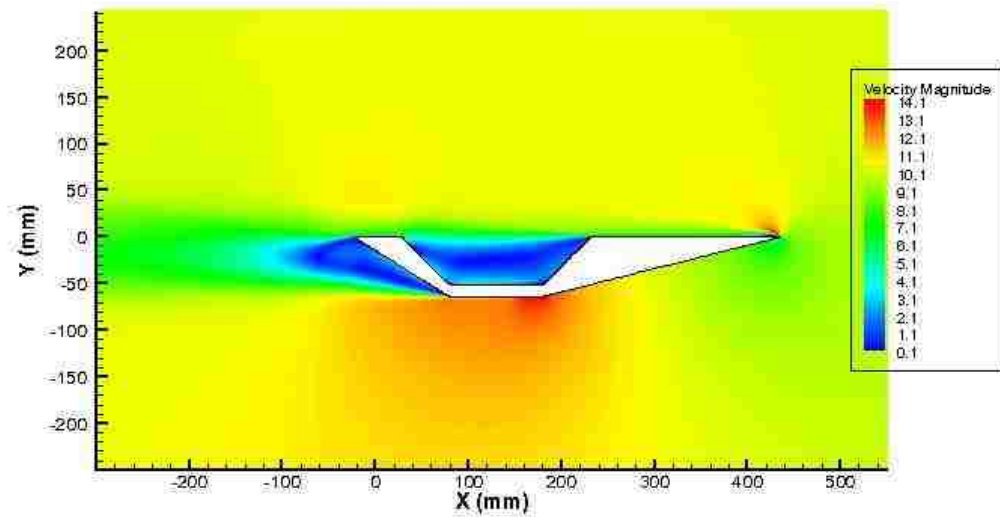
Fig. 4.10. Velocity contour around the cavity
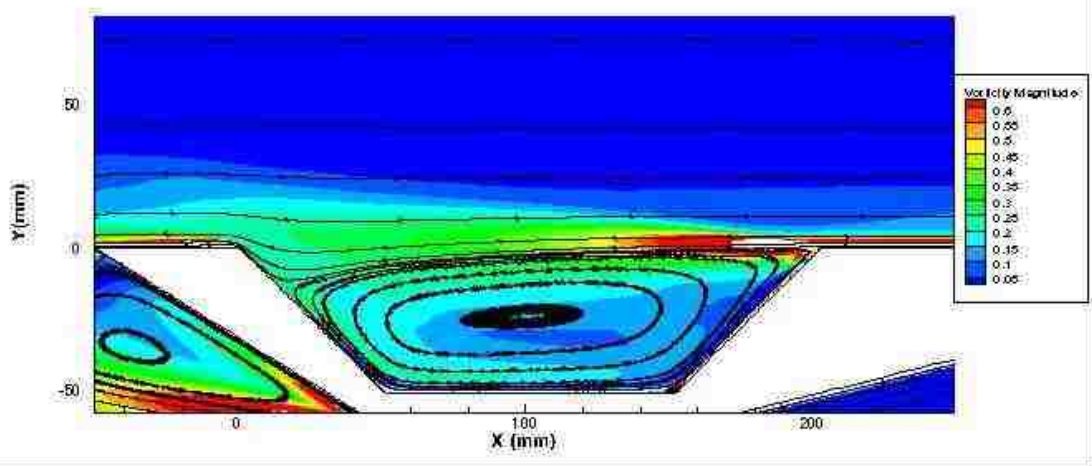
Fig. 4.11.Vorticity contour inside the cavity

A very high vorticity area is visible at the very opening of the cavity because of the sudden expansion of flow. At this area an intense thin shear layer starts to form and that created this very high vorticity area there. This area has been omitted from the contour to see the vorticity gradient inside the cavity better. It can be seen that vorticity magnitude is higher at the trailing edge as expected as the flow rotates close to the trailing edge. However, due to the diffusive nature of turbulence, the vorticity has been diffused toward the leading edge (Grace and Dewar, 2004). In addition, it can be seen that vorticity magnitude in the mouth of the cavity is of a higher order in comparison with the vorticity magnitude inside the vortex.

Moreover, as explained before, the cavity is placed suspended inside the wind tunnel. A comparison between the case that cavity is installed at the bottom of cavity and this study has been done numerically. A CFD model was developed to simulate the cavity placed at the bottom of the wind tunnel. There has been an effort to use the same meshing scheme and boundary conditions for both cases. Figure 4.12 shows flow streamlines for two cases and Fig.4.13. shows the static pressure contour for both scenarios.
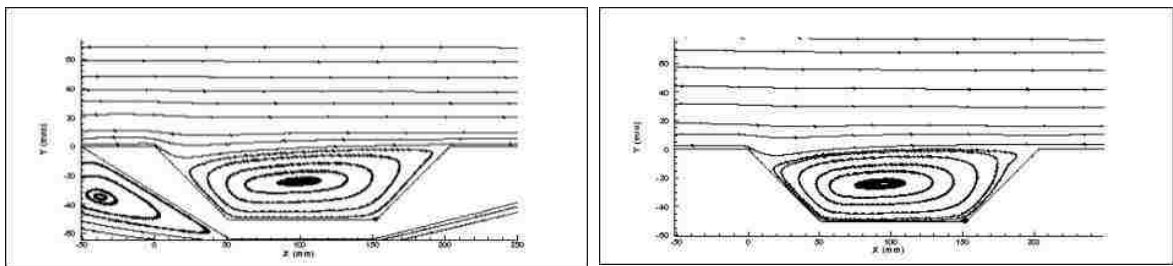
Fig. 4.12. Flow streamlines (Left side: suspended cavity, right: cavity at the bottom)

44
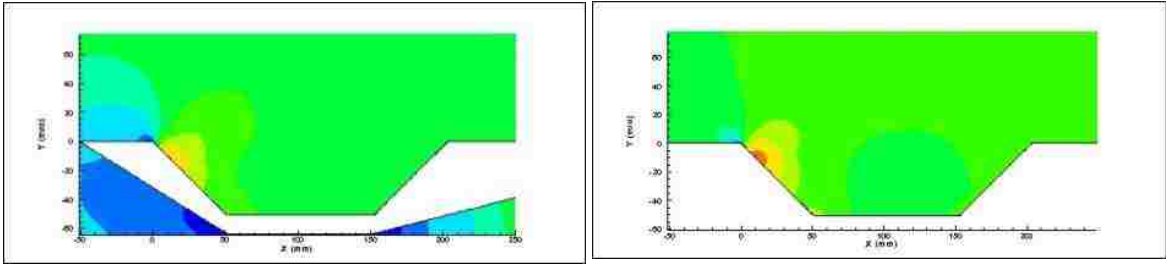
Fig. 4.13. Static pressure contour inside the cavity (Left side: suspended cavity, right: cavity at the bottom)

In both cases the cavity is found to be open and a single dominant vortex is detectable inside the cavity and static pressure contours show that both cases are quite similar. However, vortex shapes are a little bit different and center of vortex is 4 mm closer to the trailing edge for the case that cavity placed in the bottom of wind tunnel.

Figure 4.14 shows the shear layer growth above the cavity on contour of X-velocity. Shear layer above cavities in this work is defined from the zero X-velocity line inside the cavity to the free stream velocity. As the vortex is rotating, on a vertical line normal to the direction of the flow, at one point the x component of the velocity goes to zero and the flow changes the direction. The line with zero X-velocity has shown in the figure as well.

It can be seen that at the boundary of flow approaching the cavity starts from the leading edge and is around 20 mm as it can be illustrated in the figure. The shear layer becomes thicker farther downstream. The maximum shear layer thickness occurs on x ≈ 50 mm and the shear layer thickness is around 50 mm. This shows that the flow above and inside the cavity are more mixed in the trailing edge of the cavity. This larger shear

45

layer thickness shows that the flow above the cavity is more dispersed into the cavity and vice versa.
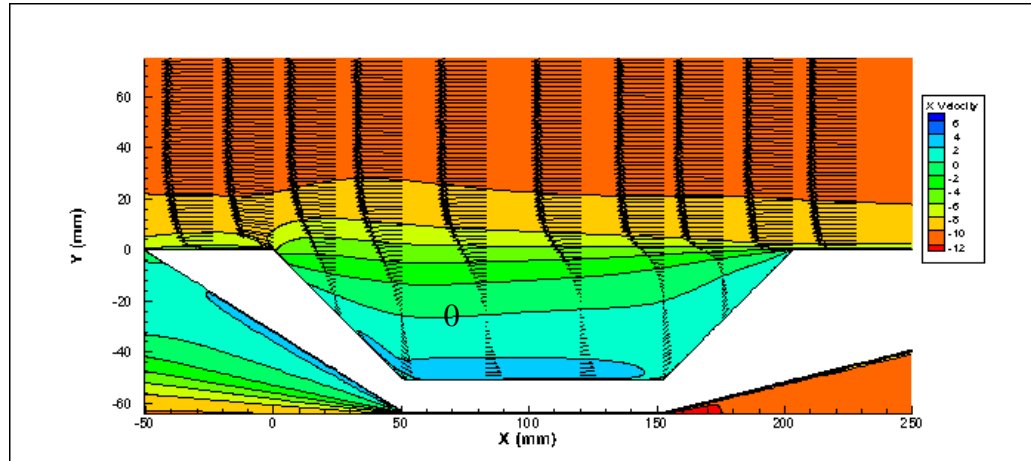
Fig. 4.14. Shear layer growth above the cavity on X-velocity contour

Moreover, a zoomed in view of the boundary layer approaching the cavity can be seen in Fig. 4.15. It can be seen that flow has been fully developed and enters the cavity perpendicularly.
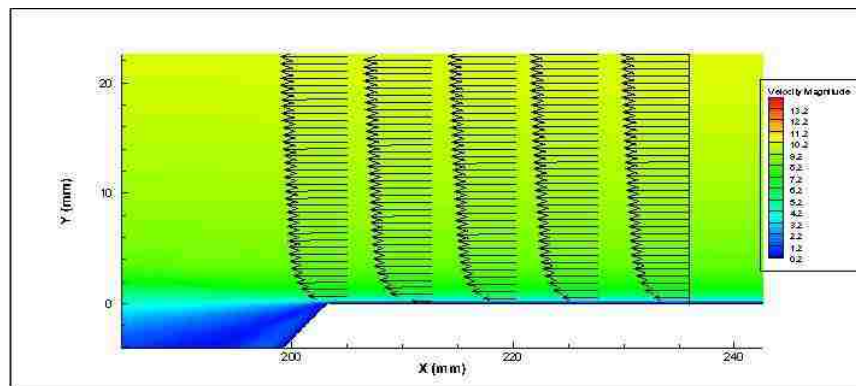
Fig. 4.15. The zoomed-in boundary layer approaching the cavity

Figure 4.16 shows Y-velocity on the mouth of the cavity. It can be seen that at the opening of the leading edge the velocity is in negative direction and at the trailing edge the value is positive. The volumetric flow rate, Q [m³/s] is defined as:

$$Q = \int V dA = L \int V dx \qquad (4.3)$$

where L is the unit length of the cavity in z direction. Therefore, the volumetric flow rate is calculated per unit length of the cavity. The net volumetric flow rate at the mouth of the cavity has to be zero as the flow is incompressible and the amount of flow that enters the cavity escapes the cavity as well. However, this integration at the portion of the mouth of the cavity in which the velocity magnitude in positive, i.e. flow is leaving the cavity, will give the amount of mass of air which is exchanged in the mouth of the cavity. For this case, this value has been calculated as to be 0.0351m³/s. This value is the volumetric flow rate that leaves the cavity. The value that enters the cavity has been calculated as to be 0.0349 m³/s. The difference between these two values is around 2%. This value can be normalized by the volume of the cavity. For the case with W/D of 2, the area of the cavity is calculated to be 0.00775 m²; hence the volume of the cavity for a unit length in z- direction will be 0.00775 m³. Therefore, the normalized exchanged air at

the mouth of the cavity will be: $\dfrac{0.0349\,\frac{m^3}{s}}{0.00775\,m^3} = 4.534\,\frac{1}{s}$.
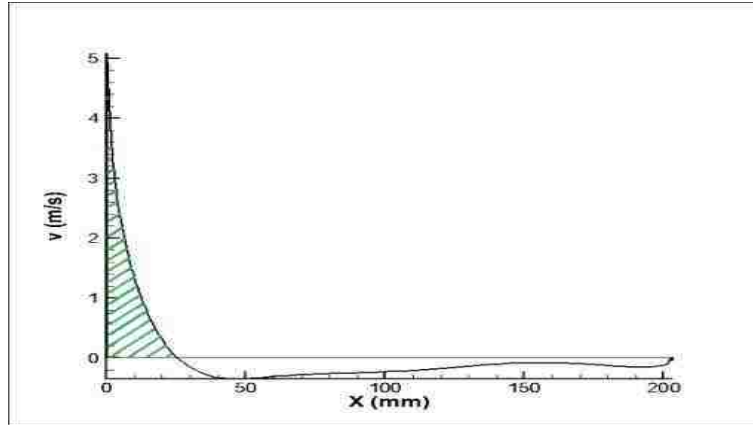
Fig. 4.16. Y-velocity profile on the line mouth of the cavity

4.3. CFD results and analysis

As explained in section 3.3, considering 3 factors and 3 levels for each, there are 27 possible combinations (see Table- 3.1). The CFD results from the 27 cases are presented. The effect of $U_{upstream}$, Tu and W/D ratio on normalized air exchanged rate from the cavity ($Q_{normalized}$), normalized position of the center of the vortex (x/L and Y/D), the type of the cavity; i.e. "open" or "closed and transitional", and the number of vortexes inside the cavity have been studied statistically.

The volumetric flow of air exchange rate at the mouth of cavity is normalized by the volume of the cavity. The horizontal position of the center of vortex (x) is normalized by the length of the cavity's mouth (L) and the vertical position of the center of vortex (y) is normalized by the depth of the cavity (D). Table- 4.1 shows the length, depth and volume of the cavity for different aspect ratios.

Table- 4.1 Length, depth and volume of the cavity for different W/D ratios

W/D	Cavity's length (mm)	Cavity's depth (mm)	Volume of the cavity (m^3)
2	203	50.8	0.00775
4	203	38.9	0.00657
6	203	25.4	0.00451

A summary of all the factors and responses are presented in Table- 4.2. In the cavity type column 0 is referring to "open" cavity and 1 is referring to "closed and transitional" cavity. Note that at each $U_{upstream}$, Re is constant for different aspect ratios.

Table- 4.2 Summary of all simulation results

#	W/D	Tu%	$U_{upstream}$ (m/s)	Re	Q (m³)	$Q_{nomalized}$ (1/s)	x (mm)	x/L	y (mm)	y/D	Cavity type	Inside Number of vortexes
1	2	0.67	5	60000	0.018	2.396	107.6	0.53	-24	-0.47	0	1
2	2	0.67	9.5	123000	0.035	4.534	99.5	0.49	-24	-0.47	0	1
3	2	0.67	15	181000	0.054	6.960	95.41	0.47	-24	-0.47	0	1
4	2	5	5	60000	0.019	2.426	111	0.54	-24	-0.47	0	1
5	2	5	9.5	123000	0.035	4.518	98.7	0.48	-24	-0.47	0	1
6	2	5	15	181000	0.054	7.005	96	0.47	-24	-0.47	0	1
7	2	15	5	60000	0.018	2.411	115.7	0.57	-24	-0.47	0	1
8	2	15	9.5	123000	0.035	4.534	107.6	0.53	-24	-0.47	0	1
9	2	15	15	181000	0.054	7.036	105.5	0.52	-24	-0.47	0	1
10	4	0.67	5	60000	0.030	4.698	146.2	0.72	-16.3	-0.42	0	1
11	4	0.67	9.5	123000	0.054	8.343	142.1	0.70	-16.3	-0.42	0	1
12	4	0.67	15	181000	0.084	12.92	142.1	0.70	-16.3	-0.42	0	1
13	4	5	5	60000	0.030	4.663	146.1	0.72	-16.3	-0.42	0	1
14	4	5	9.5	123000	0.054	8.361	144.1	0.71	-16.3	-0.42	0	1
15	4	5	15	181000	0.085	12.95	142.1	0.70	-16.3	-0.42	0	1
16	4	15	5	60000	0.030	4.645	146.2	0.72	-16.3	-0.42	0	1
17	4	15	9.5	123000	0.055	8.397	144.1	0.71	-16.3	-0.42	0	1
18	4	15	15	181000	0.085	12.92	144.1	0.71	-16.3	-0.42	0	1
19	6	0.67	5	60000	0.042	9.318	162.4	0.80	-12.9	-0.51	1	2
20	6	0.67	9.5	123000	0.078	17.31	160.4	0.79	-12.9	-0.51	1	2
21	6	0.67	15	181000	0.122	27.02	160.4	0.79	-12.9	-0.51	1	2
22	6	5	5	60000	0.042	9.293	162.4	0.80	-12.9	-0.51	1	2
23	6	5	9.5	123000	0.077	17.21	160.4	0.79	-12.9	-0.51	1	2
24	6	5	15	181000	0.122	27.02	160.4	0.79	-12.9	-0.51	1	2
25	6	15	5	60000	0.042	9.37	164.4	0.81	-12.9	-0.51	1	2
26	6	15	9.5	123000	0.078	17.26	162.4	0.80	-12.9	-0.51	1	2
27	6	15	15	181000	0.121	26.99	160.4	0.79	-12.9	-0.51	1	2

The significant factors on each response are listed in Table- 4.3. For all the cases the full model with all factors and possible interactions was initially tested and insignificant factors were omitted from the model (See Appendix. A.9).

The percentage of R-Squared that has explained by each factor with the total R-Squared and Adjusted R- Squared are listed in the table as well. It can be seen that aspect ratio is the dominant factor affecting all 5 responses and it explained the biggest portion of R-Squared.

Table- 4.3 Significant factors on responses

Response	Individual factors (% variance explained)	Interaction (% variance explained)	R-Sq	Adj-R-Sq
$Q_{normalized}$	W/D (58%) $U_{upstream}$ (32.6%)	W/D*$U_{upstream}$ (9.6%)	100%	100%
x/L	W/D (97.2%) $U_{upstream}$ (1.13%) Tu% (0.5%)	W/D*$U_{upstream}$ (0.57%) W/D*Tu (0.48%)	99.94%	99.80%
y/D	W/D (100%)		100%	100%
Cavity type	W/D (100%)		100%	100%
Number of vortex	W/D (100%)		100%	100%

Effect of factors on $Q_{normalized}$

Main effects and interaction plot for $Q_{normalized}$ is shown in Fig. 4.17. Tu has little effect on $Q_{normalized}$. With increasing W/D ratio and $U_{upstream}$, $Q_{normalized}$ increases. By increasing W/D from 4 to 6, $Q_{normalized}$ increases more than when increasing W/D from 2 to 4. This happens because the cavity changes from "open" to "closed and transitional" and more amount of air is exchanged at the mouth of the cavity. (Table- 4.2)

51

There is significant interaction between W/D and $U_{upstream}$. However, it explains only around 10% of R-Sq. This interaction is seen in Fig.4.17.b. The response is more sensitive to $U_{upstream}$ in W/D of 6 in comparison with W/D of 2 and 4.
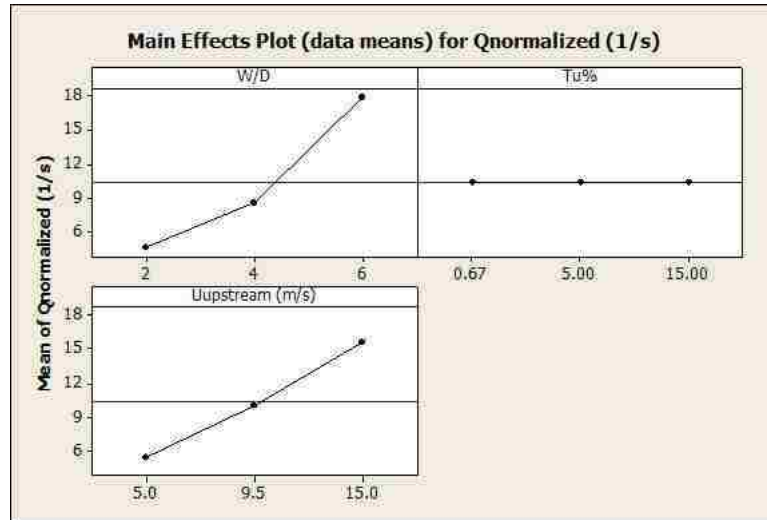
a) Main effect plot for $Q_{normalized}$
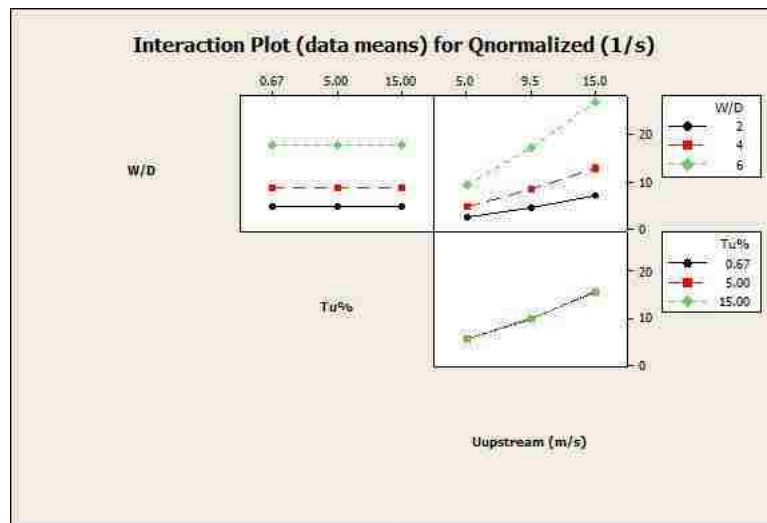
b) Interaction plot $Q_{normalized}$

Fig. 4.17. Main effects and interaction plots for Qnormalized

Effect of factors on x/L

Figure 4.18 shows the main effects and interaction plots for x/L as the response. With increasing W/D ratio, the center of vortex moves toward the leading edge (x/L increases). The center of vortex movement is more significant when increasing W/D from 2 to 4 in comparison with increasing W/D from 4 to 6. With increasing Tu from 0.67 to 5% the center of vortex does not move significantly however, with increasing Tu from 5% to 15% the center of vortex moves toward the leading edge. With increasing $U_{upstream}$ the center of vortex moves toward the trailing edge (x/L decreases).

There is significant interaction between "W/D and $U_{upstream}$" and "W/D and Tu". However, these interactions explain only around 1% of R-Sq together. In aspect ratio of 2 the sensitivity of the response on the effect of Tu is more in comparison with W/D of 4 and 6 (see Fig. 4.18.b).
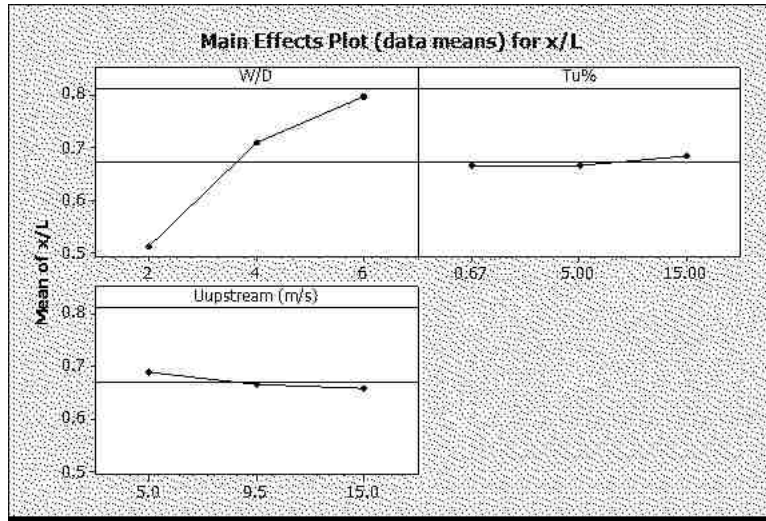
a) Main effect plot for x/L
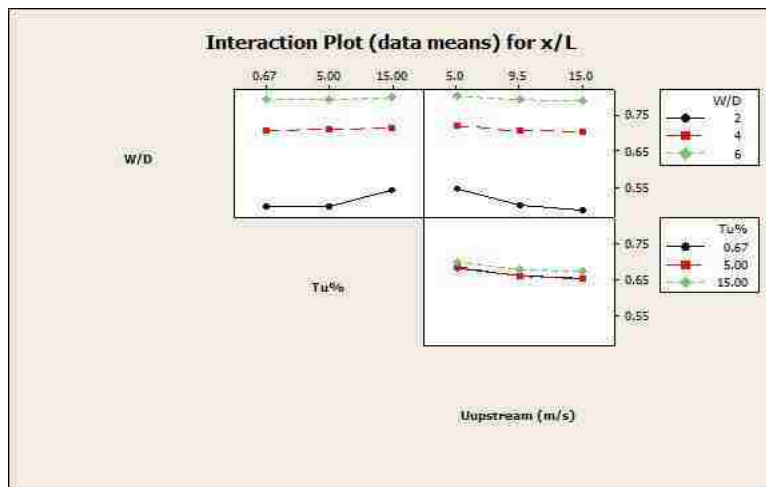
b) Interaction plot for x/L

Fig. 4.18. Main effects and interaction plots for x/L

Effect of factors on y/D

Figure 4.19 shows the main effect plot for y/D. For this response, the only significant factor is W/D ratio. It can be seen that the absolute value of y/D decreases (center of vortex moves up) with increasing from 2 to 4 and increases with increasing the aspect ratio from 4 to 6 (center of vortex goes deeper into the cavity).

54
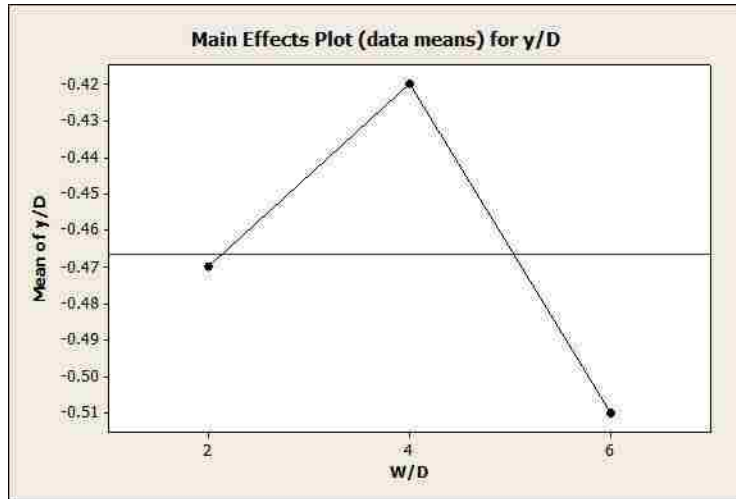
Fig. 4.19. Main effect plots for y/D

Effect of factors on cavity type

Figure 4.20 shows the main effect plot for cavity type. For this response, the only significant factor is W/D ratio. The cavity is "open" for aspect ratios of 2 and 4 and the cavity alters to "closed and transitional" in W/D of 6.
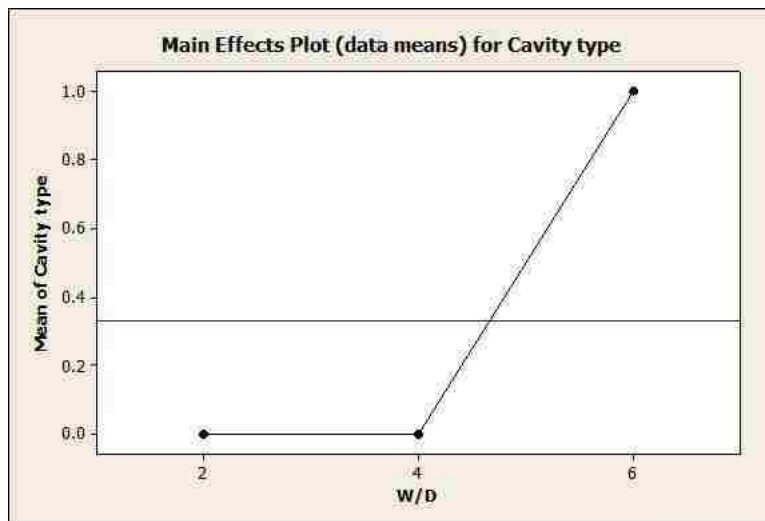
Fig. 4.20. Main effect plots for the cavity type

Effect of factors on number of vortex

Figure 4.21 shows the main effect plot for number of vortexes inside the cavity. In aspect ratios of 2 and 4, only one vortex is detectable inside the cavity. In aspect ratio of 6, two vortexes are inside the cavity. This sudden change happens because the cavity changes from "open" to "closed and transitional" with increasing W/D from 4 to 6.
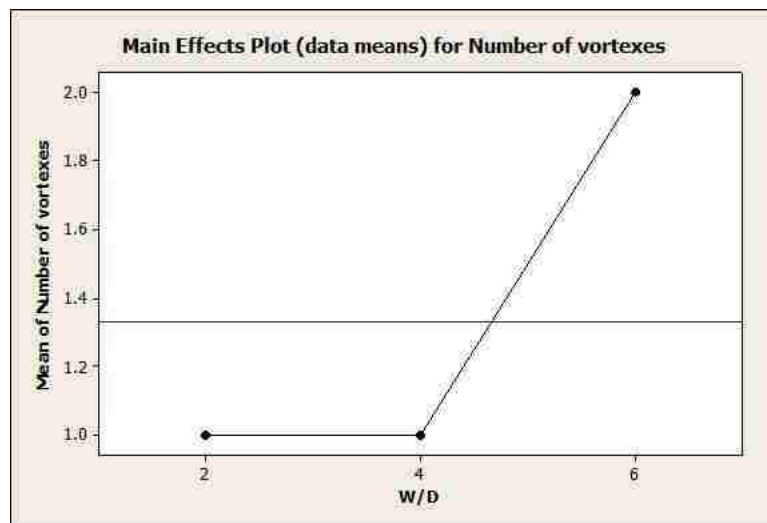
Fig. 4.21. Main effect plots for the number of vortexes inside the cavity

The effect of W/D ratio, upstream velocity and Tu is now discussed individually and in more details. To study the effect of each parameter, all the factors have been kept constant and only that factor varies. Seven cases from 27 possible cases have been chosen.

Effect of upstream velocity

Upstream stream velocity has been varied in three levels (5 m/s, 9.5 m/s and 15 m/s) resulting Re of (60000, 123000 and 181000) on cavity with aspect ratio of 2 and with Tu of 5%. Other factors (Tu and W/D) have been set constant for all the three cases. Figure 4.22 show the flow streamlines above and inside the cavity.

a) $U_{upstream} = 5$ m/s,   b) $U_{upstream} = 9.5$ m/s

c) $U_{upstream} = 15$ m/s
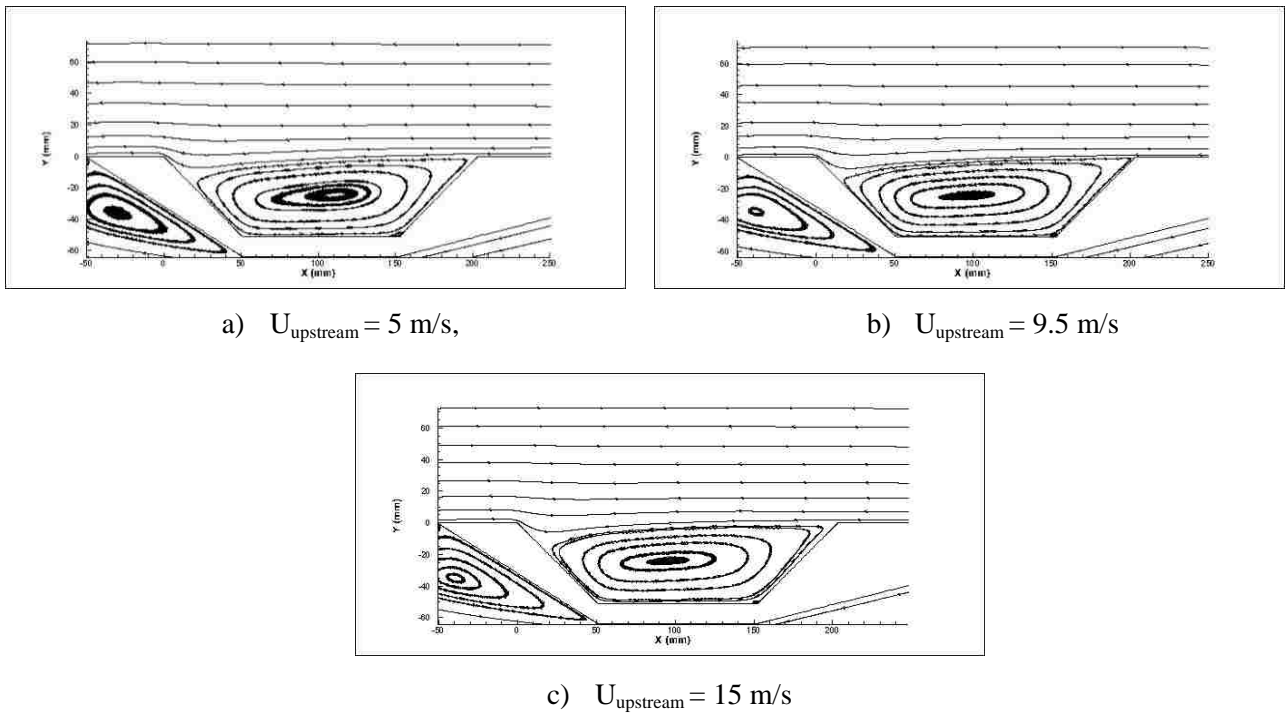
Fig. 4.22. Flow streamlines above and inside the cavity for W/D=2 and Tu=5%

It is illustrated that with increasing the upstream velocity the vortex becomes more aligned with the bottom of the cavity and the center of vortex inside moves toward the trailing edge (as explained previously). However, the vertical position of the center of vortex remains constant.

Fig. 4.23 shows the velocity vectors above and inside the cavity on contour of X-velocity. It can be seen that in all the cases the shear layer growth and thickness of the

shear layer is quite the same. In all the cases, an intense thin shear layer forms at the leading edge of the cavity and the shear layer grows toward the trailing edge and the maximum thickness of the shear layer is around 50 mm from the trailing edge. After this point, the shear layer becomes narrower because of the effect of trailing edge.
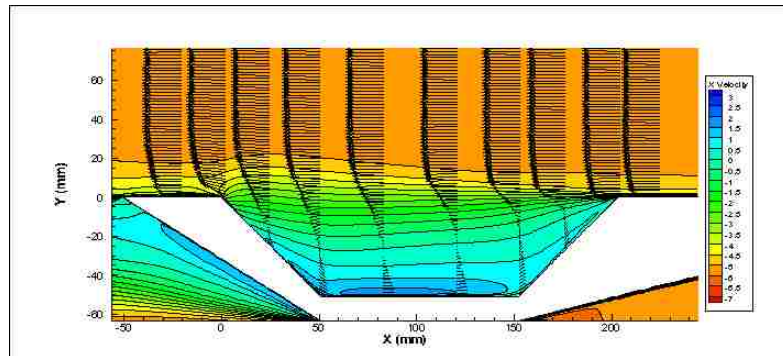
a) $U_{upstream}=5m/s$
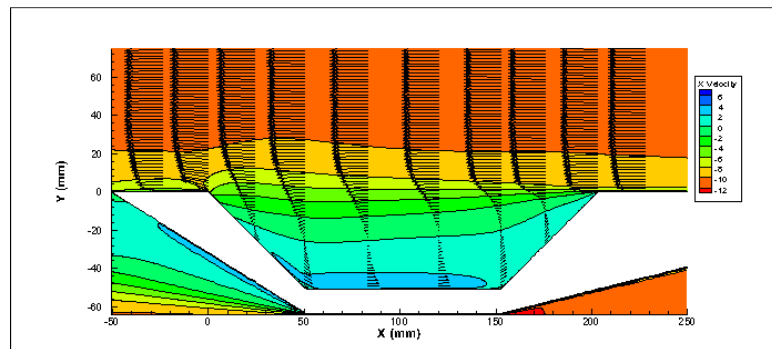
b) $U_{upstream}=9.5m/s$
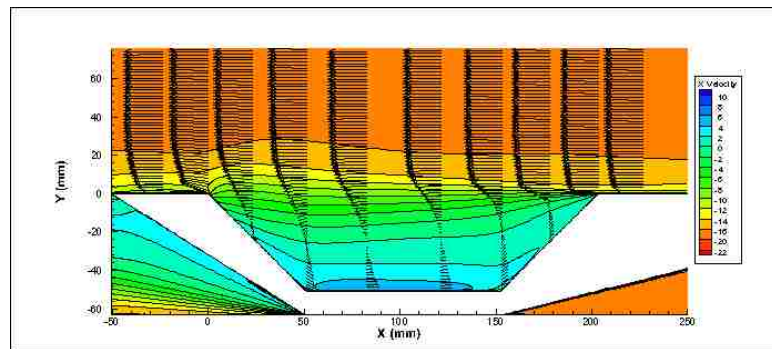
c) $U_{upstream}=15m/s$

Fig. 4.23. Shear layer growth above the cavity (W/D=2, Tu =5%)

Figure 4.24 shows the normalized X-velocity ($\frac{u}{U_{upstream}}$) with normalized vertical

position (Y/D) on Line b2. It can be seen with that with increasing upstream velocity, the

non-normalized velocity profiles do not alter significantly. These profiles have been

checked for other lines as well and no significant change was observed.
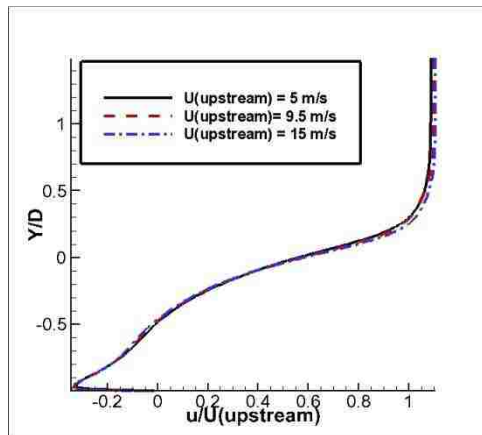
Fig. 4.24. Normalized X velocity on Line b2

Figure 4.25 shows the normalized Y-velocity profiles for Lines b1, b2 and b3. It can

be seen that at the mouth of the cavity (Y/D = 0) flow has a negative vertical component

of velocity which shows that flow above the cavity is interacting with the flow inside the

cavity. Moving toward the trailing edge of the cavity, Y-velocity increases. On Line b2

the magnitude of normalized Y-velocity is larger for upstream velocity of 5 m/s which is

because of the fact that at this velocity flow has lower momentum in the x direction,

therefore, it is more affected by the expansion due to the cavity.
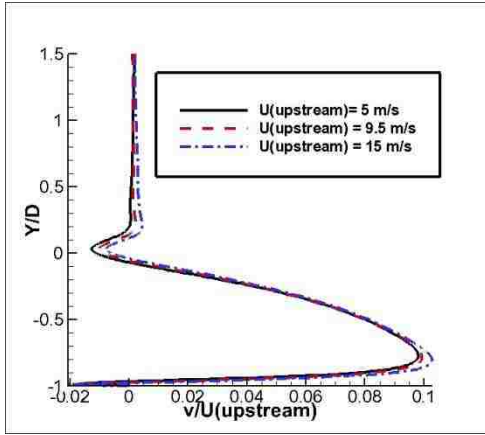
a)   Line b1
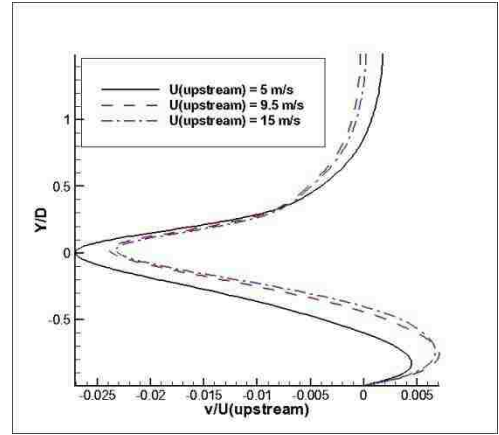
b)   Line b2
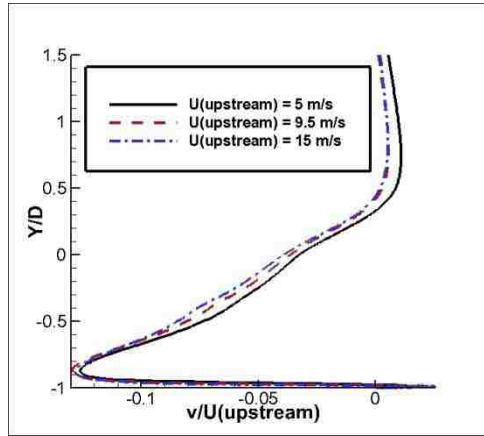
a) Line b3

Fig. 4.25. Normalized Y-velocity profiles on lines b1, b2 and b3

Figure 4.26 shows the vertical velocity profile at the mouth the cavity for three upstream velocities and the normalized volumetric flow rate of exchanged air from the cavity ($Q_{normalized}$) has been calculated based on the method explained using these profiles. $Q_{normalized}$ increases with increasing $U_{upstream}$ as explained before.
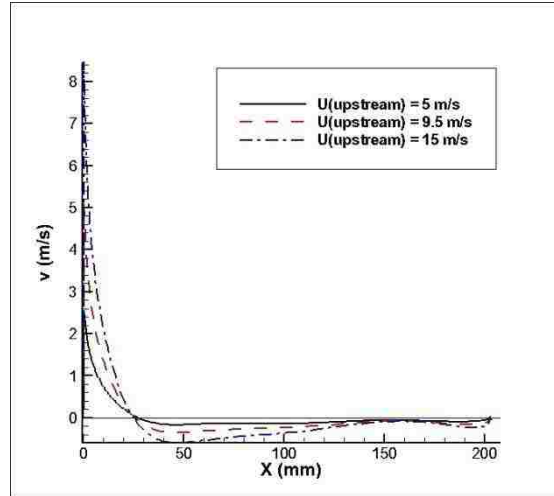
Fig. 4.26.Y-velocity at the mouth of the cavity at different upstream velocities

Figure 4.27 shows the vorticity plots on a portion of Lines b1, b2 and b3. The plot is zoomed in to the region of vortex presence. The idea of this comparison was borrowed from the paper by (Grace and Dewar, 2004). They omitted the very high vorticity region at the mouth of the cavity and close to the walls for two vortexes and compared the maximum value of vorticity in them.

In this work, the vorticity plots on three lines among the cavity's mouth have been compared. If the value of vorticity for one vortex be higher on three lines, it can be concluded that that vortex has more strength. In addition, for each case, as expected, the value of vorticity magnitude increases moving toward the trailing edge. With increasing the upstream velocity, the vorticity magnitude is higher; hence, the vortex has more strength.
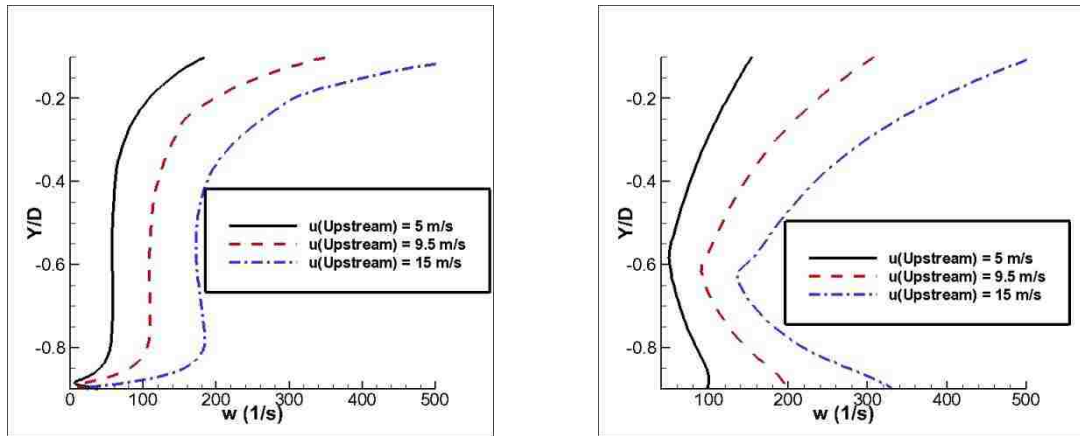
a) Line b1   b) Line b2
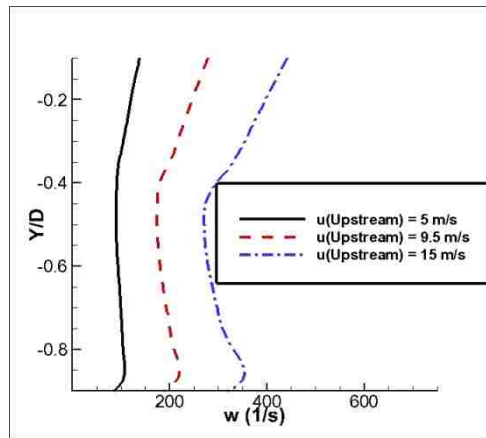
c) Line b3

Fig. 4.27. Vorticity plots on Lines b1,b2 and b3

Effect of turbulence intensity

In aspect ratio of 2 and upstream velocity of 9.5 m/s, Tu varies for 0.67, 5 and 15%. Figure 4.28 shows flow streamlines above the cavity at different turbulence intensities.

62

  a) Tu = 0.67%   b) Tu= 5%

c) Tu =15%
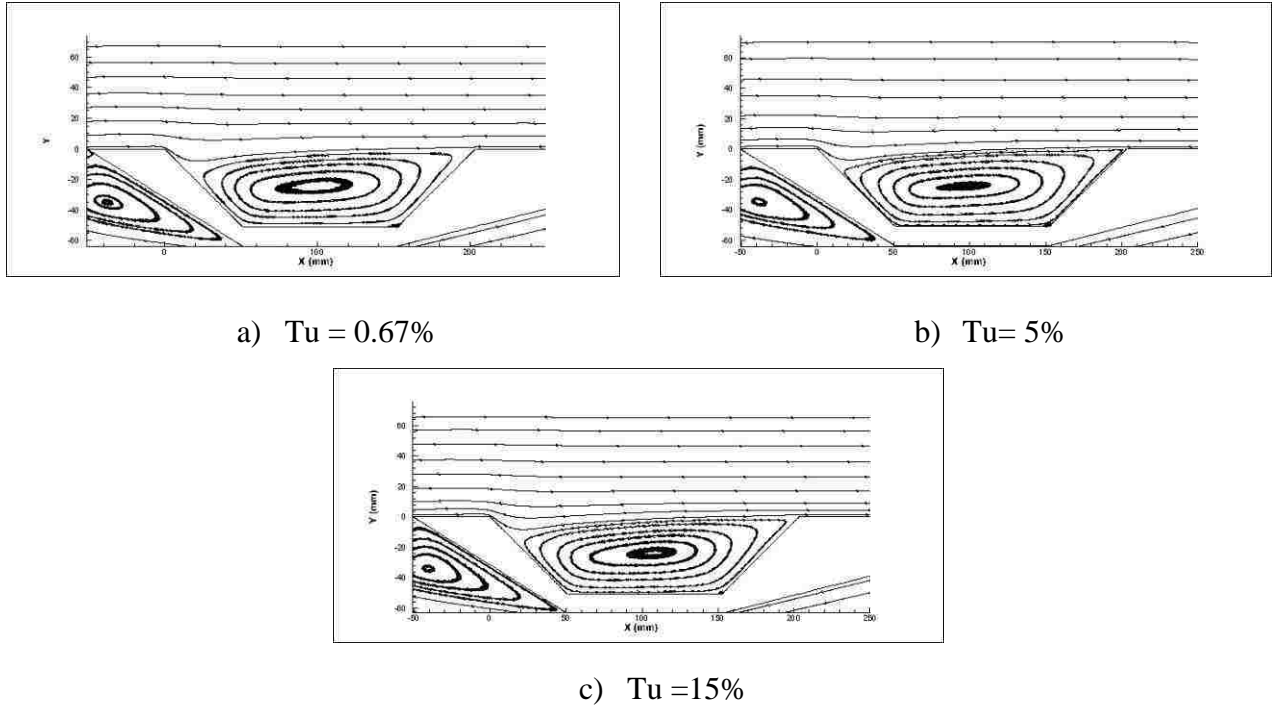
Fig. 4.28. Flow streamlines above and inside the cavity (W/D=2, Uupstream =9.5 m/s)

  Flow streamlines have not altered significantly with increasing turbulence intensity. However, the center of vortex moves toward leading edge with increasing turbulence intensity from 5% to 15%. In this study, Tu values are the set at inlet. The center of vortex for both cases of 0.67% and 5% are at ≈ 100 mm. However, for the case with Tu=15% the center of vortex has been moved 8 mm toward the leading edge. This can be explained based on the diffusive nature of turbulence. Basically, with increasing level of turbulence, the momentum of the flow diffuses more into the cavity when hitting the wall of the cavity.

  Figure 4.29 show the shear layer growth above the cavity at different Tu values. It can be seen that the shear layer growth does not change significantly.
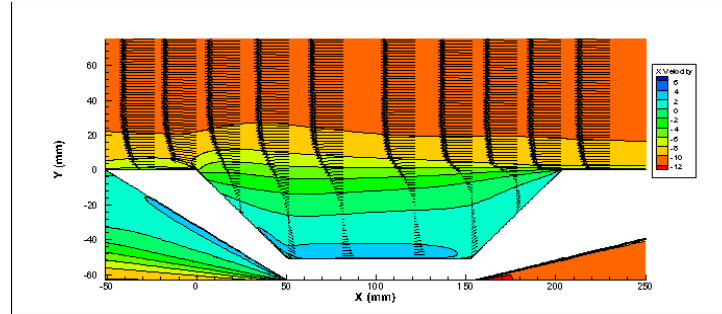
a)   Tu = 0.67%
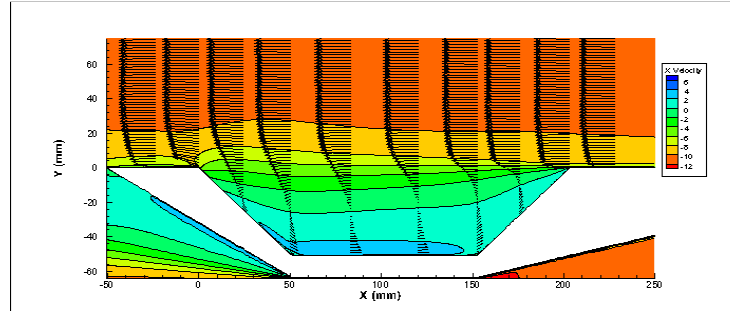
b)   Tu = 5%
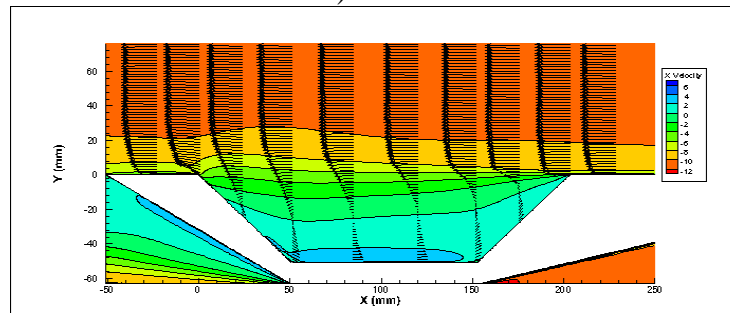
c)   Tu =15%

Fig. 4.29. Shear layer growth above the cavity with increasing Tu

Fig. 4.30. shows the normalized X-velocity ($\frac{u}{U_{upstream}}$) with normalized vertical position (Y/D) for the Line b2. With increasing upstream velocity, the non-dimensionalized velocity profile does not alter significantly. These profiles have been checked for other lines as well and no significant change was observed.
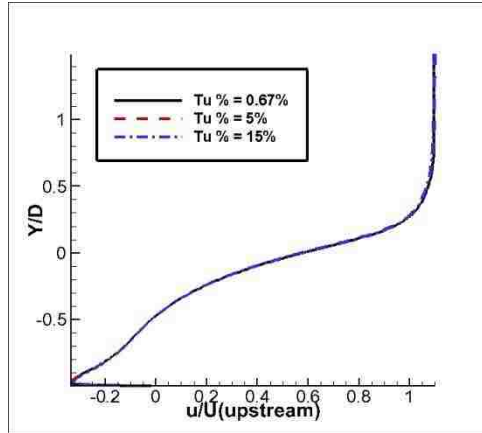
Fig. 4.30. Normalized X-velocity profile on the Line b2

Figure 4.31 shows the normalized Y-velocity profiles for Lines b1, b2 and b3. At the mouth of the cavity (Y/D = 0) flow has a negative vertical component of velocity which shows that flow above the cavity is interacting with the flow inside the cavity. The biggest difference in plots occurs at the mouth of cavity on line b2. This line is in the middle of the cavity and is less affected by the effect of leading and trailing edge of the cavity. On the mouth of the cavity the case with 15% of turbulence intensity shows the biggest normalized y-velocity component.

a) Line b1

b) Line b2

c) Line b3
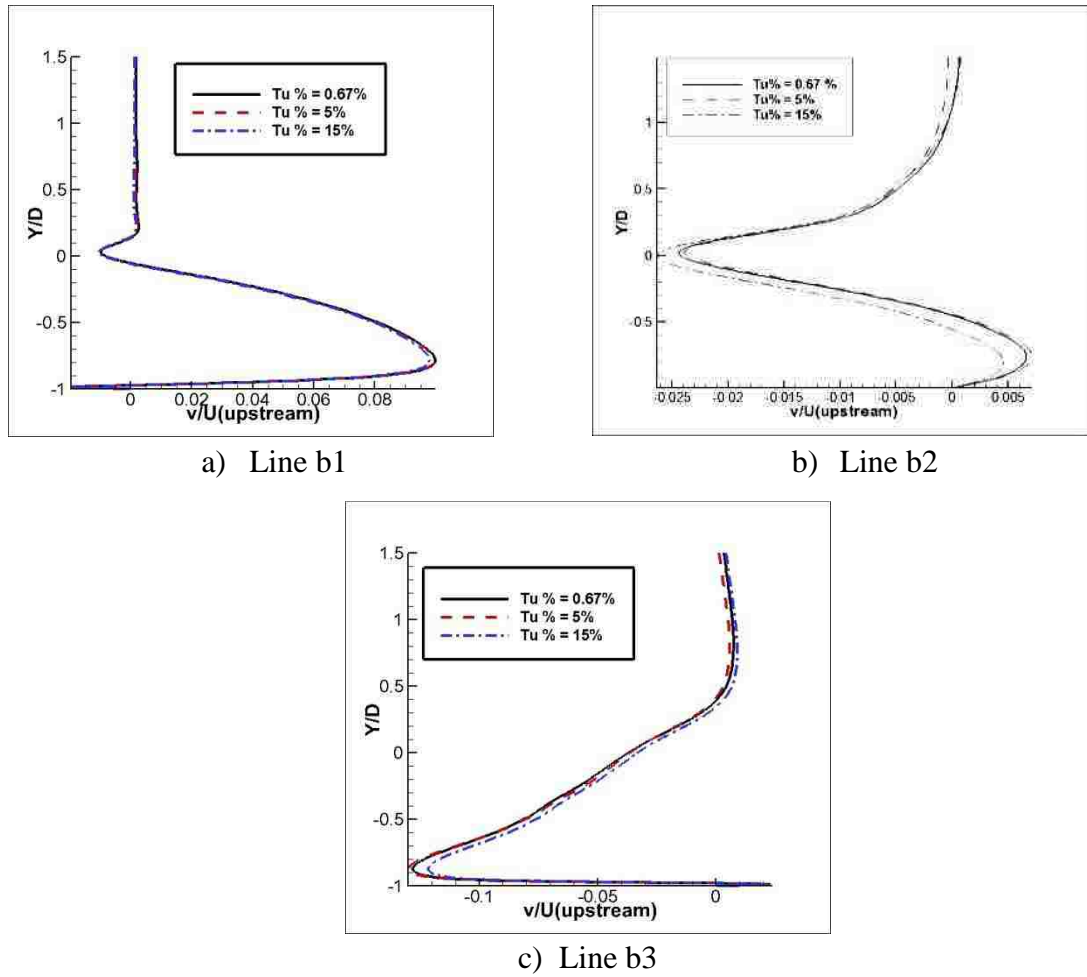
Fig. 4.31. Normalized Y-velocity profiles on lines b1, b2 and b3

Figure 4.32 shows the vertical velocity profile at the mouth of the cavity for three levels of turbulence and the normalized volumetric air exchange flow rate ($Q_{normalized}$) has been calculated using these plots. Therefore, no significant difference in the values of $Q_{normalized}$ for these three cases is expected.
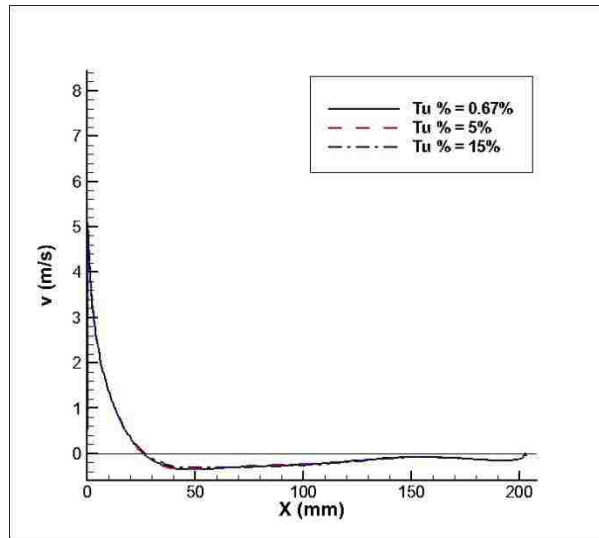
Fig. 4.32.Y-velocity at the mouth of the cavity at different Tu levels

Figure 4.33 shows the vorticity plots on portions of Lines b1, b2 and b3. The vortexes have the same strength based on the method introduced previously. The effect of Tu is not very significant. Two main reasons for this can be listed. First, the Tu is set in the inlet of the CFD model and as explained the level of turbulence drops when flow reaches the setup due to energy dissipation (See Appendix A.7). Hence, for the two cases with Tu of 0.67% and 5% there is not much difference in Tu of flow when it reaches to the cavity (see Appendix A.7). Moreover, in all the cases boundary layer formed on the leading edge of the cavity is turbulent. The reason is that the presence of setup by itself generates turbulence as the cavity is suspended inside the wind tunnel. Hence, due to the limitation of this work the comparison between laminar and turbulent boundary layer entering the cavity is not possible.

67

a) Line b1   b) Line b2

c) Line b3
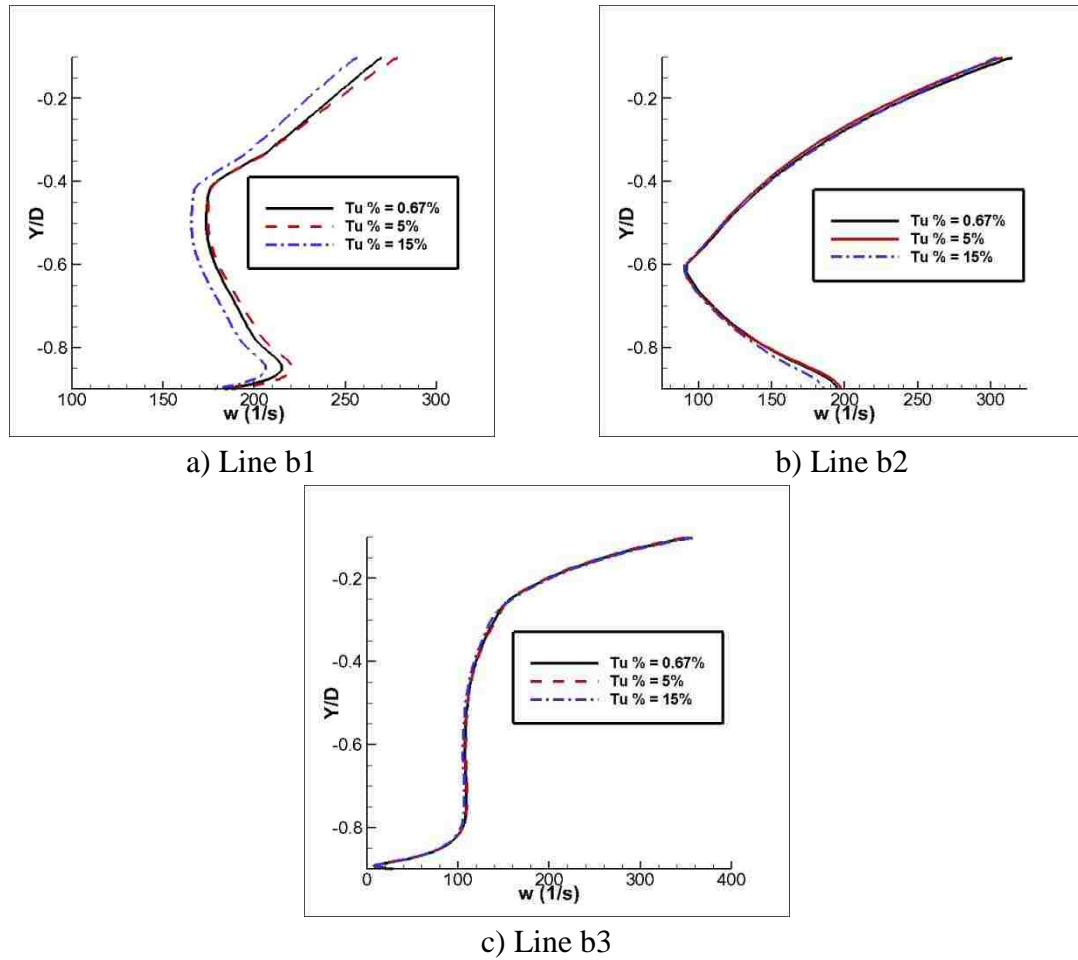
Fig. 4.33. Vorticity magnitude plots on different sections among the cavity mouth

Effect of aspect ratio (W/D)

Two aspect ratios larger than two have been studied to find out how W/D ratio affects vortex characteristics and the shear layer growth above the cavity. The aspect ratios of 2, 4 and 6 have been studied under upstream velocity of 9.5 m/s (Re= 123000) and Tu of 5%.

Figure 4.34 shows the flow streamlines above and inside the cavity for the aspect ratios of 2, 4 and 6. With increasing the aspect ratio from 2 to 4 the dominant vortex

68

inside has become more stretched and the center of vortex has been moved to the leading edge. For the cavity with W/D of 6 the flow re attaches on the bottom of the cavity and flow cannot bridge the cavity. It should be mentioned that the definition of "open" and "closed and transitional" cavity has been borrowed from rectangular cavities into this work. Therefore, according to the definition, the cavity with aspect ratio of 6 is "closed and transitional".

a) W/D = 2   b) W/D = 4

c) W/D = 6
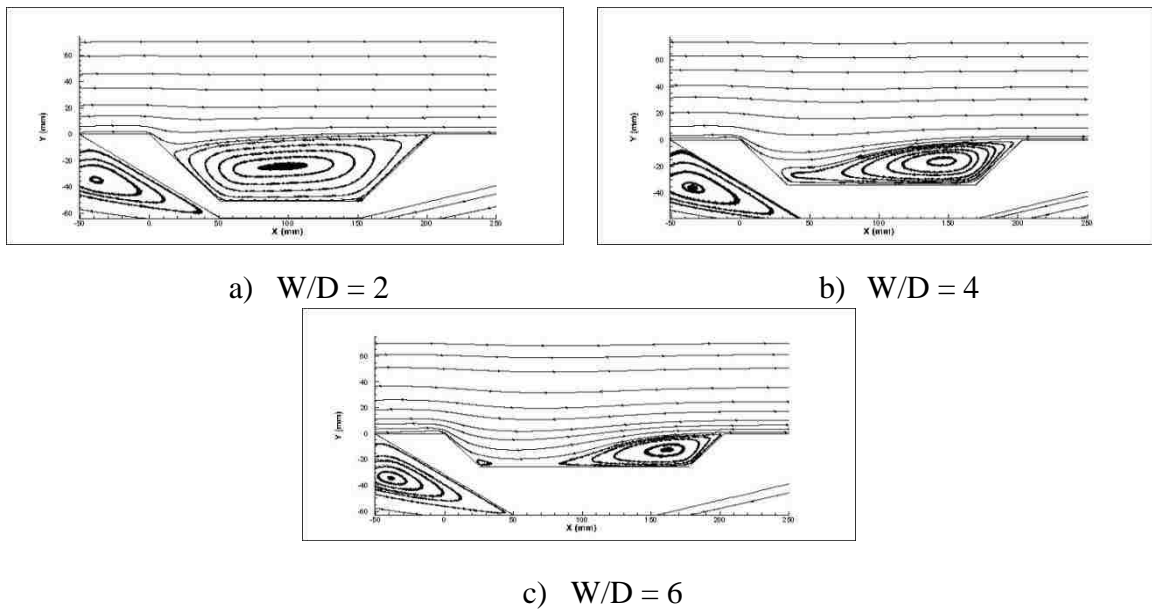
Fig. 4.34. Flow streamlines above cavity for Uupstream = 9.5 m/s, Tu = 5%

Figure 4.35 shows the shear layer growth above the cavity. With increasing the aspect ratio the shear layer becomes thicker. In Fig. 4.35.c the shear layer on the bottom of cavity after flow reattachment is also visible. After the reattachment of the flow, a boundary layer is formed on the bottom of the cavity.
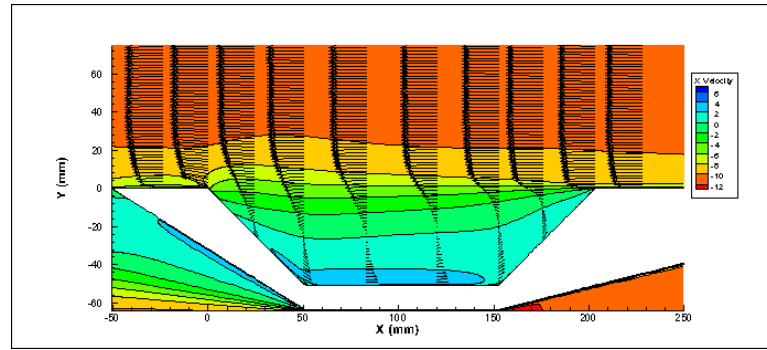
a) W/D =2
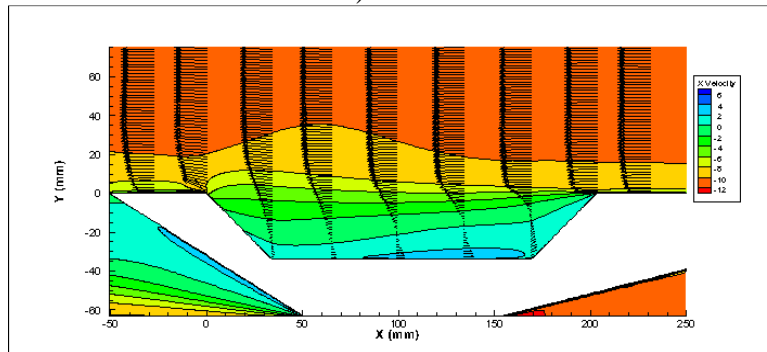
b) W/D = 4
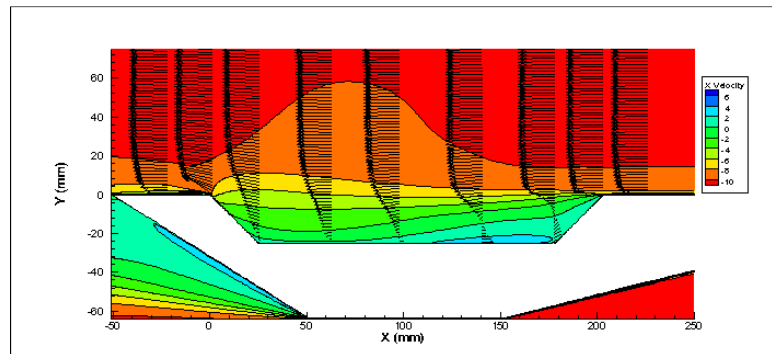
c) W/D =6

Fig. 4.35. Boundary layer growth above the cavity at different aspect ratios

Figure 4.36 shows the Y-velocity profile on the mouth of the cavity in different aspect ratios and $Q_{normalized}$ is calculated using these profiles. Flow leaves the cavity closer to the trailing edge for W/D of 2 and in aspect ratio of 6 flow leaves the cavity around at 70 mms from the trailing edge.
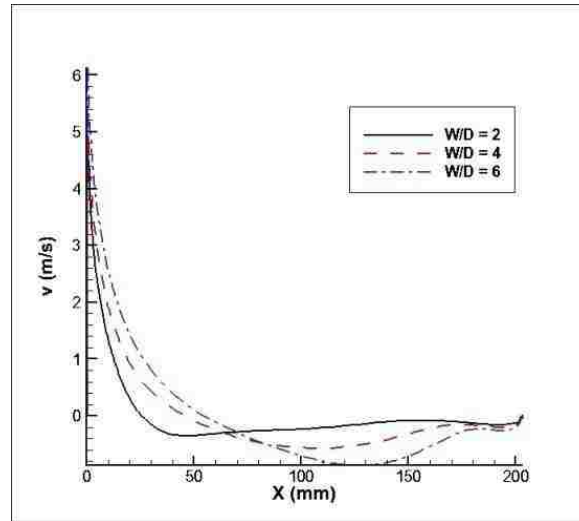
Fig. 4.36. Y-velocity at the mouth of the cavity at different W/D ratios

With increasing W/D, $Q_{normalized}$ increases drastically which has been proofed statistically, as well. It can be seen in Fig. 4.34. that for the cavity with W/D of 2 only one streamline enters the cavity and leaves it without interaction with the vortex inside. However, in the cavity with W/D ratio of 4, two stream lines enter the cavity and leave it. In W/D ratio of 6, the cavity changes from "open" into "closed and transitional" and 5 streamlines enter the cavity and leave the cavity.

In this chapter, the results from CFD case study were presented. The effect of aspect ratio, $U_{upstream}$ and Tu was statistically analyzed on normalized flow air exchanged rate at the mouth of the cavity, the normalized horizontal and vertical position of the center of the vortex, the cavity type and number of vortexes inside the cavity. The aspect ratio was found to be the most significant factor affecting $Q_{normalized}$, the position of center of the vortex and flow characteristics above and inside the cavity.

71

CHAPTER V

CONCLUSIONS AND RECOMMENDATIONS

5.1. Conclusions

In this work a trapezoidal cavity was studied using a CFD model. The cavity was studied for aspect ratios of 2, 4 and 6; Re = 60000, 123000 and 181000 ($U_{upstream}$= 5 m/s, 9.5 m/s and 15 m/s); and Tu = 0.67%, 5% and15%.

A CFD model was developed and validated using experimental data collected from wind tunnel experiments. Different turbulence modeling schemes were tested and k-kl-ω was chosen for this study because with this turbulence modeling scheme, the CFD results are in a better agreement with experimental results. This turbulence modeling has reasonable computational cost too. Vortex characteristics and vorticity contour inside; shear layer growth above the cavity were analyzed with the CFD results from the case that was used for model validation (W/D =2, $U_{upstream}$= 9.5 m/s and Tu = 0.67%).

The CFD model was run for all 27 possible cases (three factors each has three levels). The effect of each individual factor and possible interactions between them was studied statistically. There are five responses; they are the normalized of air exchanged volumetric flow rate at the mouth of the cavity ($Q_{normalized}$), the normalized horizontal position (x/L) and normalized vertical position (y/D) of the vortex, the cavity type and number of vortexes inside the cavity. The effect of each factor was analyzed in more details as well.

The aspect ratio was found to be the most significant factor affecting all the responses whereas Tu did not show any major effect on any of the responses. W/D ratio was the

only significant factor on the normalized vertical position of the cavity (y/D), cavity type and number of vortexes inside the cavity. W/D ratio and $U_{upstream}$ and the interaction between them were significant factors affecting $Q_{normalized}$. W/D ratio, $U_{upstream}$, Tu and interactions between W/D×$U_{upstream}$ and W/D×Tu were the significant factors affecting x/L.

With increasing W/D ratio, $Q_{normalized}$ increased significantly. The increase in $Q_{normalized}$ was more when increasing the aspect ratio from 4 to 6, in comparison with when increasing W/D from 2 to 4. This significant increase in $Q_{normalized}$ is explained by the change of the cavity type from "open" to "closed and transitional". Moreover, with increasing $U_{upstream}$, $Q_{normalized}$ increased and this increase was more significant in aspect ratio of 6.

With increasing W/D ratio, the center of vortex was moved toward the leading edge of the cavity. Furthermore, with increasing $U_{upstream}$, the center of vortex moved toward the trailing edge. The effect of Tu was significant in W/D of 2. With increasing Tu from 0.67% to 5% the center of vortex did not move significantly, whereas, with increasing the level of turbulence from 5% to 15%, the center of vortex was found to move toward the leading edge a bit.

With increasing W/D ratio the normalized vertical position of the center of vortex (y/D) moved up but with increasing the aspect ratio from 4 to 6, y/D was moved toward the bottom of the cavity.

Only in aspect ratio of 6, two vortexes were detectable inside the cavity whereas, in aspect ratios of 2 and 4 one dominant vortex were detectable inside the cavity.

Furthermore, the cavity was found to be "closed and transitional" in aspect ratio of 6. In W/D ratios of 2 and 4 the cavity was found to be "open".

Moreover, for the cavity with aspect ratio of 2, detailed analysis on the effect of $U_{upstream}$ and Tu showed that neither of those factors affect shear layer growth above the cavity and normalized X-velocity. Vorticity magnitude inside the vortex increased with increasing $U_{upstream}$. Hence, the vortex inside has more strength at higher upstream velocities. Tu did not show a significant effect on vorticity inside the cavity. The vorticity plot on line b1 (close to the leading edge of the cavity) is slightly higher for Tu= 15%.

5.2. Recommendations

In this work a 2D CFD model was used to study flow characteristics inside and above a trapezoidal cavity. In future studies, a 3D CFD model could be used which will require high computational cost.

Specific road configurations, i.e. below-grades, with trapezoidal section can be modeled as a trapezoidal cavity. Although this work was not reflecting exactly the same conditions of a real below grade, scaling study will show how to interpret the results of this work for the real case geometry. In addition, pollutant dispersion can be included in the model by adding a point source of pollution or a pollutant flux at the bottom of the cavity.

The effect of Tu was not found to be significant on all the responses. The boundary layer entering the cavity was turbulent in all the cases as the setup is suspended inside the (i.e. turbulence is generated due to the presence of the setup). A setup that can generate

laminar boundary layer on the leading edge of the cavity should be designed to better understand the effect of Tu.

In this study, the experimental results were only conducted for a cavity with aspect ratio of 2. A comparison between experimental and CFD model results for the cavities with other aspect ratios (i.e. 4 and 6) improves the model validation.

REFERENCES

K. Ahmad, M. Khare, K.K. Chaudhry, Wind tunnel simulation studies on dispersion at urban street canyons and intersections—a review, (2005), Journal of Wind Engineering and Industrial Aerodynamics, 93, (697–717).

C.K. Aidun, N.G. Triantafillopoulos, J.D. Benson, Global stability of a lid-driven cavity with through flow: flow visualization studies, (1991), Physics of Fluids A, 3, (2081–2091).

O.J. Akinlade, Effects of surface roughness on the flow characteristics in a turbulent boundary layer, (2005), PhD dissertation, University of Saskatchewan.

ANSYS FLUENT, Manual,(2012), ANSYS Inc.

V.D. Assimakopoulos, H.M. ApSimona, N. Moussiopoulos, A numerical study of atmospheric pollutant dispersion in different two-dimensional street canyon configurations, (2002), Atmospheric Environment, 37, (4037–4049).

J.B. Barlow., H. William. RAE. A. Pope. Low-speed wind tunnel testing, (1999), 3rd edition, Wiley-Interscience.

S. Chen, GD Doolen, Lattice Boltzmann method for fluid flows, (1998), Annual Review of Fluid Mechanics, 30, (329–64).

G. Comte-Bellot, Hot-Wire Anemometry, (1976), Annual Review of Fluid Mechanics, 8, (209-231).

E. Erturk, Discussions on driven cavity flow, (2009), International Journal for Numerical Methods in Fluids, 60, (275-294).

M.J. Esteve, P. Reulet, P. Millan, Flow field characterisation within a rectangular cavity (2000), 10th symposium applications of laser techniques.

T.M. Faure, P. Adrianos, F. Lusseyran, L. Pastur, Visualizations of the flow inside an open cavity at medium range Reynolds numbers, (2007), Experiments in Fluids, 42, (169-184).

J. Fenger, Urban air quality, (1999), Atmospheric Environment 33, (4877–4900).

P. H. Gaskell, H. M. Thompson, M. D. Savage, A finite element analysis of steady viscous flow in triangular cavities, (1999), Journal of Mechanical Engineering Science, 213, (263-276).

M. Glauser, http://www.lcs.syr.edu/faculty/glauser/mae315/fluids/MAE315 Lab4Week1.htm [online].

S. M. Grace, W. G. Dewar, D. E. Wroblewski, Experimental investigation of the flow characteristics within a shallow wall cavity for both laminar and turbulent upstream boundary layers, (2004), Experiments in Fluids, 36, (791–804).

J. C. Hardin, P. J. W. Block, Evaluation of a vortex model of turbulent cavity flow, (1979), NASA Technical Paper, No. 1505.

R. Kunz, N. Moussiopoulos, Simulation of the wind field in Athens using refined boundary conditions (1995). Atmospheric Environment, (29), (3575–3591).

L. Larchevequ, P. Sagaut, T-H. Le, P.Comte, Large-eddy simulation of a compressible flow in a three-dimensional open cavity at high Reynolds number, (2003), Journal of Fluid Mechanics, 516, (265-301).

B. E. Launder, B .I. Sharma, Application of the energy dissipation model of turbulence to the calculation of flow near a spinning disc, (1974) Letters in Heat and Mass Transfer, 1, (131-138).

B. E. Launder, D. B. Spalding, Lectures in Mathematical Models of Turbulence. (1972) Academic Press, London, England.

S. J. Lawson, G. N. Barakos, Review of numerical simulations for high-speed, turbulent cavity flows, (2011), Progress in Aerospace Science 47, (186-216).

J.C. Lin, D. Rockwell Organized oscillations of initially turbulent flow past a cavity (2001). The American Institute of Aeronautics and Astronautics Journal, 39, (1139–1151).

A. Melling, Tracer particles and seeding for particle image velocimetry, (1997), Measurement Science and Technology, 8, (1406–1416).

F. R. Menter, M. Kuntz, R. Bender, A scale-adaptive simulation model for turbulent flow predictions, (2003). The American Institute of Aeronautics and Astronautics Journal.

Minitab help (2012), Minitab Inc.

C. Ozalp, A. Pinarbasi, B. Sahin, Experimental measurement of flow past cavities of different shapes, (2010), Experimental Thermal and Fluid Science, 34, (505–515).

E. Ozsoy, P. Rambaud, A. Stitou, M.L. Riethmuller, Vortex characteristics in laminar cavity flow at very low Mach number, (2005) Experiment in Fluids, 38, (133-145).

S. V. Patankar, D. B. Spalding, A calculation procedure for heat, mass and momentum transfer in three-dimensional parabolic flows,(1972), International Journal of Heat and Mass Transfer,15, (1787-1806) .

S. V. Patankar, Numerical Heat Transfer and Fluid Flow, (1980), Tylor and Francis.

S. B. Pope, Turbulent flows, (2000) , Cambridge University Press.

J. Proakis, D. Manolakis, Digital Signal Processing: Principles, Algorithms, and Applications, (1992), New York: Macmillan Publishing Company.

S. A. Ritchie, N.J. Lawson, K. Knowles, A PIV and CFD investigation of cavity flows in the transonic flow regime, (2004), 24th, International congress of the aeronautical sciences.

A. Roshko, Some measurements of flow in rectangular cutout, (1995), National advisory committee for aeronautics, Technical note 3488.

P. Sagaut, C. Meneveaue, Large Eddy Simulation of incompressible flows, An introduction (1998), third edition, Springer.

P. Salizzoni, M. Marro • L. Soulhac, N. Grosjean, R. J. Perkins, Turbulent Transfer Between Street Canyons and the Overlying Atmospheric Boundary Layer, (2010), Boundary-Layer Meteorology, 141, (393-414).

S. Sarkar, l. balakrishnan, Application of a Reynolds Stress Turbulence model to the compressible shear layer, NASA Contractor Report 182002, ICASE Report No. 90-18

P. N. Shankar, M. D. Deshpande, Fluid mechanics in the driven cavity, (2000), Annual Reports in Fluid Mechanics, 32, (93-136).

C. Tropea, Laser Doppler anemometry: recent developments and future challenges, (1995) Measurement Science and Technology, 6 (605-619).

D. K. Walters, D. Cokljat, A three-equation eddy-viscosity model for Reynolds-averaged Navier-Stokes simulations of transitional flows, (2008), Journal of Fluids Engineering

F. M. White, Fluid Mechanics, (2003), McGraw-Hill, 5th Edition.

D. C. Wilcox. Turbulence Modeling for CFD, (1998), DCW Industries, Inc. La Canada, California.

M. William, C. J. Ribbens, and C. Y. Wang. and Watson, Layne T. Steady Viscous Flow in a Trapezoidal Cavity. (1992) Technical Report TR-92-58, Computer Science, Virginia Polytechnic Institute and State University.

Y. Yang, A.G. Straatman, R.J. Martinuzzi, E.K. Yanful, A study of laminar flow in low aspect ratio lid driven cavities,(2002) Canadian Journal of Civil Engineering, 29 (436–447).

T. Zhang, B. Shi, Z. Chai, Lattice Boltzmann simulation of lid-driven flow in trapezoidal cavities, (2010), Computers & Fluids, 39, (1977–1989).

APPENDICES

A.1. Modeling Approaches

There are different approaches to tackle different engineering problems. However, they can be classified into: Reduced Scaled Experiments, Computational Fluid Dynamics (CFD) and Full Scale Experiments. In this appendix, a brief introduction on these methods is presented.

A.1.1. Reduced Scaled Models

These models are based on similarity principles with which real geometries can be scaled down into a wind tunnel or water tank geometry. Therefore, the real geometry of the case can be scaled down in an order of 1/20 or even more. The dimensions of the reduced scaled model are limited to the blockage effect inside the wind tunnel and therefore, they are limited to the dimension of the wind tunnel. There are some different techniques such as flow visualization (Lawson and Barakos, 2011) and "Laser Doppler velocimetry" or Particle Image Velocimetry or are used to measure velocity or concentrations. Hot-wire probes are also been used to find velocity profile in wind tunnels.

<u>Scaling</u>

Scaling in wind tunnels is performed based on flow similarity. If we write Navier-Stokes equations in a dimensionless form, two dimensionless coefficients appear: Reynolds number and Froude number and dimensionless energy equation will contain another dimensionless coefficient that is called Mach number.

Considering effective volume of air as kl^3 where l is the characteristic length and k is a constant regarding to the shape of body we will have:

$$\text{Inertia force} \sim \frac{\rho l^3 V}{t} \qquad\qquad (A.1.1)$$

where ρ is density (kg/m³), V is velocity of the body (m/s) and t is time(s). According to definition of velocity t=l/V and if this substituted with t then we will have:

$$\text{Inertia force} \sim \rho l^2 V^2 \qquad\qquad (A.1.2)$$

viscous and elastic forces according to their definition can be written as:

$$\text{Viscous force} \sim \mu V l \qquad\qquad (A.1.3)$$

$$\text{Elastic force} \sim \rho a^2 l^2 \qquad\qquad (A.1.4)$$

where "a" is speed of sound and gravity force is simply gravity acceleration mass of air:

$$\text{Gravity force} \sim \rho l^3 g \qquad\qquad (A.1.5)$$

dividing inertia force by others gives us three dimensionless coefficients:

$$\text{Mach number} = \frac{inertia\ force}{elasticity\ force} = \frac{V}{a} \qquad\qquad (A.1.6)$$

$$\text{Froude number} = \frac{inertia\ force}{gravity\ force} = \sqrt{\frac{V^2}{lg}} \qquad\qquad (A.1.7)$$

$$\text{Reynolds number} = \frac{inertia\ force}{viscouse\ force} = \frac{\rho V l}{\mu} \qquad\qquad (A.1.8)$$

For wind tunnel experiments these dimensionless numbers are used to scale down the real case geometry into the dimensions of wind tunnel. For stationary setups inside the wind tunnel, Reynolds number is used for scaling. Hence, for the scaled down setup and real case geometry Reynolds number should be equal. Froude number is a very important

81

parameter when model motion is involved. For compressible flow in wind tunnel, Mach numbers should be taken into account (Barlow 1999, White 2002).

A.1.2. CFD models

Computational Fluid Dynamics (CFD) has been used to solve some of fluid dynamics' problems for the past 50 years. CFD models analyze a system with fluid flow, heat transfer and any other associated phenomenon such as chemical reactions. In CFD models numerical methods are used to solve the governing equations simultaneously. There are some methods used in CFD as listed below: "Finite Element Method (FEM)", "Finite Difference Method (FDM)", "Finite Volume Method (FVM)" and other Methods ("such as Spectral Methods, Boundary Element Method", etc.) (Karniadakis 1998)

The difference between these models is their approximation of properties. Each method has its advantages and disadvantages and they can be applied to different problems with respect to problem's geometry, boundary conditions, and other specifications. However, for all of them two major equation is solved:

- "Mass conservation (continuity)" equation
- "Three momentum conservation (Navier-Stokes)" equations

Some other equations can be added to these three main equations if needed such as equations of state, mass transfer kinetics equations These equations are used when the pollutants react with each other, also it should be noticed that the adding these equations can raise computational cost of the model. (Esfahanian 2008, Huffman 2000)

A.1.3. Full Scale experiments

In field researches experiments are done on the real geometry. Hence, this method has some limitations. Most importantly, the cost of doing field experiments is usually very high in comparison to CFD and reduced scale models. In addition, the time that takes to get the results is way more than the other two methods. Furthermore, in field experiments there are many extraneous factors affecting the experiment directly. Nonetheless, the results of these experiments are closest to the reality. In reduced scale models and CFD there are some assumptions which make the conditions of them far from the reality. It is worth noting that in field researches usually regression analysis (Johnson 2001) or Artificial Neural Networks (ANN) (Samarasinghe, 2006) are used to relate the independent variable(s) to dependent variable(s). ANN has been found to be more applicable in the cases that there is nonlinearity in the nature of the problem.

A.2 Sampling size and frequency

Choosing sampling size and frequency are very important in an experiment. For this study, experiments are conducted in 80 KHz frequency and the sampling size is 2×10^6. Figures A.2.1 and A.2.2, show the values of mean velocity and turbulence intensity with respect to sampling size. The sampling size has been increased from 1000 to 2×10^6 by 1000 each time. It can be seen that from sample size of 10^6 on the value of mean velocity and turbulence intensity calculated starts to stabilize and from sample size of 1.8×10^6 both the values are stabled. Thus, the sampling size of 2×10^6 is large enough. These graphs are for a point located 2.2 inches above the cavity in at the leading edge.
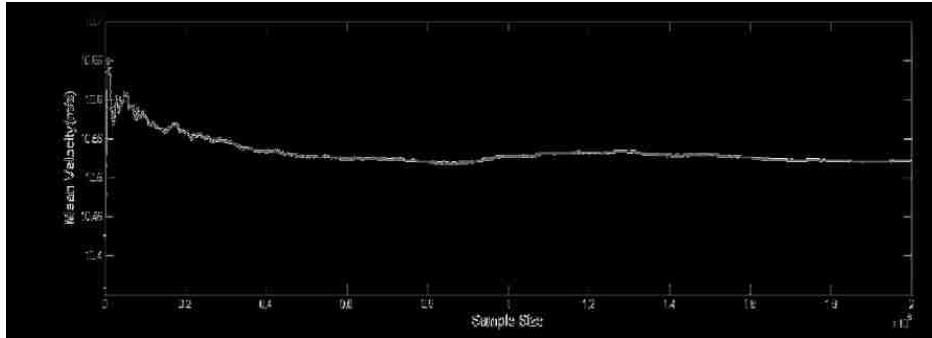
Fig. A.2.1. Mean Velocity Vs. Sampling Size
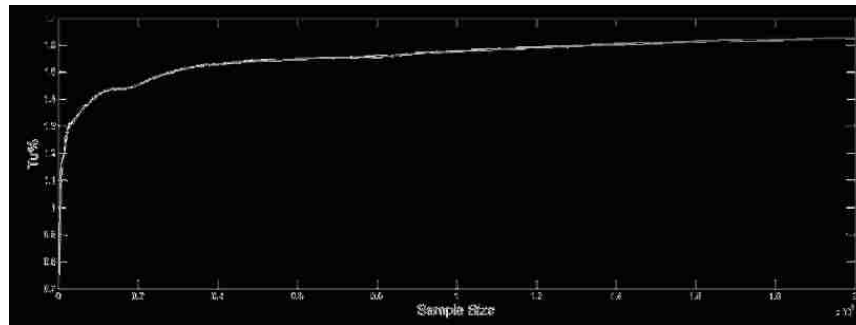
Fig. A.2.2. Turbulence intensity Vs. Sampling size

A.3. Roughness measurement

To make the conditions of the wind tunnel experiment and the CFD model, the surface roughness of the experimental setup has been measured and imported into the CFD model. Therefore, a small piece of the same wood that the experimental setup was made out of was used for the roughness measurement experiment. The surface of the sample wood was painted twice and sanded to create the same surface as the setup. Roughness measurement experiments were conducted by Wyko NT1100 optical profiling system in "Lightweight Materials for Automotive Products and Manufacturing Processes" lab. The results of the experiment can be seen in Fig. A.3. 1 & A.3.2.
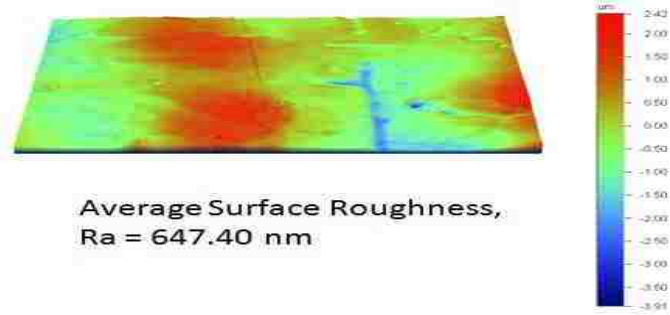
Fig. A.3.1. Average surface roughness contour

Average height: 0.83 ± 0.4 μm
Maximum height: 2.34 μm

Fig. A.3.2. Roughness height plot and average roughness height

A.4. Governing Equations

In order to model flow field in the wind tunnel and over the cavity, governing equations are solved simultaneously. The governing equations include conservation of mass, momentum, energy and species as well as turbulence model. (ANSYS FLUENT manual)

A.4.1. Conservation of mass

The equation for conservation of mass is presented as follows:

$$\frac{\partial \rho}{\partial t} + \vec{\nabla}.(\rho \vec{v}) = S_m \tag{A.4.1}$$

where ρ is the density, $\vec{v}$ is the velocity vector and S_m is the mass source. Mass source is

equal to zero in the flow field except in locations where mass is injected to the flow.

A.4.2. Conservation of momentum

The equation for conservation of momentum is presented in Eq. (A.4.2).

$$\frac{\partial}{\partial t}(\rho\vec{v}) + \nabla.(\rho\vec{v}\vec{v}) = -\nabla p + \nabla.\bar{\bar{\tau}} + \rho\vec{g} + \vec{F} \qquad \text{(A.4.2)}$$

where p is the static pressure, $\bar{\bar{\tau}}$ is the stress tensor, $\rho\vec{g}$ is the gravitational body force and

$\vec{F}$ represents other external body forces. Stress tensor can be explained by Eq. (A.4.3).

$$\bar{\bar{\tau}} = \mu\left[\left(\nabla\vec{v} + \nabla\vec{v}^{\mathrm{T}}\right) - \frac{2}{3}\nabla.\vec{v}I\right] \qquad \text{(A.4.3)}$$

where μ is the molecular viscosity, I is the unit tensor and $\nabla\vec{v}^{\mathrm{T}}$ presents the volume

dilation effect.

A.4.3. Turbulence modeling

Turbulence is always tied with chaos manner and fluctuation. A fluctuating property

can be written in the form of:

$$\varphi = \bar{\varphi} + \varphi' \qquad \text{(A.4.4)}$$

where $\bar{\varphi}$ is the mean value and $\acute{\varphi}$ is the fluctuation part. Therefore, if we replace v in

conservation of mass equation and conservation of momentum and assuming the density

to be constant, there will be some newly generated terms as $\rho\overline{u_i u_j}$ (shear stress) and

turbulent fluxes. Therefore, the number of unknowns will be more than equations and

some additional equations are required. These additional equations are called turbulence

modeling. There is different turbulence modeling approaches developed for Reynolds Averaged Navier Stokes (RANS) – based solution:

- Algebric (zero equation models)

- One equation models : k-model, μ_t models

- Two equation models : k-ε model, k-ω model

- Three equation models $: k$-kl-ω model

- Reynolds Stress Model (RSM)

For this study k-ε (Launder 1974), k-ω standard, (Wilcox 1998), k-ω SST (Menter, 2003), k-kl-ω (Walters, 2008) k-ω SST, k-kl-ω and RSM model have been tested. Among these models k-kl-ω and RSM have shown better agreement with the experimental results. However, k-kl-ω was chosen by some considerations. The k-kl-ω model is a three equation turbulence modeling which has known to have a very good accuracy in predicting boundary layer and transition between laminar and turbulent regime. The model is based on k-ω framework with slightly difference. The third transport equation is included to predict the magnitude of "low-frequency velocity fluctuations" in the pretransitional boundary layer.

The concept of k-ε, k-ω standard, k-ω SST and k-kl-ω are close to each other. They all have turbulent kinetic energy and dissipation rate equations and the difference is in their formulation. Here, the formulation of k-ω SST has been brought as an example. The shear-stress transport (SST) k-ω model which is presented by considering low Reynolds number correction is a modified version of k-ω which is known to have better accuracy in low Re turbulence, i.e. close to the wall region. The SST k-ω model is presented by a

couple of equations based on turbulence kinetic energy (k) and specific dissipation rate (ω) as follows:

$$\frac{\partial}{\partial t}(\rho k) + \nabla.(\rho k \vec{v}) = \nabla.(\Gamma_k \nabla k) + \tilde{G}_k - Y_k \tag{A.4.5}$$

$$\frac{\partial}{\partial t}(\rho \omega) + \nabla.(\rho \omega \vec{v}) = \nabla.(\Gamma_\omega \nabla \omega) + G_\omega - Y_\omega + D_\omega \tag{A.4.6}$$

where $\tilde{G}_k$, G_ω, Γ_k, Γ_ω and D_ω are representing the generation of turbulent kinetic energy, generation of ω, effective diffusivity of turbulent kinetic energy, effective diffusivity of specific dissipation rate and the cross-diffusion term, respectively. Also, Y_k and Y_ω are the dissipation of turbulent kinetic energy and specific dissipation rate, respectively.

Generation of turbulent kinetic energy is defined based on exact equation for its transport as follows:

$$\tilde{G}_k = min(G_k, 10\rho\beta^* k\omega) \tag{A.4.7}$$

$$G_k = -\rho \overline{u_i' u_j'} \frac{\partial u_j}{\partial x_i} \tag{A.4.8}$$

In order to make a consistent definition of G_k with Boussinesq hypothesis it is written as follows:

$$G_k = \mu_t S^2 \tag{A.4.9}$$

where μ_t is the turbulent viscosity and S is the modulus of the mean rate strain-tensor as presented in Eq. (A.4.10).

$$S = \sqrt{2S_{ij}S_{ij}} \tag{A.4.10}$$

The generation of ω is defined as follows:

88

$$G_\omega = \frac{\alpha}{\nu_t} \tilde{G}_k \qquad (A.4.11)$$

where coefficient α is defined as follows:

$$\alpha = \frac{\alpha_\infty}{\alpha^*} \left(\frac{\alpha_0 + Re_t/R_\omega}{1 + Re_t/R_\omega} \right) \qquad (A.4.12)$$

where:

$$\alpha^* = \frac{\beta_i}{3} \qquad (A.4.13)$$

$$\alpha_\infty = F_1 \alpha_{\infty,1} + (1 - F_1)\alpha_{\infty,2} \qquad (A.4.14)$$

$$\alpha_{\infty,1} = \frac{\beta_{i,1}}{\beta_\infty^*} - \frac{\kappa^2}{\sigma_{\omega,1}\sqrt{\beta_0^*}} \qquad (A.4.15)$$

$$\alpha_{\infty,2} = \frac{\beta_{i,2}}{\beta_\infty^*} - \frac{\kappa^2}{\sigma_{\omega,2}\sqrt{\beta_0^*}} \qquad (A.4.16)$$

$$\kappa = 0.41 \qquad (A.4.17)$$

$$F_1 = \tanh(\Phi_1^4) \qquad (A.4.18)$$

$$\Phi_1 = min\left[max\left(\frac{\sqrt{k}}{0.09\omega y}, \frac{500\mu}{\rho y^2 \omega}\right), \frac{4\rho k}{\sigma_{\omega,2}D_\omega^+ y^2}\right] \qquad (A.4.19)$$

$$D_\omega^+ = max\left[2\rho\frac{1}{\sigma_{\omega,2}}\frac{1}{\omega}\frac{\partial k}{\partial x_j}\frac{\partial \omega}{\partial x_j}, 10^{-10}\right] \qquad (A.4.20)$$

$$\beta_i = 0.072 \qquad (A.4.21)$$

$$Re_t = \frac{\rho k}{\mu\omega} \qquad (A.4.22)$$

$$R_\omega = 2.95 \qquad (A.4.23)$$

Dissipation of turbulent kinetic energy is presented in Eq. (A.4.24).

$$Y_k = \rho\beta^*k\omega \tag{A.4.24}$$

Dissipation of specific dissipation rate (Y_ω) equation is presented as follows:

$$Y_\omega = \rho\beta_i\omega^2 \tag{A.4.25}$$

where β_i is defined as presented in Eq. (D.26).

$$\beta_i = F_1\beta_{i,1} + (1 - F_1)\beta_{i,2} \tag{A.4.26}$$

Finally, Eq. (A.4.27) represents the cross-diffusion term.

$$D_\omega = 2(1 - F_1)\rho\sigma_{\omega,2}\frac{1}{\omega}\frac{\partial k}{\partial x_j}\frac{\partial\omega}{\partial x_j} \tag{A.4.27}$$

A.5. Uncertainty in Reynolds number

$$\text{Re} = \frac{\rho \times U_o \times D}{\mu} \tag{A.5.1}$$

Hence the uncertainty of Re would be:

$$W_{\text{Re}} = \sqrt{(\frac{\partial\text{Re}}{\partial\rho}W_\rho)^2 + (\frac{\partial\text{Re}}{\partial U_o}W_{U_o})^2 + (\frac{\partial\text{Re}}{\partial D}W_D)^2} \tag{A.5.2}$$

$$W_{\text{Re}} = \sqrt{(\frac{U_o \times D}{\mu}W_\rho)^2 + (\frac{\rho \times D}{\mu}W_{U_o})^2 + (\frac{\rho \times U_o}{\mu}W_D)^2} \tag{A.5.3}$$

the absolute uncertainty in temperature is:

$$W_T = \sqrt{(W_T)^2{}_{\text{Resolution}} + (W_T)^2{}_{\text{Accuracy}}} \tag{A.5.4}$$

The device used has a resolution of 1^oC, and the accuracy is $\pm1^oC$.

$$W_T = \sqrt{(\frac{0.1}{2})^2 + (1)^2} \cong 1°C \qquad \text{(A.5.5)}$$

The manometer used in the lab has a resolution of 0.01 inHg, and the accuracy is ± 0.05 inHg. Thus, the absolute uncertainty in pressure is:

$$W_P = \sqrt{(\frac{0.1}{2})^2 + (0.05)^2} \cong 170.33 \text{ Pa} \qquad \text{(A.5.6)}$$

Considering the ideal gas equation:

$$P = \rho \times R \times T \qquad \text{(A.5.7)}$$

Hence, the uncertainty allocated with the density will be :

$$W_\rho = \sqrt{(\frac{\partial \rho}{\partial P} W_P)^2 + (\frac{\partial \rho}{\partial T} W_T)^2} \qquad \text{(A.5.8)}$$

$$W_\rho = \sqrt{(\frac{W_P}{RT})^2 + (-\frac{P \times W_T}{R \times T^2})^2} \qquad \text{(A.5.9)}$$

where, the gas constant is:

$$R = 287.05 \frac{J}{kg \times K} \qquad \text{(A.5.10)}$$

The pressure and temperature of the lab are measured to be 99200 Pa and 294 K:

$$W_\rho = \sqrt{(\frac{170.33}{287.05 \times 294})^2 + (-\frac{99200 \times 1}{287.05 \times (294)^2})^2} = 0.00446 \frac{kg}{m^3} \qquad \text{(A.5.11)}$$

As the mean velocity is calculated by Eq. (A.5.12)

$$U_o = \sqrt{\frac{2 \times \Delta P}{\rho_{air}}} \qquad \text{(A.5.12)}$$

The uncertainty allocated with the velocity will be:

$$W_{U_o} = \sqrt{\left(\frac{\partial U_o}{\partial \Delta P} W_{\Delta P}\right)^2 + \left(\frac{\partial U_o}{\partial \rho} W_\rho\right)^2} \qquad \text{(A.5.13)}$$

$$W_{U_o} = \sqrt{\left(\sqrt{\frac{\rho}{2 \times \Delta P}} \times \frac{W_{\Delta P}}{\rho}\right)^2 + \left(\sqrt{\frac{\rho}{2 \times \Delta P}} \times \left(-\frac{\Delta P \times W_{\Delta P}}{\rho^2}\right)^2\right)} \qquad \text{(A.5.14)}$$

The manometer has hysteresis of $\pm\,0.1\%$ which leads to the accuracy is $\pm\,0.5\%$ of the full scale and neglecting the precision error:

$$W_{\Delta P} = \sqrt{(W_{\Delta P})^2{}_{Resolution} + (W_{\Delta P})^2{}_{Hysteresis}} \qquad \text{(A.5.15)}$$

$$W_{\Delta P} = 0.00127 \text{ Kpa} \qquad \text{(A.5.16)}$$

In this study, the manometer reading was $\Delta P = 0.0532$ kPa for $U_o = 9.5\,\frac{m}{s}$, hence:

$$W_{U_o} = \sqrt{\left(\sqrt{\frac{1.18}{2 \times 53.2}} \times \frac{1.27}{1.18}\right)^2 + \left(\sqrt{\frac{1.18}{2 \times 53.2}} \times \left(-\frac{53.2 \times 0.00448}{1.18^2}\right)^2\right)} = 0.119\,\frac{m}{s} \qquad \text{(A.5.17)}$$

The digital caliper has 0.01 mm resolution giving the accuracy is ± 0.025 mm.

$$W_D \sqrt{(W_D)^2{}_{Resolution} + (W_D)^2{}_{Accuracy}} = 0.0255\ mm \qquad \text{(A.5.18)}$$

Now importing the values into equation (A.5.3) will give the uncertainty for Reynolds number = 123112

$$W_{Re} = \sqrt{\left(\frac{9.5 \times 0.2032}{1.83 \times 10^{-5}} \times 0.00446\right)^2 + \left(\frac{1.18 \times 0.2032}{1.83 \times 10^{-5}} \times 0.119\right)^2 + \left(\frac{1.18 \times 9.5}{1.83 \times 10^{-5}} \times 0.0000255\right)^2} = 471$$

$$Re = 123112 \pm 471$$

A.6. Uncertainty of hot-wire data

The uncertainty in hot-wire measurement comes from three sources:

- Uncertainty in calibration process

- Uncertainty in data acquisition

- Uncertainty in post processing

Uncertainty in calibration process has been reported to be ≈ 3% (Jorgenson, 2002). The uncertainty in data acquisition can have different sources such as humidity change and pressure change during the measurement. In addition, the resolution of the data acquisition card is an important factor to be taken into account.

Among the factors important for uncertainty allocated with data acquisition, uncertainty due to the A/D bar resolution and uncertainty of the change in pressure while running the experiment are considered.

The uncertainty of hot-wire voltage is ½ of the resolution of the A/D bar. The A/D board used in this work is 12- bit which leads to a resolution of 2^{12}. As the output voltage is within the range of 10 volts, the total uncertainty of the output voltage can be written as:

$$\Delta E = \pm \left(\frac{1}{2}\right) \times 10 \times 2^{-12} = 0.0012 \tag{A.6.1}$$

As the velocity is calculated via the voltage outputs, the propagation of this uncertainty in the spontaneous velocity calculation would be:

$$\Delta U_{aqu,1} = \frac{dU}{dE} \Delta E \tag{A.6.2}$$

The outcome of calibration process is five coefficients which relate the voltage outcome to velocity as explained in chapter 3.

$$U = C_0 + C_1 E + C_2 E^2 + C_3 E^3 + C_4 E^4 \qquad \text{(A.6.3)}$$

Hence, $\frac{\Delta E_{aqu,1}}{U}$ can be written in the form of:

$$\frac{\Delta E_{aqu,1}}{U} = \left(\frac{C_1 + 2C_2 E + 3C_3 E^2 + 4C_4 E^3}{C_0 + C_1 E + C_2 E^2 + C_3 E^3 + C_4 E^4}\right) \Delta E \qquad \text{(A.6.4)}$$

In addition the uncertainty allocated with change in ambient pressure during the experiment has been recorded as: (Jorgenson, 2002)

$$\frac{\Delta E_{aqu,2}}{U} = \pm 0.006 \qquad \text{(A.6.5)}$$

Therefore:

$$\frac{\Delta E_{aqu,tot}}{U} = \pm \sqrt{\left(\frac{\Delta E_{aqu,1}}{U}\right)^2 + \left(\frac{\Delta E_{aqu,2}}{U}\right)^2} \qquad \text{(A.6.6)}$$

In the post processing of hot-wire data, there is a small amount of uncertainty allocated with truncation error in the calculation by MATLAB. As the accuracy used in all the calculations is 0.0001, hence:

$$\frac{\Delta E_{post}}{U} = \pm \frac{0.0001}{2} = \frac{\pm 0.00005}{U} \qquad \text{(A.6.7)}$$

In summary, the uncertainty of one spontaneous value of velocity calculated at each point can be written in the form of:

$$\frac{\Delta U}{U} = \pm \sqrt{\left(\frac{\Delta E_{cal,tot}}{U}\right)^2 + \left(\frac{\Delta E_{aqu,tot}}{U}\right)^2 + \left(\frac{\Delta E_{post,tot}}{U}\right)^2} \qquad \text{(A.6.8)}$$

where:

$$\frac{\Delta E_{cal,tot}}{U} = \pm 0.03 \qquad \text{(A.6.9)}$$

It has been mentioned in chapter IV that the value of mean velocity at each point of measurement is calculated by averaging all the spontaneous voltage values. Assuming a sample of the size N is in hand velocity at each point can be written as:

$$U_{mean} = \frac{1}{N}\sum_{i=1}^{N} U_i \qquad \text{(A.6.10)}$$

Considering $\frac{\Delta U}{U} = \vartheta$ and $\overline{\Delta U} = \Delta \overline{U}$ it can be written that:

$$\overline{\Delta U}_{mean} = \overline{\vartheta U} = \vartheta \overline{U} = \vartheta U_{mean} \qquad \text{(A.6.11)}$$

$$\frac{\overline{\Delta U}_{mean}}{U_{mean}} = \vartheta = \frac{\Delta U}{U} \qquad \text{(A.6.12)}$$

A MATLAB code was developed to calculate the total amount of uncertainty and the relative uncertainty was calculated as to be 3.0005%. However, this is the bias uncertainty allocated with the hotwire measurements. In this work, for Lines 1, 2 and 3 (see chapter IV) five replications of hotwire measurements were in hand. Therefore, the total uncertainty consists of both relative uncertainty that has been calculated above and the uncertainty in measurements from 5 replications.

Hotwire results are known to have the biggest uncertainty very close to walls and boundaries. Therefore, the total uncertainty has been calculated at on Line 3 that has the closest distance to wall as an example.

The total uncertainty would be:

$$W_{Tot} = \sqrt{(W_{Bias})^2 + (W_{Rep})^2} \qquad (A.6.13)$$

In this work, 5 replications are available, and for the closest point on Line 3 to the wall the velocity measurements are:

Experiment A = 7.75 [m/s], Experiment B = 7.14 [m/s], Experiment C = 7.68 [m/s], Experiment D = 8.6 [m/s] and Experiment E = 8.12 [m/s].

Hence, U_{mean} = 7.85 [m/s] and the standard deviation of the measurements would be 0.54.

Therefore, $W_{Bias} = \Delta U = 7.85 \times 0.03 = 0.23$ [m/s].

Moreover, according to the definition and using student's t-distribution with confidence interval of 95% we have:

$$W_{Rep} = \frac{t_{\vartheta,0.95} \times S}{\sqrt{N}} \qquad (A.6.14)$$

where N is the number of measurements and ϑ is the degree of freedom and is N-1 =4. Hence, from the table, $t_{4,0.95}$ = 2.776 and W_{Rep} = 0.67 [m/s].

and

$$W_{Tot} = \sqrt{(0.23)^2 + (0.67)^2} = 1.13 \qquad (A.6.15)$$

and the relative total uncertainty is

$$\frac{W_{Tot}}{U_{mean}} = \frac{1.13}{7.85} = 14\%. \qquad (A.6.16)$$

A.7. Turbulence Decay

As explained in the thesis, the value of Tu is set at the inlet and the level of turbulence drops till flow reaches to the cavity. Figures A.7.1, A.7.2 and A.7.3 show the turbulence intensity at inlet and 1 inch (25.4 mm) before the setup. These plots are for $U_{upstream}$ of 9.5 m/s and cavity with aspect ratio of 2.
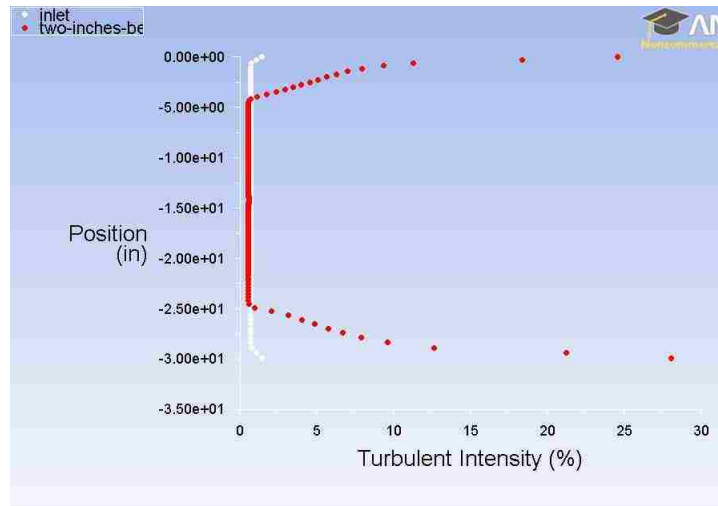
Fig.A.7.1. Turbulence decay for the case with Tu= 0.67% at inlet
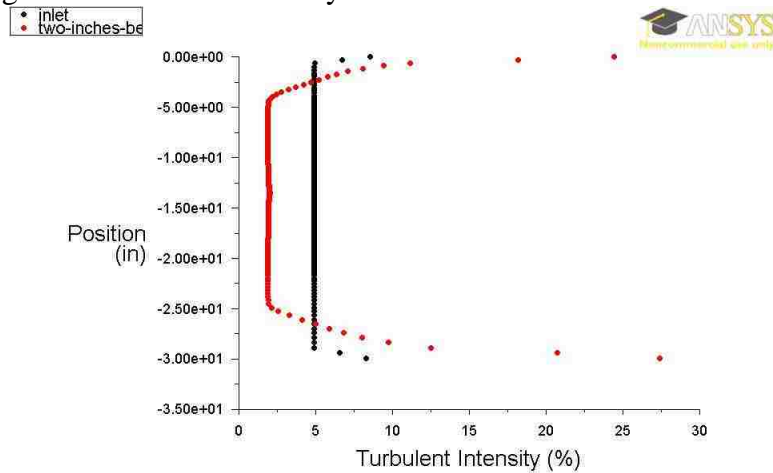
Fig.A.7.2. Turbulence decay for the case with Tu= 5% at inlet
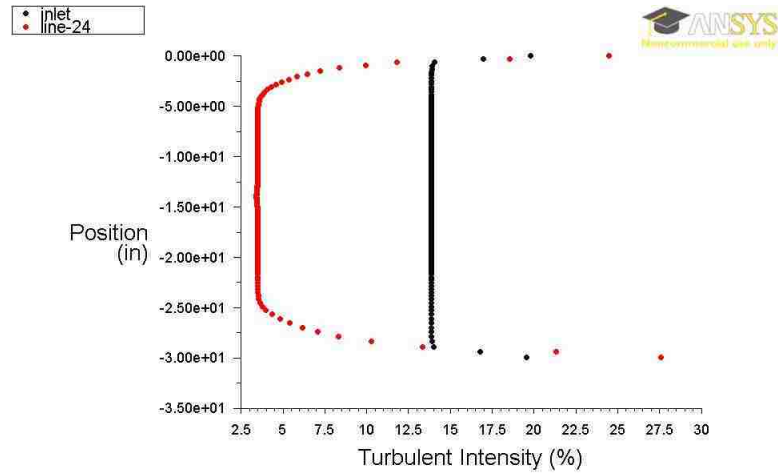
Fig.A.7.3. Turbulence decay for the case with Tu= 15% at inlet

It can be seen that for the case with Tu of 15% at inlet the turbulence decay is most severe. For the case with 0.67% of turbulence at inlet, the level of turbulence is 0.67% when flow reaches to the cavity and for the case with Tu of 5% at inlet, the level of turbulence is 1.2% before the cavity and for the case with Tu of 15% at inlet, flow has 4.1% turbulence intensity when it reaches to the cavity.

A.8. Results from the cases not included in parametric study

In this section, results from CFD simulation that have not been presented in the body of thesis are presented.

A.8.1. Effect of upstream velocity

The effect of upstream velocity was studied for the cavity with aspect ratio of 2 and Tu of 5% for three upstream velocities (5, 9.5 and 15 m/s). In this section, the effect of $U_{upstream}$ is studied for other turbulence intensities and aspect ratios. Figure A.8.1shows flow streamlines for different upstream velocities for the cavity with W/D of 2 and at Tu of 0.67%.

a) $U_{upstream}$ = 5 m/s,   b) $U_{upstream}$ = 9.5 m/s

c) $U_{upstream}$ = 15 m/s
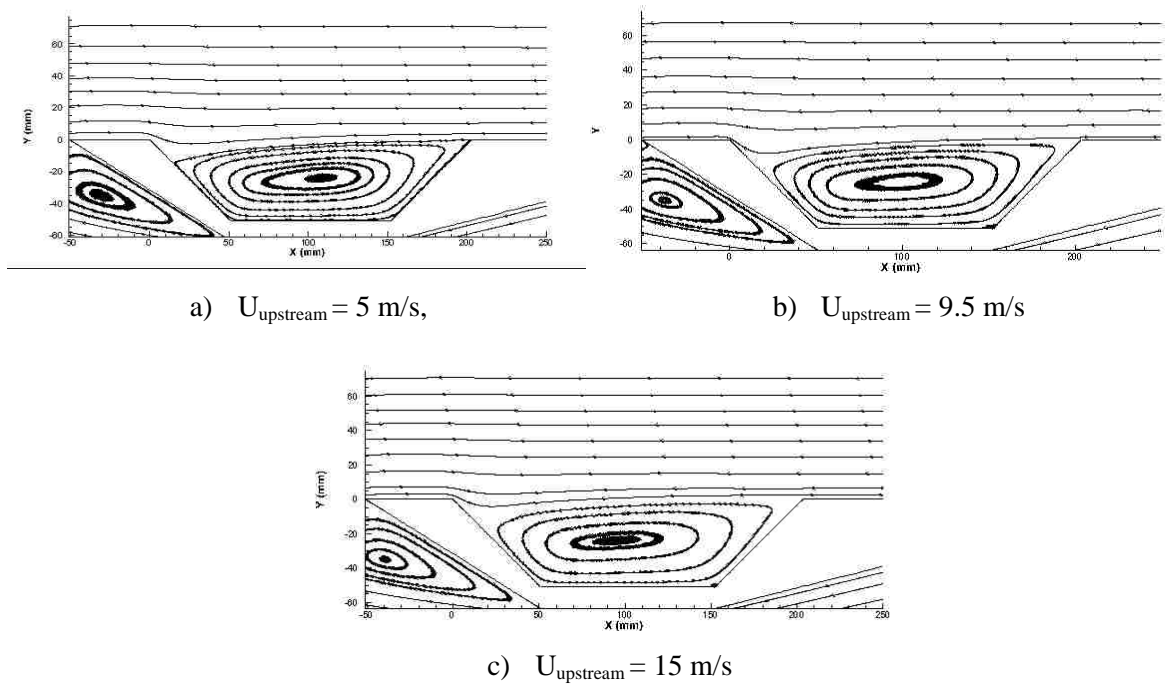
Fig. A.8.1. Flow streamlines above and inside the cavity for (W/D=2, Tu=0.67%)

Figure A.8.2 shows flow streamlines for three upstream velocities for the cavity with aspect ratio of 4 and at Tu of 5%.

a) $U_{upstream} = 5$ m/s,

b) $U_{upstream} = 9.5$ m/s

c) $U_{upstream} = 15$ m/s
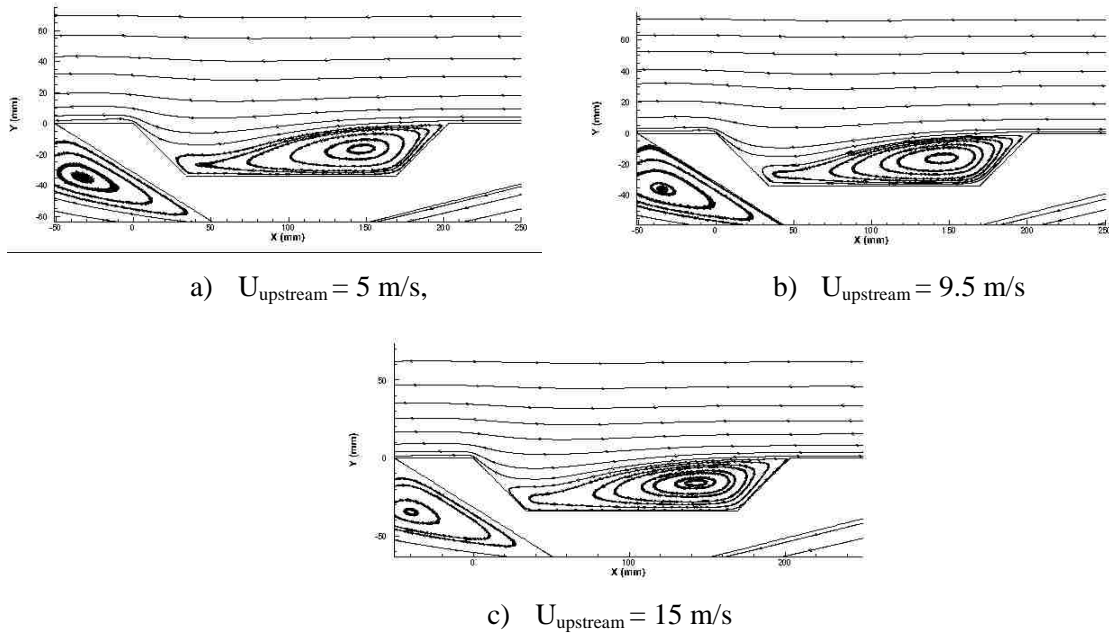
Fig. A.8.2. Flow streamlines above and inside the cavity for (W/D=4, Tu= 5%)

Figure A.8.3 shows flow streamlines for three upstream velocities for the cavity with aspect ratio of 6 and at Tu of 5%.

a) $U_{upstream} = 5$ m/s,

b) $U_{upstream} = 9.5$ m/s

c) $U_{upstream} = 15$ m/s
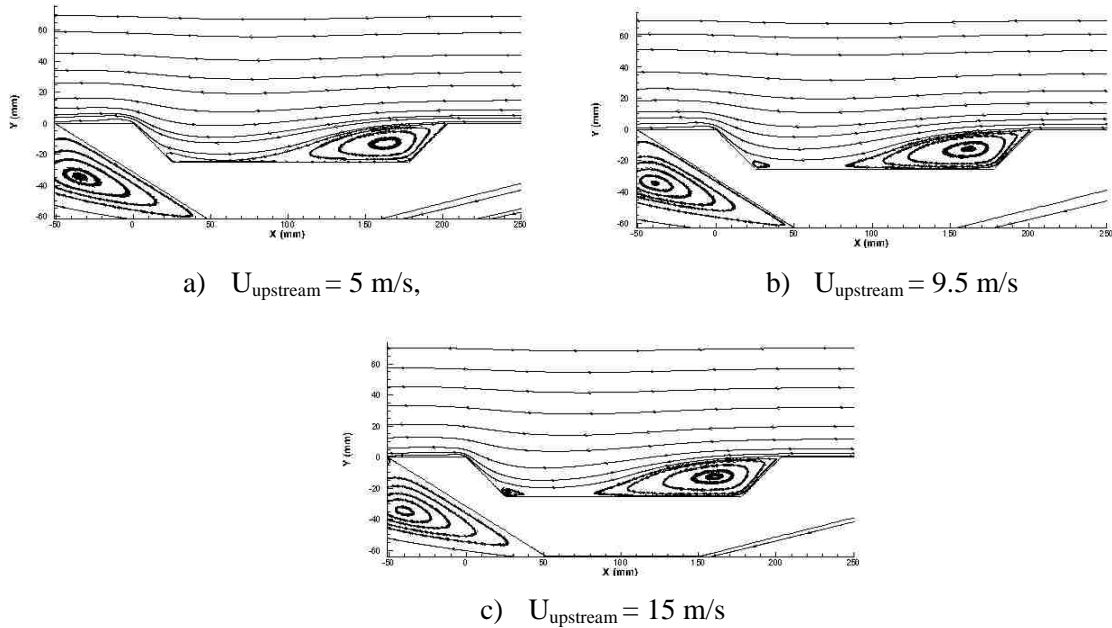
Fig. A.8.3. Flow streamlines above and inside the cavity for (W/D=6, Tu= 5%)

It can be seen that for all the cases with increasing $U_{upstream}$, the center of vortex has been moved toward the leading edge and the normalized volumetric flow rate of air exchanged at the mouth of cavity increases. These results are in agreement with the results presented in the body of the thesis and lead to the same conclusion. However, it can be seen that for cavity with aspect ratio of 2, this movement of the center of vortex is more detectable.

A.8.2. Effect of turbulence intensity

The effect of turbulence intensity was studied for the cavity with aspect ratio of 2 and with upstream velocity of 9.5 m/s for three levels of turbulence at inlet (0.67%, 5% and 15%). In this section, the effect of Tu is clarified for other upstream velocities and

aspect ratios. Figure A.8.4 shows flow streamlines for different upstream velocities for the cavity with W/D of 2 and at $U_{upstream}$ of 5 m/s.

a) Tu= 0.67%   b) Tu= 5%

c) Tu= 15%
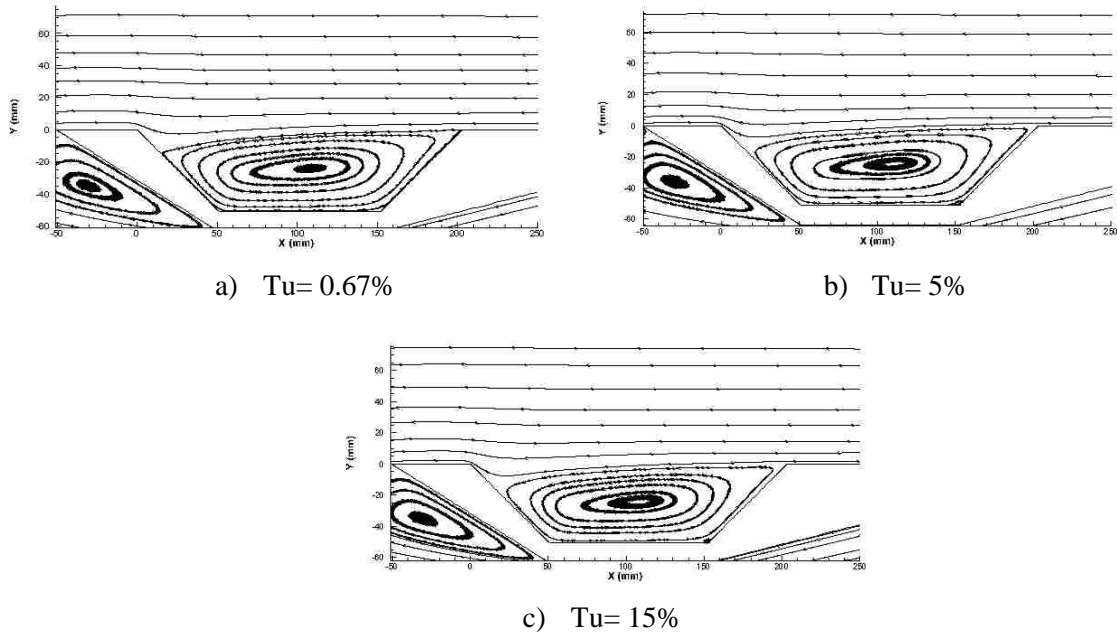
Fig. A.8.4. Flow streamlines above and inside the cavity for (W/D=2, Uupstream = 5 m/s)

Figure A.8.5 shows flow streamlines for different upstream velocities for the cavity with W/D of 4 and at $U_{upstream}$ of 15 m/s.

a)   Tu= 0.67%   b)   Tu= 5%
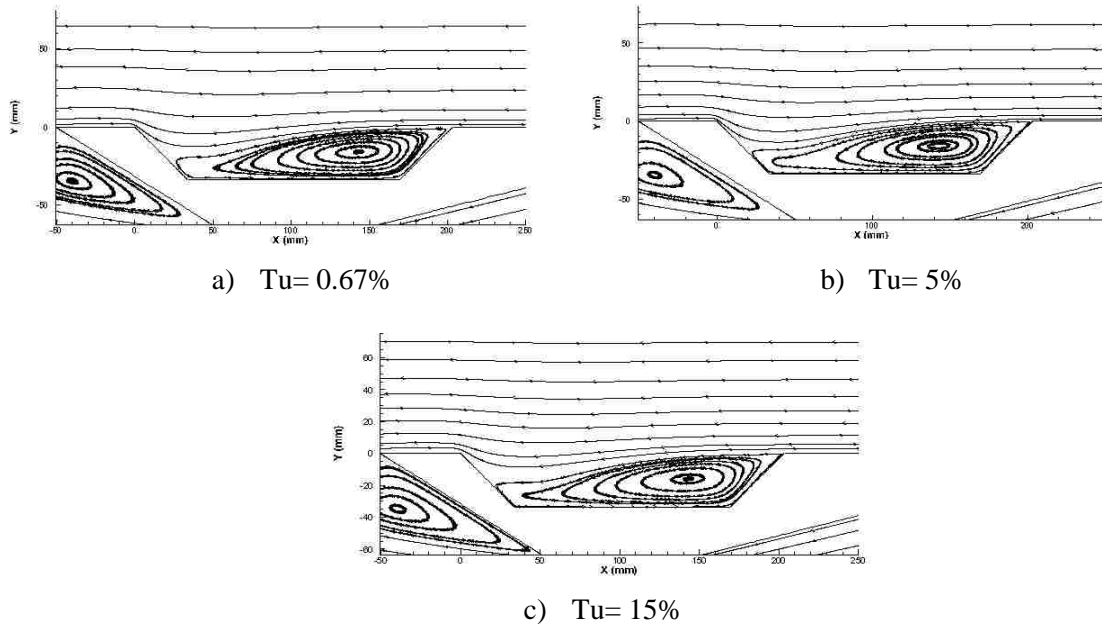
c)   Tu= 15%

Fig. A.8.5. Flow streamlines above and inside the cavity for (W/D=4, Uupstream =15 m/s)

Figure A.8.6 shows flow streamlines for different upstream velocities for the cavity with W/D of 4 and at $U_{upstream}$ of 15 m/s.

a)   Tu= 0.67%   b)   Tu= 5%
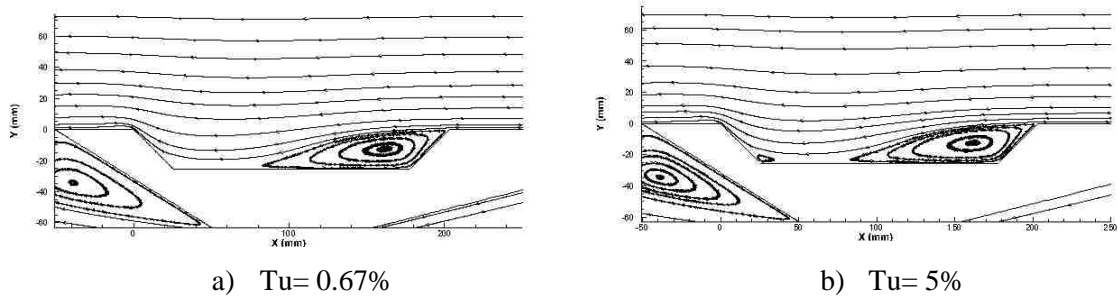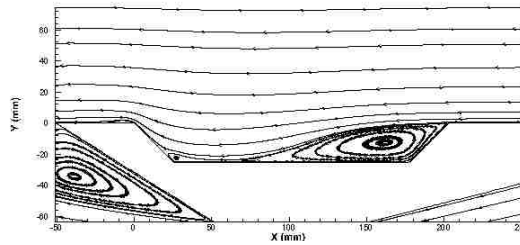
c) Tu= 15%

Fig. A.8.6. Flow streamlines above and inside the cavity for (W/D=4, Uupstream =9.5 m/s)

It can be seen that Tu does not affect the position of X and Y and $Q_{normalized}$ significantly. However, it can be seen that in aspect ratio of 2 the center of vortex is moved toward the leading edge a bit.

A.8.3. Effect of aspect ratio

The effect of aspect ratio was studied for the cavity with $U_{upstream}$ of 9.5 m/s and with Tu of 5% for three aspect ratios (2, 4 and 6). In this section, the effect of W/D ratio is clarified for other upstream velocities and aspect ratios. Figure A.8.7 shows flow streamlines for different upstream velocities for the cavity with $U_{upstream}$ of 9.5 m/s and Tu of 0.67%.

a) W/D= 2

b) W/D= 4

c) W/D= 6
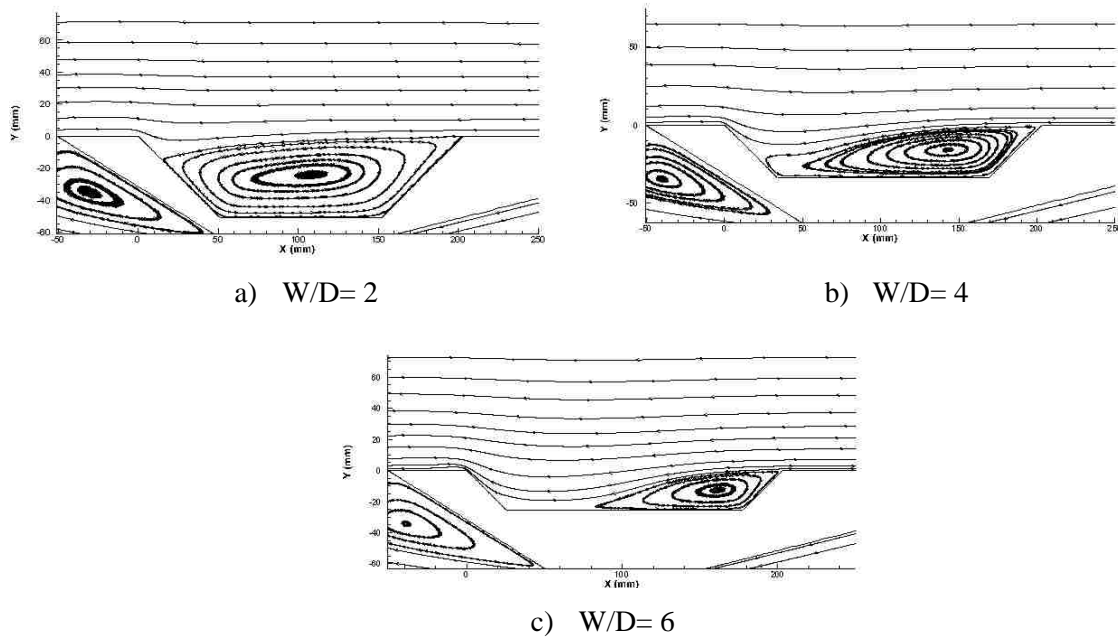
Fig. A.8.7. Flow streamlines above and inside the cavity for (Uupstream = 9.5 m/s, Tu = 0.67%)

It can be illustrated that with increasing the aspect ratio, the normalized volumetric flow rate of exchanged air at the mouth of the cavity increases drastically. Moreover, the center of vortex moves toward the leading edge. These conclusions are in agreement with the conclusions made from the parametric study designed.

A.9. Statistical model selection

As explained in the thesis, for the statistical analysis, only significant factors were included and insignificant factors were omitted from the model. All the factors and interactions between them were imported in to the full model. Then, insignificant factors were dropped.

For $Q_{normalized}$ as the response and using the full factorial model:

```
Factor            Type   Levels  Values
W/D               fixed      3   2, 4, 6
Tu%               fixed      3   0.67, 5.00, 15.00
Uupstream (m/s)   fixed      3   5.0, 9.5, 15.0


Analysis of Variance for Qnormalized (1/s), using Adjusted SS for Tests

Source                    DF     Seq SS    Adj SS    Adj MS    F  P
W/D                       2     826.928   826.928   413.464   **
Tu%                       2       0.001     0.001     0.000   **
Uupstream (m/s)           2     467.688   467.688   233.844   **
W/D*Tu%                   4       0.004     0.004     0.001   **
W/D*Uupstream (m/s)       4     137.399   137.399    34.350   **
Tu%*Uupstream (m/s)       4       0.003     0.003     0.001   **
W/D*Tu%*Uupstream (m/s)   8       0.009     0.009     0.001   **
Error                     0          *         *         *
Total                    26    1432.031

** Denominator of F-test is zero.


S = *
```

It can be seen that the model cannot give results and this happens when one of the factors has correlation with others and is not significant. Dropping the second order interaction (W/D*Tu*$U_{upstream}$) the results will be:

```
Source                 DF     Seq SS    Adj SS    Adj MS          F      P
W/D                    2     826.928   826.928   413.464   379534.47  0.000
Tu%                    2       0.001     0.001     0.000        0.35  0.715
Uupstream (m/s)        2     467.688   467.688   233.844   214654.43  0.000
W/D*Tu%                4       0.004     0.004     0.001        0.82  0.549
W/D*Uupstream (m/s)    4     137.399   137.399    34.350    31530.96  0.000
Tu%*Uupstream (m/s)    4       0.003     0.003     0.001        0.63  0.654
Error                  8       0.009     0.009     0.001
Total                 26    1432.031
```

```
S = 0.0330060    R-Sq = 100.00%    R-Sq(adj) = 100.00%
```

It can be seen that Tu% and interactions of Tu% are not significant as the P-values of them are greater than 0.05. Hence, these variables have been omitted in the model presented in the thesis.

And final model will be:

```
Factor              Type   Levels  Values
W/D                 fixed       3  2, 4, 6
Uupstream (m/s)     fixed       3  5.0, 9.5, 15.0


Analysis of Variance for Qnormalized (1/s), using Adjusted SS for Tests

Source                DF   Seq SS  Adj SS  Adj MS          F      P
W/D                    2   826.88  826.88  413.44  455053.27  0.000
Uupstream (m/s)        2   467.65  467.65  233.83  257359.57  0.000
W/D*Uupstream (m/s)    4   137.41  137.41   34.35   37810.22  0.000
Error                 18     0.02    0.02    0.00
Total                 26  1431.96


S = 0.0301423    R-Sq = 100.00%    R-Sq(adj) = 100.00%


Unusual Observations for Qnormalized (1/s)

      Qnormalized
Obs        (1/s)      Fit  SE Fit  Residual  St Resid
 20      17.3100  17.2580  0.0174    0.0520     2.11 R
 23      17.2060  17.2580  0.0174   -0.0520    -2.11 R

R denotes an observation with a large standardized residual.
```

<u>For x/L as the response the full model's result will be:</u>

```
Factor              Type   Levels  Values
W/D                 fixed       3  2, 4, 6
Tu%                 fixed       3  0.67, 5.00, 15.00
Uupstream (m/s)     fixed       3  5.0, 9.5, 15.0


Analysis of Variance for x/L, using Adjusted SS for Tests

Source                DF    Seq SS    Adj SS    Adj MS   F   P
W/D                    2  0.383356  0.383356  0.191678  **
Tu%                    2  0.002022  0.002022  0.001011  **
```

```
Uupstream (m/s)             2  0.004467  0.004467  0.002233   **
W/D*Tu%                     4  0.001889  0.001889  0.000472   **
W/D*Uupstream (m/s)         4  0.002244  0.002244  0.000561   **
Tu%*Uupstream (m/s)         4  0.000044  0.000044  0.000011   **
W/D*Tu%*Uupstream (m/s)     8  0.000244  0.000244  0.000031   **
Error                       0      *         *         *
Total                      26  0.394267

** Denominator of F-test is zero.


S = *
```

And deleting the interaction of (W/D*Tu%*U$_{upstream}$) the model gives:

```
Factor           Type   Levels  Values
W/D              fixed      3    2, 4, 6
Tu%              fixed      3    0.67, 5.00, 15.00
Uupstream (m/s)  fixed      3    5.0, 9.5, 15.0


Analysis of Variance for x/L, using Adjusted SS for Tests

Source              DF    Seq SS    Adj SS    Adj MS        F      P
W/D                  2  0.383356  0.383356  0.191678  6273.09  0.000
Tu%                  2  0.002022  0.002022  0.001011    33.09  0.000
Uupstream (m/s)      2  0.004467  0.004467  0.002233    73.09  0.000
W/D*Tu%              4  0.001889  0.001889  0.000472    15.45  0.001
W/D*Uupstream (m/s)  4  0.002244  0.002244  0.000561    18.36  0.000
Tu%*Uupstream (m/s)  4  0.000044  0.000044  0.000011     0.36  0.828
Error                8  0.000244  0.000244  0.000031
Total               26  0.394267


S = 0.00552771   R-Sq = 99.94%   R-Sq(adj) = 99.80%
```

It can be seen that all factors except the interaction of Tu% and U$_{upstream}$ are significant and this variable has been omitted from the model presented in the thesis.

And the final model is:

```
Factor           Type   Levels  Values
W/D              fixed      3    2, 4, 6
Tu%              fixed      3    0.67, 5.00, 15.00
Uupstream (m/s)  fixed      3    5.0, 9.5, 15.0


Analysis of Variance for x/L, using Adjusted SS for Tests

Source              DF    Seq SS    Adj SS    Adj MS        F      P
W/D                  2  0.383356  0.383356  0.191678  6273.09  0.000
Tu%                  2  0.002022  0.002022  0.001011    33.09  0.000
Uupstream (m/s)      2  0.004467  0.004467  0.002233    73.09  0.000
W/D*Tu%              4  0.001889  0.001889  0.000472    15.45  0.001
```

```
W/D*Uupstream (m/s)   4  0.002244  0.002244  0.000561   18.36  0.000
Error                 8  0.000244  0.000244  0.000031
Total                26  0.394267


S = 0.00552771   R-Sq = 99.94%   R-Sq(adj) = 99.80%
```

Considering y/D as the response, the full model results:

```
Factor           Type  Levels  Values
W/D              fixed      3  2, 4, 6
Tu%              fixed      3  0.67, 5.00, 15.00
Uupstream (m/s)  fixed      3  5.0, 9.5, 15.0


Analysis of Variance for y/L, using Adjusted SS for Tests

Source                  DF     Seq SS     Adj SS     Adj MS   F  P
W/D                      2  0.0366000  0.0366000  0.0183000  **
Tu%                      2  0.0000000  0.0000000  0.0000000  **
Uupstream (m/s)          2  0.0000000  0.0000000  0.0000000  **
W/D*Tu%                  4  0.0000000  0.0000000  0.0000000  **
W/D*Uupstream (m/s)      4  0.0000000  0.0000000  0.0000000  **
Tu%*Uupstream (m/s)      4  0.0000000  0.0000000  0.0000000  **
W/D*Tu%*Uupstream (m/s)  8  0.0000000  0.0000000  0.0000000  **
Error                    0          *          *          *
Total                   26  0.0366000

** Denominator of F-test is zero.


S = *
```

And omitting the interaction of (W/D*Tu%*U$_{upstream}$) the model gives:

```
Factor           Type  Levels  Values
W/D              fixed      3  2, 4, 6
Tu%              fixed      3  0.67, 5.00, 15.00
Uupstream (m/s)  fixed      3  5.0, 9.5, 15.0


Analysis of Variance for y/L, using Adjusted SS for Tests

Source               DF     Seq SS     Adj SS     Adj MS   F  P
W/D                   2  0.0366000  0.0366000  0.0183000  **
Tu%                   2  0.0000000  0.0000000  0.0000000  **
Uupstream (m/s)       2  0.0000000  0.0000000  0.0000000  **
W/D*Tu%               4  0.0000000  0.0000000  0.0000000  **
W/D*Uupstream (m/s)   4  0.0000000  0.0000000  0.0000000  **
Tu%*Uupstream (m/s)   4  0.0000000  0.0000000  0.0000000  **
Error                 8  0.0000000  0.0000000  0.0000000
Total                26  0.0366000

** Denominator of F-test is zero.


S = 7.985378E-18   R-Sq = 100.00%   R-Sq(adj) = 100.00%
```

Deleting the other interactions will lead to:

```
Factor              Type   Levels  Values
W/D                 fixed      3   2, 4, 6
Tu%                 fixed      3   0.67, 5.00, 15.00
Uupstream (m/s)     fixed      3   5.0, 9.5, 15.0


Analysis of Variance for y/L, using Adjusted SS for Tests

Source             DF      Seq SS      Adj SS      Adj MS   F   P
W/D                 2   0.0366000   0.0366000   0.0183000  **
Tu%                 2   0.0000000   0.0000000   0.0000000  **
Uupstream (m/s)     2   0.0000000   0.0000000   0.0000000  **
Error              20   0.0000000   0.0000000   0.0000000
Total              26   0.0366000

** Denominator of F-test is zero.


S = 9.342556E-18   R-Sq = 100.00%   R-Sq(adj) = 100.00%
```

This shows that only one factor is affecting y/D. One way ANOVA analysis on

y/D with Tu%, $U_{upstream}$ and W/D will show which one of the factors are significant:

One-way ANOVA: y/L versus W/D

```
Source  DF          SS          MS   F   P
W/D      2   0.0366000   0.0183000   *   *
Error   24   0.0000000   0.0000000
Total   26   0.0366000

S = 0   R-Sq = 100.00%   R-Sq(adj) = 100.00%


                                Individual 95% CIs For Mean Based on
                                Pooled StDev
Level  N       Mean      StDev  ----+---------+---------+---------+-----
2      9  -0.470000   0.000000                      *
4      9  -0.420000   0.000000                                      *
6      9  -0.510000   0.000000  *
                                ----+---------+---------+---------+-----
                                 -0.500    -0.475    -0.450    -0.425

Pooled StDev = 0.000000
```

One-way ANOVA: y/L versus Tu%

```
Source  DF        SS        MS      F       P
Tu%      2   0.00000   0.00000   0.00   1.000
Error   24   0.03660   0.00153
Total   26   0.03660

S = 0.03905   R-Sq = 0.00%   R-Sq(adj) = 0.00%
```

```
                              Individual 95% CIs For Mean Based on
                              Pooled StDev
Level   N     Mean    StDev  --------+---------+---------+---------+
 0.67   9  -0.46667  0.03905 (----------------*----------------)
 5.00   9  -0.46667  0.03905 (----------------*----------------)
15.00   9  -0.46667  0.03905 (----------------*----------------)
                              --------+---------+---------+---------+
                                   -0.480    -0.465    -0.450    -0.435

Pooled StDev = 0.03905
```

One-way ANOVA: y/L versus Uupstream (m/s)

```
Source           DF      SS      MS      F      P
Uupstream (m/s)   2  0.00000  0.00000  0.00  1.000
Error            24  0.03660  0.00153
Total            26  0.03660

S = 0.03905   R-Sq = 0.00%   R-Sq(adj) = 0.00%


                              Individual 95% CIs For Mean Based on
                              Pooled StDev
Level   N     Mean    StDev  --------+---------+---------+---------+
 5.0    9  -0.46667  0.03905 (----------------*----------------)
 9.5    9  -0.46667  0.03905 (----------------*----------------)
15.0    9  -0.46667  0.03905 (----------------*----------------)
                              --------+---------+---------+---------+
                                   -0.480    -0.465    -0.450    -0.435

Pooled StDev = 0.03905
```

Therefore, Tu% and $U_{upstream}$ are not significant factors and W/D explains 100% of R-Sq. This can be observed from Table- 6 as well. It can be seen that y/D only varies with W/D ratio.

For cavity type and number of vortexes exactly same manner can be observed.

For the cavity type as the response:

```
Factor           Type   Levels  Values
W/D              fixed      3   2, 4, 6
Tu%              fixed      3   0.67, 5.00, 15.00
Uupstream (m/s)  fixed      3   5.0, 9.5, 15.0


Analysis of Variance for Cavity type, using Adjusted SS for Tests

Source                   DF   Seq SS   Adj SS   Adj MS    F   P
W/D                       2  6.00000  6.00000  3.00000   **
```

```
Tu%                           2  0.00000  0.00000  0.00000  **
Uupstream (m/s)               2  0.00000  0.00000  0.00000  **
W/D*Tu%                       4  0.00000  0.00000  0.00000  **
W/D*Uupstream (m/s)           4  0.00000  0.00000  0.00000  **
Tu%*Uupstream (m/s)           4  0.00000  0.00000  0.00000  **
W/D*Tu%*Uupstream (m/s)       8  0.00000  0.00000  0.00000  **
Error                         0        *        *        *
Total                        26  6.00000

** Denominator of F-test is zero.



S = *
```

And omitting the (W/D*Tu%*U$_{upstream}$) interaction:

```
Factor            Type   Levels  Values
W/D               fixed      3   2, 4, 6
Tu%               fixed      3   0.67, 5.00, 15.00
Uupstream (m/s)   fixed      3   5.0, 9.5, 15.0


Analysis of Variance for Cavity type, using Adjusted SS for Tests

Source                   DF   Seq SS   Adj SS   Adj MS    F  P
W/D                       2  6.00000  6.00000  3.00000  **
Tu%                       2  0.00000  0.00000  0.00000  **
Uupstream (m/s)           2  0.00000  0.00000  0.00000  **
W/D*Tu%                   4  0.00000  0.00000  0.00000  **
W/D*Uupstream (m/s)       4  0.00000  0.00000  0.00000  **
Tu%*Uupstream (m/s)       4  0.00000  0.00000  0.00000  **
Error                     8  0.00000  0.00000  0.00000
Total                    26  6.00000

** Denominator of F-test is zero.


S = 9.668031E-17   R-Sq = 100.00%   R-Sq(adj) = 100.00%
```

And omitting other interaction the model will give:

```
Factor            Type   Levels  Values
W/D               fixed      3   2, 4, 6
Tu%               fixed      3   0.67, 5.00, 15.00
Uupstream (m/s)   fixed      3   5.0, 9.5, 15.0


Analysis of Variance for Cavity type, using Adjusted SS for Tests

Source              DF  Seq SS  Adj SS  Adj MS    F  P
W/D                  2  6.0000  6.0000  3.0000  **
Tu%                  2  0.0000  0.0000  0.0000  **
Uupstream (m/s)      2  0.0000  0.0000  0.0000  **
Error               20  0.0000  0.0000  0.0000
Total               26  6.0000
```
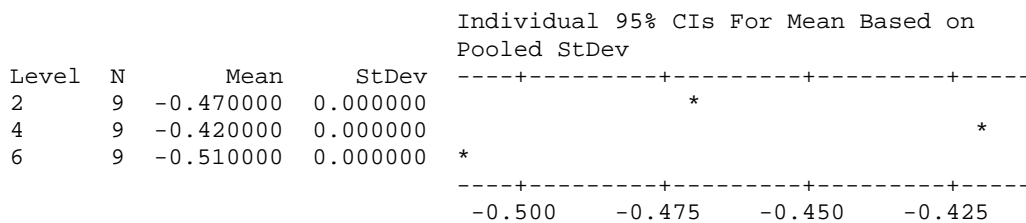
```
** Denominator of F-test is zero.


S = 9.093855E-17   R-Sq = 100.00%   R-Sq(adj) = 100.00%
```

One-way ANOVA: Cavity type versus W/D

```
Source  DF        SS        MS    F   P
W/D      2  6.000000  3.000000  *   *
Error   24  0.000000  0.000000
Total   26  6.000000


S = 0   R-Sq = 100.00%   R-Sq(adj) = 100.00%



                                  Individual 95% CIs For Mean Based on Pooled
                                  StDev
Level  N    Mean    StDev    +---------+---------+---------+---------
2      9  0.00000  0.00000    *
4      9  0.00000  0.00000    *
6      9  1.00000  0.00000                                          *
                             +---------+---------+---------+---------
                             0.00      0.25      0.50      0.75

Pooled StDev = 0.00000
```

One-way ANOVA: Cavity type versus Tu%

```
Source  DF    SS     MS     F      P
Tu%      2  0.000  0.000  0.00  1.000
Error   24  6.000  0.250
Total   26  6.000


S = 0.5   R-Sq = 0.00%   R-Sq(adj) = 0.00%



                                  Individual 95% CIs For Mean Based on
                                  Pooled StDev
Level  N    Mean    StDev    -+---------+---------+---------+--------
 0.67  9  0.3333  0.5000   (----------------*----------------)
 5.00  9  0.3333  0.5000   (----------------*----------------)
15.00  9  0.3333  0.5000   (----------------*----------------)
                           -+---------+---------+---------+--------
                           0.00      0.20      0.40      0.60

Pooled StDev = 0.5000
```
One-way ANOVA: Cavity type versus Uupstream (m/s)

```
Source          DF    SS     MS     F      P
Uupstream (m/s)  2  0.000  0.000  0.00  1.000
Error           24  6.000  0.250
```

```
Total            26  6.000

S = 0.5   R-Sq = 0.00%   R-Sq(adj) = 0.00%


                            Individual 95% CIs For Mean Based on
                            Pooled StDev
Level  N   Mean    StDev   -+---------+---------+---------+--------
 5.0   9  0.3333  0.5000   (-----------------*----------------)
 9.5   9  0.3333  0.5000   (-----------------*----------------)
15.0   9  0.3333  0.5000   (-----------------*----------------)
                           -+---------+---------+---------+--------
                           0.00      0.20      0.40      0.60

Pooled StDev = 0.5000
```

It can be observed that Tu% and $U_{upstream}$ are not significant as the P-value of them are greater than 0.05.

For the number of vortexes as response:

The full model gives:

```
Factor           Type   Levels  Values
W/D              fixed     3    2, 4, 6
Tu%              fixed     3    0.67, 5.00, 15.00
Uupstream (m/s)  fixed     3    5.0, 9.5, 15.0


Analysis of Variance for Number of vortexes, using Adjusted SS for Tests

Source                    DF   Seq SS   Adj SS   Adj MS   F   P
W/D                        2  6.00000  6.00000  3.00000  **
Tu%                        2  0.00000  0.00000  0.00000  **
Uupstream (m/s)            2  0.00000  0.00000  0.00000  **
W/D*Tu%                    4  0.00000  0.00000  0.00000  **
W/D*Uupstream (m/s)        4  0.00000  0.00000  0.00000  **
Tu%*Uupstream (m/s)        4  0.00000  0.00000  0.00000  **
W/D*Tu%*Uupstream (m/s)    8  0.00000  0.00000  0.00000  **
Error                      0        *        *        *
Total                     26  6.00000

** Denominator of F-test is zero.


S = *
```

Omitting the interactions the model will result:

```
actor            Type   Levels  Values
W/D              fixed     3    2, 4, 6
Tu%              fixed     3    0.67, 5.00, 15.00
```

```
Uupstream (m/s)  fixed        3  5.0, 9.5, 15.0


Analysis of Variance for Number of vortexes, using Adjusted SS for Tests

Source          DF  Seq SS  Adj SS  Adj MS   F   P
W/D              2  6.0000  6.0000  3.0000  **
Tu%              2  0.0000  0.0000  0.0000  **
Uupstream (m/s)  2  0.0000  0.0000  0.0000  **
Error           20  0.0000  0.0000  0.0000
Total           26  6.0000

** Denominator of F-test is zero.


S = 8.388386E-17   R-Sq = 100.00%   R-Sq(adj) = 100.00%
```
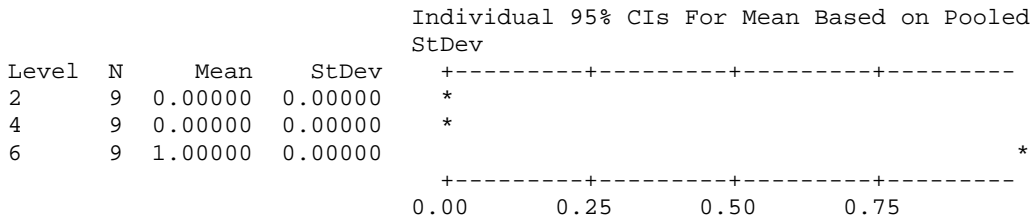
Hence, it is obvious that only one factor is affecting the response and one way ANOVA analysis leads to the conclusion that W/D is the only factor significant for number of vortexes as it can be understood from Table- 6 as well.

One-way ANOVA: Number of vortexes versus W/D
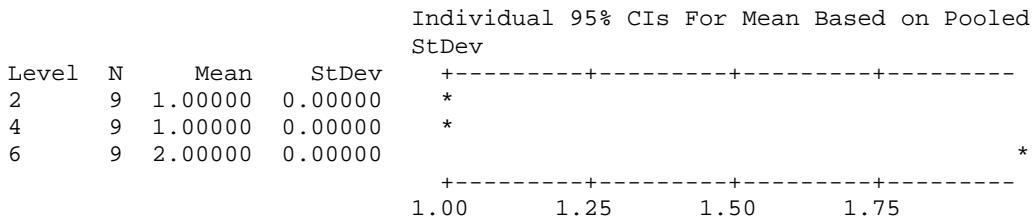
```
Source  DF       SS        MS    F   P
W/D      2  6.000000  3.000000  *   *
Error   24  0.000000  0.000000
Total   26  6.000000


S = 0   R-Sq = 100.00%   R-Sq(adj) = 100.00%


                                Individual 95% CIs For Mean Based on Pooled
                                StDev
Level  N    Mean     StDev    +---------+---------+---------+---------
2      9  1.00000  0.00000    *
4      9  1.00000  0.00000    *
6      9  2.00000  0.00000                                         *
                             +---------+---------+---------+---------
                             1.00      1.25      1.50      1.75

Pooled StDev = 0.00000
```
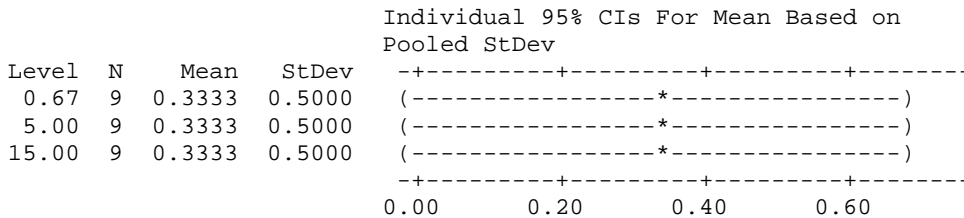
One-way ANOVA: Number of vortexes versus Tu%

```
Source  DF     SS      MS     F       P
Tu%      2  0.000   0.000   0.00   1.000
Error   24  6.000   0.250
Total   26  6.000


S = 0.5   R-Sq = 0.00%   R-Sq(adj) = 0.00%


                                Individual 95% CIs For Mean Based on
                                Pooled StDev
```
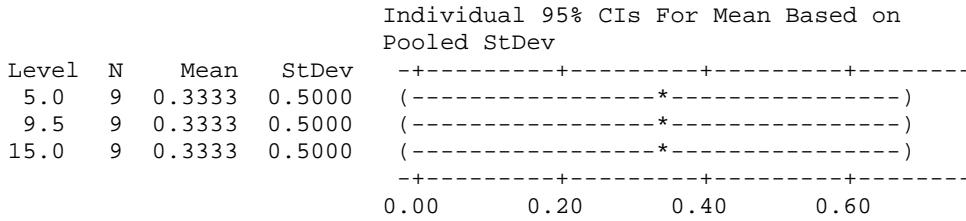
```
Level   N    Mean    StDev   -+---------+---------+---------+--------
 0.67   9   1.3333   0.5000  (----------------*----------------)
 5.00   9   1.3333   0.5000  (----------------*----------------)
15.00   9   1.3333   0.5000  (----------------*----------------)
                             -+---------+---------+---------+--------
                            1.00      1.20      1.40      1.60

Pooled StDev = 0.5000
```

One-way ANOVA: Number of vortexes versus Uupstream (m/s)

```
Source           DF    SS     MS     F     P
Uupstream (m/s)   2  0.000  0.000  0.00  1.000
Error            24  6.000  0.250
Total            26  6.000

S = 0.5   R-Sq = 0.00%   R-Sq(adj) = 0.00%


                           Individual 95% CIs For Mean Based on
                           Pooled StDev
Level   N    Mean    StDev   -+---------+---------+---------+--------
  5.0   9   1.3333   0.5000  (----------------*----------------)
  9.5   9   1.3333   0.5000  (----------------*----------------)
 15.0   9   1.3333   0.5000  (----------------*----------------)
                             -+---------+---------+---------+--------
                            1.00      1.20      1.40      1.60

Pooled StDev = 0.5000
```

Hence, W/D ratio is the only significant factor as P-value is greater than 0.05 for

$U_{upstream}$ and Tu%.

REFERENCES

J.B. Barlow., H. William. RAE. A. Pope. Low-speed wind tunnel testing, (1999), 3rd edition, Wiley-Interscience.

R.A. Johnson. Miller & Freund's Probability and statistics for engineers, (2011), Pearson Education, 8th edition.

F.E. Jorgenson, How to measure turbulence with hot-wire anemometers, a practical guide, (2002), Dantec Dynamics.

B.E. Launder, B.I. Sharma, Application of the energy dissipation model of turbulence to the calculation of flow near a spinning disc, (1974) Letters in Heat and Mass Transfer, 1, (131-138).

F.R. Menter, M. Kuntz, R. Bender, A scale-adaptive simulation model for turbulent flow predictions, (2003). The American Institute of Aeronautics and Astronautics Journal.

S. Samarasinghe, Neural Networks for applied sciences and engineering, (2006), Auerbach Publications, Boston, MA, USA.

P. Salizzoni, M. Marro, L. Soulhac, N. Grosjean, R. J. Perkins, Turbulent transfer between street canyons and the overlying atmospheric boundary layer, (2011), Boundary- Layer Meteorol, 141, (393-414).

D. K. Walters, D. Cokljat, A three-equation eddy-viscosity model for Reynolds-averaged Navier-Stokes simulations of transitional flows, (2008), Journal of Fluids Engineering

F. M. White, Fluid Mechanics, (2003), McGraw-Hill, 5th Edition.

D. C. Wilcox. Turbulence Modeling for CFD, (1998), DCW Industries, Inc. La Canada, California.

A.10. Figure copyright permission

1. This is a License Agreement between Saeed Zeinalidanaloo ("You") and Springer ("Springer") provided by Copyright Clearance Center ("CCC"). The license consists of your order details, the terms and conditions provided by Springer, and the payment terms and conditions.

All payments must be made in full to CCC. For payment instructions, please see information listed at the bottom of this form.

License Number: 3018820904009

License date: Oct 30, 2012

Licensed content publisher: Springer

Licensed content publication: Experiments in Fluids

Licensed content title: Experimental investigation of the flow characteristics within a shallow wall cavity for both laminar and turbulent upstream boundary layers

Licensed content author: Sheryl Grace

Licensed content date: May 1, 2004, Volume number: 36, Issue number: 5

Type of Use: Thesis/Dissertation, Portion: Figures

Author of this Springer article: No

Order reference number

Title of your thesis / dissertation: FLOW OVER A TRAPEZOIDAL CAVITY UNDER VARYING REYNOLDS NUMBER AND TURBULENCE CHARACTERISTICS

Expected completion date: Oct 2012

Estimated size (pages): 120

Total: 0.00 USD

2. This is a License Agreement between Saeed Zeinalidanaloo ("You") and Springer ("Springer") provided by Copyright Clearance Center ("CCC"). The license consists of your order details, the terms and conditions provided by Springer, and the payment terms and conditions.

All payments must be made in full to CCC. For payment instructions, please see information listed at the bottom of this form.

License Number: 3018811273526

License date: Oct 30, 2012

Licensed content publisher: Springer

Licensed content publication: Experiments in Fluids

Licensed content title: Visualizations of the flow inside an open cavity at medium range Reynolds numbers

Licensed content author: Thierry M. Faure

Licensed content date: Jan 1, 2006

Volume number: 42, Issue number: 2. Type of Use: Thesis/Dissertation

Portion: Figures

Author of this Springer article: No

Order reference number

Title of your thesis / dissertation: FLOW OVER A TRAPEZOIDAL CAVITY UNDER VARYING REYNOLDS NUMBER AND TURBULENCE CHARACTERISTICS

Expected completion date: Oct 2012

Estimated size (pages): 120

Total: 0.00 USD

3. This is a License Agreement between Saeed Zeinalidanaloo ("You") and Elsevier ("Elsevier") provided by Copyright Clearance Center ("CCC"). The license consists of your order details, the terms and conditions provided by Elsevier, and the payment terms and conditions.

All payments must be made in full to CCC. For payment instructions, please see information listed at the bottom of this form.

Supplier: Elsevier Limited, The Boulevard,Langford Lane, Kidlington,Oxford,OX5 1GB,UK

Registered Company Number: 1982084

Customer name: Saeed Zeinalidanaloo

Customer address: 347 Indian Rd, Windsor, ON N9C 2M1

License number: 3018821339874

License date: Oct 30, 2012

Licensed content publisher: Elsevier

Licensed content publication: Computers & Fluids

Licensed content title: Lattice Boltzmann simulation of lid-driven flow in trapezoidal cavities

Licensed content author: Ting Zhang,Baochang Shi,Zhenhua Chai

Licensed content date: December 2010

Licensed content volume number: 39, Licensed content issue number: 10

Number of pages: 13, Start Page: 1977-End Page: 1989

Type of Use: reuse in a thesis/dissertation

Intended publisher of new work: other

Portion: figures/tables/illustrations

Number of figures/tables/illustrations: 1

Format: both print and electronic

Are you the author of this Elsevier article? No

Will you be translating? No

Order reference number

Title of your thesis/dissertation: FLOW OVER A TRAPEZOIDAL CAVITY UNDER VARYING REYNOLDS NUMBER AND TURBULENCE CHARACTERISTICS

Expected completion date: Oct 2012

Estimated size (number of pages): 120

Elsevier VAT number: GB 494 6272 12

Permissions price: 0.00 USD

VAT/Local Sales Tax: 0.0 USD / 0.0 GBP

Total: 0.00 USD

4. This is a License Agreement between Saeed Zeinalidanaloo ("You") and Elsevier ("Elsevier") provided by Copyright Clearance Center ("CCC"). The license consists of your order details, the terms and conditions provided by Elsevier, and the payment terms and conditions.

All payments must be made in full to CCC. For payment instructions, please see information listed at the bottom of this form.

Supplier: Elsevier Limited, The Boulevard,Langford Lane, Kidlington,Oxford,OX5 1GB,UK.

Registered Company Number: 1982084

Customer name: Saeed Zeinalidanaloo

Customer address: 347 Indian Rd, Windsor, ON N9C 2M1,

License number: 3018821153825

License date: Oct 30, 2012

Licensed content publisher: Elsevier

Licensed content publication: Atmospheric Environment

Licensed content title: A numerical study of atmospheric pollutant dispersion in different two-dimensional street canyon configurations

Licensed content author: V.D Assimakopoulos,H.M ApSimon,N Moussiopoulos

Licensed content date: September 2003

Licensed content volume number: 37, Licensed content issue number: 29

Number of pages: 13, Start Page: 4037, End Page: 4049

Type of Use: reuse in a thesis/dissertation

Intended publisher of new work: other

Portion: figures/tables/illustrations

Number of figures/tables/illustrations: 1

Format: both print and electronic

Are you the author of this Elsevier article? No

Will you be translating? No

Order reference number

Title of your thesis/dissertation: FLOW OVER A TRAPEZOIDAL CAVITY UNDER VARYING REYNOLDS NUMBER AND TURBULENCE CHARACTERISTICS

Expected completion date: Oct 2012

Estimated size (number of pages): 120

Elsevier VAT number: GB 494 6272 12

Permissions price: 0.00 USD

VAT/Local Sales Tax: 0.0 USD / 0.0 GBP

Total: 0.00 USD

5. This is a License Agreement between Saeed Zeinalidanaloo ("You") and Elsevier ("Elsevier") provided by Copyright Clearance Center ("CCC"). The license consists of your order details, the terms and conditions provided by Elsevier, and the payment terms and conditions.

All payments must be made in full to CCC. For payment instructions, please see information listed at the bottom of this form.

Supplier: Elsevier Limited, The Boulevard,Langford Lane, Kidlington,Oxford,OX5 1GB,UK

Registered Company Number: 1982084

Customer name: Saeed Zeinalidanaloo

Customer address: 347 Indian Rd, Windsor, ON N9C 2M1

License number: 3001021400796

License date: Oct 02, 2012

Licensed content publisher: Elsevier

Licensed content publication: Progress in Aerospace Sciences

Licensed content title: Review of numerical simulations for high-speed, turbulent cavity flows

Licensed content author: S.J. Lawson,G.N. Barakos

Licensed content date: April 2011

Licensed content volume number: 47

Licensed content issue number: 3

Number of pages: 31, Start Page: 186, End Page: 216

Type of Use: reuse in a thesis/dissertation

Portion: figures/tables/illustrations

Number of figures/tables/illustrations: 2

Format: both print and electronic

Are you the author of this Elsevier article? No

Will you be translating? No

Order reference number

Title of your thesis/dissertation: FLOW OVER A TRAPEZOIDAL CAVITY UNDER VARYING REYNOLDS NUMBER AND TURBULENCE CHARACTERISTICS

Expected completion date: Oct 2012

Estimated size (number of pages): 120

Elsevier VAT number: GB 494 6272 12

Permissions price: 0.00 USD

VAT/Local Sales Tax: 0.0 USD / 0.0 GBP

Total: 0.00 USD

INTRODUCTION

1. The publisher for this copyrighted material is Elsevier. By clicking "accept" in connection with completing this licensing transaction, you agree that the following terms and conditions apply to this transaction (along with the Billing and Payment terms and conditions established by Copyright Clearance Center, Inc. ("CCC"), at the time that you opened your Rightslink account and that are available at any time at http://myaccount.copyright.com).

GENERAL TERMS

2. Elsevier hereby grants you permission to reproduce the aforementioned material subject to the terms and conditions indicated.

3. Acknowledgement: If any part of the material to be used (for example, figures) has appeared in our publication with credit or acknowledgement to another source, permission must also be sought from that source. If such permission is not obtained then that material may not be included in your publication/copies. Suitable acknowledgement to the source must be made, either as a footnote or in a reference list at the end of your publication, as follows:

"Reprinted from Publication title, Vol /edition number, Author(s), Title of article / title of chapter, Pages No., Copyright (Year), with permission from Elsevier [OR APPLICABLE SOCIETY COPYRIGHT OWNER]." Also Lancet special credit - "Reprinted from The Lancet, Vol. number, Author(s), Title of article, Pages No., Copyright (Year), with permission from Elsevier."

4. Reproduction of this material is confined to the purpose and/or media for which permission is hereby given.

5. Altering/Modifying Material: Not Permitted. However figures and illustrations may be altered/adapted minimally to serve your work. Any other abbreviations, additions, deletions and/or any other alterations shall be made only with prior written authorization of Elsevier Ltd. (Please contact Elsevier at permissions@elsevier.com)

6. If the permission fee for the requested use of our material is waived in this instance, please be advised that your future requests for Elsevier materials may attract a fee.

7. Reservation of Rights: Publisher reserves all rights not specifically granted in the combination of (i) the license details provided by you and accepted in the course of this licensing transaction, (ii) these terms and conditions and (iii) CCC's Billing and Payment terms and conditions.

8. License Contingent Upon Payment: While you may exercise the rights licensed immediately upon issuance of the license at the end of the licensing process for the transaction, provided that you have disclosed complete and accurate details of your proposed use, no license is finally effective unless and until full payment is received from you (either by publisher or by CCC) as provided in CCC's Billing and Payment terms and

conditions.   If full payment is not received on a timely basis, then any license preliminarily granted shall be deemed automatically revoked and shall be void as if never granted. Further, in the event that you breach any of these terms and conditions or any of CCC's Billing and Payment terms and conditions, the license is automatically revoked and shall be void as if never granted. Use of materials as described in a revoked license, as well as any use of the materials beyond the scope of an unrevoked license, may constitute copyright infringement and publisher reserves the right to take any and all action to protect its copyright in the materials.

9. Warranties: Publisher makes no representations or warranties with respect to the licensed material.

10. Indemnity: You hereby indemnify and agree to hold harmless publisher and CCC, and their respective officers, directors, employees and agents, from and against any and all claims arising out of your use of the licensed material other than as specifically authorized pursuant to this license.

11. No Transfer of License: This license is personal to you and may not be sublicensed, assigned, or transferred by you to any other person without publisher's written permission.

12. No Amendment Except in Writing: This license may not be amended except in a writing signed by both parties (or, in the case of publisher, by CCC on publisher's behalf).

13. Objection to Contrary Terms: Publisher hereby objects to any terms contained in any purchase order, acknowledgment, check endorsement or other writing prepared by you, which terms are inconsistent with these terms and conditions or CCC's Billing and Payment terms and conditions. These terms and conditions, together with CCC's Billing and Payment terms and conditions (which are incorporated herein), comprise the entire agreement between you and publisher (and CCC) concerning this licensing transaction. In the event of any conflict between your obligations established by these terms and conditions and those established by CCC's Billing and Payment terms and conditions, these terms and conditions shall control.

14. Revocation: Elsevier or Copyright Clearance Center may deny the permissions described in this License at their sole discretion, for any reason or no reason, with a full refund payable to you. Notice of such denial will be made using the contact information provided by you. Failure to receive such notice will not alter or invalidate the denial. In no event will Elsevier or Copyright Clearance Center be responsible or liable for any costs, expenses or damage incurred by you as a result of a denial of your permission request, other than a refund of the amount(s) paid by you to Elsevier and/or Copyright Clearance Center for denied permissions.

LIMITED LICENSE

The following terms and conditions apply only to specific license types:

15. Translation: This permission is granted for non-exclusive world English rights only unless your license was granted for translation rights. If you licensed translation rights you may only translate this content into the languages you requested. A professional translator must perform all translations and reproduce the content word for word preserving the integrity of the article. If this license is to re-use 1 or 2 figures then permission is granted for non-exclusive world rights in all languages.

16. Website: The following terms and conditions apply to electronic reserve and author websites:

Electronic reserve: If licensed material is to be posted to website, the web site is to be password-protected and made available only to bona fide students registered on a relevant course if:

This license was made in connection with a course,

This permission is granted for 1 year only. You may obtain a license for future website posting,

All content posted to the web site must maintain the copyright information line on the bottom of each image,

A hyper-text must be included to the Homepage of the journal from which you are licensing at http://www.sciencedirect.com/science/journal/xxxxx or the Elsevier homepage for books at http://www.elsevier.com , and

Central Storage: This license does not include permission for a scanned version of the material to be stored in a central repository such as that provided by Heron/XanEdu.

17. Author website for journals with the following additional clauses:

All content posted to the web site must maintain the copyright information line on the bottom of each image, and the permission granted is limited to the personal version of your paper. You are not allowed to download and post the published electronic version of your article (whether PDF or HTML, proof or final version), nor may you scan the printed edition to create an electronic version. A hyper-text must be included to the Homepage of the journal from which you are licensing at http://www.sciencedirect.com/science/journal/xxxxx . As part of our normal production process, you will receive an e-mail notice when your article appears on Elsevier's online service ScienceDirect (www.sciencedirect.com). That e-mail will include the article's Digital Object Identifier (DOI). This number provides the electronic link to the published article and should be included in the posting of your personal version. We ask that you wait until you receive this e-mail and have the DOI to do any posting.

Central Storage: This license does not include permission for a scanned version of the material to be stored in a central repository such as that provided by Heron/XanEdu.

18. Author website for books with the following additional clauses:

Authors are permitted to place a brief summary of their work online only.

A hyper-text must be included to the Elsevier homepage at http://www.elsevier.com . All content posted to the web site must maintain the copyright information line on the bottom of each image. You are not allowed to download and post the published electronic version of your chapter, nor may you scan the printed edition to create an electronic version.

Central Storage: This license does not include permission for a scanned version of the material to be stored in a central repository such as that provided by Heron/XanEdu.

19. Website (regular and for author): A hyper-text must be included to the Homepage of the journal from which you are licensing at http://www.sciencedirect.com/science/journal/xxxxx. or for books to the Elsevier homepage at http://www.elsevier.com

20. Thesis/Dissertation: If your license is for use in a thesis/dissertation your thesis may be submitted to your institution in either print or electronic form. Should your thesis be published commercially, please reapply for permission. These requirements include permission for the Library and Archives of Canada to supply single copies, on demand, of the complete thesis and include permission for UMI to supply single copies, on demand, of the complete thesis. Should your thesis be published commercially, please reapply for permission.

21. Other Conditions:

If you would like to pay for this license now, please remit this license along with your payment made payable to "COPYRIGHT CLEARANCE CENTER" otherwise you will be invoiced within 48 hours of the license date. Payment should be in the form of a check or money order referencing your account number and this invoice number RLNK500869308.

Once you receive your invoice for this order, you may pay your invoice by credit card. Please follow instructions provided at that time.

Make Payment To: Copyright Clearance Center, Dept 001, P.O. Box 843006, Boston, MA 02284-3006

For suggestions or comments regarding this order, contact RightsLink Customer Support: customercare@copyright.com or +1-877-622-5543 (toll free in the US) or +1-978-646-2777.

Gratis licenses (referencing $0 in the Total field) are free. Please retain this printable license for your reference. No payment is required.

VITA AUCTORIS

NAME	Saeed Zeinalidanaloo
PLACE OF BIRTH	Tehran
YEAR OF BIRTH	1987
EDUCATION	University of Tehran, Tehran, Iran 2010, B.Sc.
	University of Windsor, Windsor, ON, Canada 2012, M.A.Sc.